Noninvasive Ultrasound Techniques for Assessment of Early Atherosclerosis

by

Robert William Stadler

B.S., Case Western Reserve University (1990)
S.M.E.E., Massachusetts Institute of Technology (1992)

Submitted to the Harvard-MIT Division of
Health Sciences and Technology
in partial fulfillment of the requirements for the degree of

Doctor of Philosophy

at the

MASSACHUSETTS INSTITUTE OF TECHNOLOGY

May 1996

Author .....
.....
Harvard-MIT Division of
Health Sciences and Technology
May 3, 1996

Certified by...
.....
Robert S. Lees
Professor of Health Sciences and Technology
Thesis Supervisor

Accepted by...
.....
Martha L. Gray
Chairman, Departmental Committee on Graduate Students

Noninvasive Ultrasound Techniques for Assessment of Early Atherosclerosis

by Robert William Stadler

Submitted to the Harvard-MIT Division of Health Sciences and Technology
on May 3, 1996, in partial fulfillment of the requirements for
the degree of Doctor of Philosophy

Abstract

Currently, the only way to predict the development of atherosclerosis is to assess risk factors for the disease. Problematically, some risk factors for atherosclerosis remain unidentified, some patients at risk will not develop atherosclerosis, and evaluation of preventative therapy is based on reduction of risk factors, not on documented cessation of the disease process. The goal of this work was to advance the assessment of early atherosclerosis by improving three noninvasive ultrasound measures of arterial health: vasoreactivity, intima-media thickness (IMT), and distensibility. Vasoreactivity was assessed by measuring brachial artery diameter and flow velocity continuously before, during, and after a 5-minute occlusion of the forearm vasculature. Arterial diameter was measured from end-diastolic B-mode images using edge detection and a new model-based diameter estimation algorithm, which reduced measurement variance by a factor of 5 over the subjective caliper-based method. Variability of the time series of diameter estimates was additionally reduced by acquiring images in the skew plane (i.e., a plane rotated about 10 degrees off-axis of the artery), and by conducting edge-detection in consistent locations over time. Multiple parameters of vasoreactivity were extracted from the time-series measurements. Measurement of IMT in the distal common carotid artery was based on automated border detection from B-mode images. The standard deviation of individual IMT measurements compared favorably with other techniques. Arterial distensibility measurements were based on digitization and storage of radio-frequency ultrasound, followed by off-line echo tracking, which allowed detection of tracking errors.

Several pilot studies were conducted with this measurement system. Whereas subjects with familial hypercholesterolemia (FH) are known to have abnormal flow-mediated dilation (FMD), we demonstrated nearly normal FMD and reduced progression of carotid IMT in FH subjects treated chronically with Heparin-induced Extracorporeal LDL Precipitation (HELP). Evidence of the individual specificity of our vasoreactivity measurements was demonstrated by consistent deviations from normality in certain HELP subjects. In a study of the effects of acute increase in plasma homocysteine on vasoreactivity, we demonstrated acute but temporary inhibition of FMD in a subject who was later shown to have fasting hyperhomocysteinemia, and a delay in the time course of FMD in normal subjects. Finally, we demonstrated reduced FMD and abnormal arterial constriction during distal vascular occlusion in smokers who refrained from smoking, but acute normalization of vasoreactivity immediately after smoking. We conclude that measurement of vasoreactivity, IMT, and distensibility with our system provides insight to arterial health and may lead to noninvasive assessment of early atherosclerosis and of therapeutic efficacy in individual subjects.

Thesis Supervisor: Robert S. Lees
Title: Professor of Health Sciences and Technology

Acknowledgments

Trust in the Lord with all your heart
and lean not on your own understanding;
in all your ways acknowledge him,
and he will make your paths straight.
– Proverbs 3:5,6.

This thesis was supported by funds from B. Braun Inc. (USA), the Boston Heart Foundation, and the Harvard/MIT Division of Health Sciences and Technology; and by equipment from the Medical Products Division of Hewlett-Packard. I will always be grateful for this opportunity to work at the Boston Heart Foundation; the free interaction between medicine and research, the creative environment, and the encouragement and support of the staff made this experience productive and enjoyable.

This work is reported in the third person to acknowledge the innumerable contributions of my coworkers, collaborators and predecessors. In particular, I would like to thank my advisor, Dr. Robert Lees, for his selfless dedication to research and teaching, endless optimism, and for sharing his multidisciplinary insight and vision. I would also like to thank my coworker Sherrif Ibrahim, for many long hours of invaluable help; Jim Fearnside of Hewlett Packard for his expert technical advice and support; my thesis committee: Kenneth Bloch, MD, W. Clem Karl, PhD, Robert Levine, MD, and Roger Mark, MD, PhD, for their time and guidance; Linda Hemphill, MD, and my officemate, Ray Chan, for help in keeping the proper perspective; Norma Holmes and Laura Naves, for scheduling and administering to subjects; Muneeb Khalid and Ted Briggs of Gage Applied Sciences for hardware help; Phil Saul, MD, for loan of a Finapres; and the more than 100 subjects for use of their arms.

Finally, this work would not have been possible without the support and guidance of my family; especially my wife, who will always be my most valued consultant and best friend.

Contents

Chapter 1

Introduction

Atherosclerosis is the most important cause of mortality and serious morbidity in developed countries. The sequelae of atherosclerosis include myocardial infarction (heart attack), cerebral infarct (stroke), claudication (ischemia of the extremities), ischemic encephalopathy, and aneurism. In the United States, about 50% of all deaths are attributed to atherosclerosis, including 20-25% from myocardial infarction [39]. The disease is primarily manifested in the large and medium-sized arteries, by the formation of artheromas or fibrofatty plaques. The plaques are focal thickenings of the intima containing smooth muscle cells, macrophages, extracellular lipid, necrotic debris, calcium deposits, and a fibrous cap.

Efforts to control atherosclerosis are severely hindered by the inability to detect the disease before it advances to potentially life-threatening stages. The most common technique for detecting and diagnosing the disease, angiography, can only detect encroachment on the lumen by atherosclerotic plaques. However, early atherosclerosis causes arterial dilation, thereby preserving lumenal patency, blood flow, and end-organ function even as plaque growth progresses [71]. Unfortunately, actively growing plaques which are asymptomatic and undetectable by angiography may cause sudden arterial occlusion with catastrophic results – stroke or sudden cardiac death, with little or no warning [66]. The many inadequacies of angiography are reviewed by Topol and

Nissen [162]. Although angiography is unlikely to be replaced for diagnosis of late-stage atherosclerosis in the coronary arteries, alternative methods must be developed for diagnosing earlier stages of the disease and for validation of preventative therapies.

The ideal diagnostic test would be inexpensive and noninvasive, would have sufficient sensitivity and specificity for the screening of individuals, and would rapidly report changes in disease status after the onset of effective therapy. At present, the closest match to these specifications is the assessment of risk factors for atherosclerosis. Screening for risk factors, and treating those at risk significantly prolongs survival [70]. However, some risk factors remain to be identified and some subjects at risk will not develop atherosclerosis. The assessment of risk factors therefore lacks sensitivity and specificity, which decreases efficiency in the application of preventative therapy [146]. The goal of this thesis is to investigate alternative methods for noninvasive assessment of early atherosclerosis.

1.1 VASOREACTIVITY

Prinzmetal showed in 1959 that symptoms and signs of coronary atherosclerosis, including chest pain and electrocardiographic changes, may arise from coronary artery spasm at the site of minimally-stenotic atheromatous lesions [130]. Subsequent studies [41, 46, 67, 116] confirmed the direct clinical relevance of abnormal arterial vasoreactivity. The first step towards recognition of the phsyiological basis of vasoreactivity was demonstration of the obligatory role of endothelium in the vasodilatory response to acetylcholine [65]. The normal vasodilatory response to acetylcholine has been attributed to the action of endothelium-derived relaxing factor [65, 123], now known to be nitric oxide (NO) or a nitroso adduct thereof [91, 121, 122]. In the absence of functional endothelium, acetylcholine causes direct vasoconstriction of the vascular smooth muscle cells. NO is also released by functional endothelium in response to serotonin [36], bradykinin [142], substance P [181], and increased arterial wall shear

stress [92, 110, 128, 134, 148].[1] The endothelium is now viewed as a complex regulator of arterial vasomotor tone [165].

Our interest in vasoreactivity stems from the connection between atherosclerosis and abnormal endothelial function. Abnormal responses of the epicardial arteries to acetylcholine, or to increases in arterial wall shear stress, are associated with atherosclerosis [41, 111, 117, 168] or with risk factors for the disease [6, 50, 79, 98, 169, 183, 185]. In subjects with atherosclerosis, coronary arteries which appear normal on angiography may, nevertheless, demonstrate grossly abnormal vasoreactivity [53, 114, 183]. The vasoreactivity of the small coronary resistance vessels, which are known to be free of atherosclerotic involvement, may also be abnormal in subjects with atherosclerosis [142, 180, 184]. This suggests that endothelial dysfunction is generalized in the "milieu" of atherosclerosis. Significantly, long-term inhibition of normal NO-mediated vasoreactivity in rabbit models has been associated with accelerated development of atherosclerotic lesions [28, 119], enhancement of NO production by supplemental L-arginine (the metabolic precursor of NO [122]) results in regression of lesions in cholesterol-fed rabbits [27], and treatment of obvious risk factors in humans with atherosclerosis has been shown to restore coronary endothelium-dependent vasoreactivity to or towards normal [4, 54, 75, 107, 163]. Thus, the above invasive studies of vasoreactivity have provided new insight into the mechanisms of atherosclerosis, including the potential role of abnormal endothelium-dependent vasoreactivity in atherogenesis. Unfortunately, the invasive nature of human coronary vasoreactivity measurements precludes routine use for screening and follow-up of disease.

An exciting recent advance is the demonstration of similar disease-related abnormalities in peripheral arterial vasoreactivity, which is much more easily measured than coronary vasoreactivity. Vasoreactivity is abnormal in the peripheral arteries of subjects with atherosclerosis [29] or risk factors for the disease [8, 30, 31, 32, 109, 150],

[1] Although two studies [92, 110] have demonstrated conclusively that NO is responsible for flow-mediated dilation in the human brachial artery, NO may not contribute significantly to flow-mediated dilation in the human coronary artery [144].

including passive smoking [33]. The vasoreactivity of the peripheral microvasculature is also abnormal in subjects with atherosclerosis or risk factors [43, 69, 93]. Measurements of microvascular vasoreactivity generally use intra-arterial injections of acetylcholine as a stimulus whereas measurements of brachial or femoral artery vasoreactivity involve reactive hyperemia after temporary cuff occlusion of the distal vasculature, and are completely noninvasive. Dilation of peripheral arteries in response to increased arterial wall shear stress (e.g., during reactive hyperemia) is known to be mediated by endothelium-derived nitric oxide [92]. Most recently, the correlation between coronary vasoreactivity in response to acetylcholine and brachial vasoreactivity in response to shear stress has been investigated [5]. Ninety-five percent (i.e., all but one) of the subjects in this study that had abnormal brachial artery vasoreactivity also had abnormal coronary artery vasoreactivity. Finally, abnormal peripheral arterial endothelium-dependent vasoreactivity can be improved with risk factor modification [170]. Therefore, noninvasive measurement of peripheral artery vasoreactivity is potentially valuable as a screening test for early atherosclerosis.

Celermajer and associates [29, 30, 31, 150] have described a convenient, noninvasive method for measuring peripheral arterial vasoreactivity. The method involves measurement of arterial diameter with ultrasonic calipers at two time points: before and after temporary ischemia induced by inflation of a blood pressure cuff around the forearm or thigh. This innovative technique has been widely used since its introduction 4 years ago. Unfortunately, as currently performed, it provides little information beyond that afforded by assessment of risk factors, is nonspecific for various types of abnormalities, and is not sufficiently reproducible to identify individuals on a routine basis as normal or abnormal. We believe that by increasing the accuracy of, and by extracting more information from, noninvasive arterial reactivity measurements, we may be able to define patterns of arterial dysfunction with individual specificity. The ability to determine the cause of the abnormality from the pattern of abnormal vasoreactivity may give us insight into the mechanisms of atherogenesis. Finally, be-

cause some subjects with risk factors for atherosclerosis may not develop disease, and some risk factors remain to be identified, noninvasive measurements of vasoreactivity may improve the efficiency of atherosclerosis prevention [146] by assessing the need for, the efficacy of, and the appropriate endpoints of antiatherosclerotic therapy in individuals.

1.2 INTIMA-MEDIA THICKNESS

Another promising technique for the noninvasive assessment of atherosclerosis is the measurement of carotid artery intima-media thickness (IMT) with noninvasive B-mode ultrasound [173]. This technique accurately and reproducibly estimates the thickness of the carotid arterial wall; increased IMT is a direct measurement of carotid atherosclerotic thickening [17]. Measurement of IMT is widely used in studies of atherosclerosis regression [44, 64, 112]. For example, one study reported a significant reduction of IMT in 14 subjects with coronary artery disease treated for one year with colestipol and niacin [112]. An angiographic trial with comparable power would require hundreds of subjects treated for several years. A recent study has shown that regression of IMT in response to cholesterol-lowering parallels improvements in coronary artery disease [44, 64, 126]. Not surprisingly, since the risk factors for coronary and carotid atherosclerosis are essentially the same [52], patients with coronary disease have significantly larger carotid IMT than patients free of coronary disease [45]. An overwhelming body of circumstantial evidence, including relatively rapid increase in IMT with time in patients at risk [112], and similar changes in IMT and coronary disease burden in the recent major study referred to above [44, 64, 126], have shown quite clearly that carotid IMT measurement is a valid noninvasive parameter of the presence of early atherosclerotic change in arteries.

1.3 DISTENSIBILITY

Arterial distensibility can be measured noninvasively with peripheral vascular ultrasound [11, 80, 166, 167], and is known to be altered by atherosclerosis [2, 80]. Arteries become less distensible with dilation of the artery during the atherosclerotic process, i.e. the Glagov effect [71]. Arterial distensibility has also been used as a parameter of the vascular effects of hypertension [77, 145], heart failure [102], and diabetes [1, 80]. Because distensibility is altered in a variety of conditions, including advanced age [11, 80], the technique is unlikely to have sufficient specificity for the early assessment of atherosclerosis. However, the technique could be used in combination with other noninvasive tests of arterial pathophysiology.

In summary, noninvasive measurements of peripheral artery vasoreactivity, intima-media thickness, and distensibility may serve as early indications of the atherosclerotic process. Peripheral vasoreactivity is a surrogate for coronary vasoreactivity; both forms of vasoreactivity are abnormal in atherosclerosis and may even be abnormal before anatomic changes of atherosclerosis occur. Improvements in current methods for noninvasive assessment of peripheral arterial vasoreactivity may result in individual sensitivity, and in specificity for different forms of abnormal vasoreactivity. Carotid IMT is a reliable parameter of carotid atherosclerosis and may therefore be used as a noninvasive estimator of a patient's atheromatous disease burden. Measurement of arterial distensibility may provide additional information of arterial pathophysiology. These three diagnostic tests can be performed noninvasively and inexpensively with ultrasound and may eventually lead to improved prevention of atherosclerosis.

1.4 THESIS OVERVIEW

The first half of the thesis (Chapters 2 through 6) describes the engineering, construction, and validation of the measurement methodology. Chapter 2 describes the application of ultrasonic echo tracking to measurements of arterial vasoreactivity and

distensibility. Chapter 3 explores model-based estimation of arterial diameter from B-mode ultrasound images, and compares the performance of this technique to that of standard, caliper-based measurements. Chapter 4 describes the incorporation of the model-based diameter estimators into a system for noninvasive measurement of peripheral arterial vasoreactivity after release of temporary vascular occlusion. The resolution of the resulting measurements demonstrates previously-unobservable human physiology. We therefore characterize the normal vasoreactivity, propose new parameters of vasoreactivity, and determine the measurement accuracy of these parameters. In Chapter 5, the measurements of Chapter 4 are extended to include measurement of vasoreactivity before and during forearm vascular occlusion. Additional vasoreactivity parameters are proposed, and measurement accuracy is determined. Chapter 6 introduces an algorithm for measurement of common carotid intima-media thickness (IMT), describes the incorporation of the algorithm into a system for in-vivo measurements, and reports the accuracy of the measurements.

Chapters 7 through 9 describe a series of pilot studies that make use of the new methodology. Chapter 7 reports the vasoreactivity and intima-media thickness of familial hypercholesterolemic subjects treated with Heparin-induced Extracorporeal LDL Precipitation (HELP). Chapter 8 describes the changes in vasoreactivity after acute increase in plasma homocysteine levels. Chapter 9 describes abnormalities of vasoreactivity in smokers. Finally, Chapter 10 contains a summary and suggestions for future work.

Chapter 2

Methods I: Echo Tracking and Doppler Processing

Ultrasonic echo tracking, as a means of measuring changes in arterial diameter, is applicable to measurements of vasoreactivity and arterial distensibility. Echo tracking involves serial measurements of the depth of a given echogenic tissue interface, derived from the echoes received from a given direction. Changes in the depth of the selected interface as small as several microns can be detected by these methods [84, 159]. Two types of information may be used to track the desired tissue: absolute position and velocity. The absolute position information is obtained by "time-of-flight" measurements; i.e., measurement of the time between pulse emission and reception of the echo. Velocity information is obtained from low frequency Doppler signals which are typically discarded by the highpass "wall filters" of pulsed-Doppler processing.

Many methods have been proposed to incorporate the position and/or velocity information into echo-tracking algorithms.[1] In 1968, Arndt described the use of radio-frequency (RF) amplitude thresholding to track the absolute position of large echoes; e.g., from the near and far walls of the artery [10]. Hokanson proposed tracking the absolute tissue position by tracking the location of a single RF zero-crossing [87].

[1]Most methods can be adapted to velocity estimation for fluids.

Kanai proposed following the location of the maximum amplitude of the complex envelope of the RF signal for echo tracking [94]. Hoeks has described various tracking algorithms based entirely upon Doppler processing [83, 84]. The tracking of absolute position by RF cross-correlation of echoes from subsequent pulses has also been proposed [18, 40]. The computational demands of the latter method are reduced by model-based interpolation of the cross-correlation [47, 48, 56, 61]. Finally, Ferrara and Algazi have proposed an algorithm for incorporation of all of the available information (position and velocity) into a maximum-likelihood motion estimator [57, 58].

Each of these methods has advantages and disadvantages, but all methods suffer from decreased robustness with increasing measurement duration or with movements of the transducer or tissue in directions other than the direction of insonation. The tracking of the non-Doppler methods is corrupted by the decorrelation of the echoes over time as a result of disparate movements of neighboring tissue reflectors or the inability to insonate the same tissues consistently. The Doppler methods track the tissue by integrating velocity estimates; the accumulation of tracking error is inherent in this approach. Nevertheless, these methods are potentially valuable for measurements of vasoreactivity and arterial distensibility.

Documentation of endothelium-dependent vasoreactivity (EDV) involves tracking changes in arterial diameter in response to certain pharmacologic stimuli or to changes in arterial wall shear stress. These measurements require long periods (> 30 seconds) of echo tracking, thus increasing the accumulation of tracking error or the likelihood of inadvertent movement. An additional difficulty in echo tracking for noninvasive measurements of EDV is the translational motion of the artery that results from noninvasive flow stimuli such as reactive hyperemia. Nevertheless, two authors have reported the successful use of echo tracking in measurements of EDV in the radial artery, using invasive [51] and noninvasive [92] stimuli.

Measurements of arterial distensibility can be conducted over a single cardiac cycle, thereby reducing the tracking error and the likelihood of inadvertent motions.

These measurements involve either the relationship between arterial diameter and blood pressure, or the pulse propagation velocity along the artery (e.g., by continuously measuring arterial diameter at two locations along an artery). Several authors have measured arterial distensibility using both Doppler and non-Doppler echo-tracking methods [11, 21, 73, 77, 105, 124].

In this chapter, we investigate the application of echo-tracking to measurements of EDV and arterial distensibility. Our primary goal is to appraise qualitatively the general value of the technique, not to compare quantitatively the performances of the various echo-tracking methods.

2.1 METHODS

2.1.1 Hardware

To investigate the application of echo tracking to EDV and arterial distensibility measurements, we constructed a system based upon analog-to-digital (A/D) conversion of the RF signals. By storing the RF data from each complete study, we were able to compare the tracking results to the initial data. A 66MHz 80486 computer served as the central component of the measurement hardware. The computer contained a modified Gage CompuScope 1012 A/D converter (Gage inc., Montreal, Quebec) for the digitization of RF ultrasound echoes for simultaneous diameter and flow velocity measurement. The optional flow velocity measurements were made available to characterize the flow stimulus for EDV. A Hewlett Packard SONOS 100 peripheral vascular ultrasound imager served as the ultrasound front end. Measurements of arterial diameter or diameter and flow velocity were obtained with the SONOS in pulsed-Doppler mode, with a 3.7 MHz transducer and 0.32 μs (0.5 mm) pulse durations. In this mode, a single direction was repetitively insonated at a pulse repetition frequency determined by the maximum velocity of the blood (typically 1500–3000 pulses/second). The A/D converter sampled the RF echoes at 14.8 million samples

per second (four times the transducer center frequency) with 12 bits of resolution, according to an external clock signal from the SONOS. This clock signal was in-phase with a line-trigger signal from the SONOS, which signaled the arrival of echoes from a given depth and the initiation of sampling.[2] After each trigger, the A/D card sampled the echoes arising from the depth of the artery (typically 200-256 samples per trigger). The data was therefore structured as an "RF matrix", with tissue depth in one dimension and time in the other dimension (although tissue depth is equivalent to time of sound propagation). Simultaneous measurement of arterial diameter and flow velocity required about 1.3 megabytes of computer memory per second of measurement. An assembly language interrupt subroutine rapidly transferred each acquisition of 200-256 samples from the A/D card to 32 megabytes of standard computer memory.

2.1.2 Software

Algorithms for calculation of arterial diameter, Doppler spectra, mean flow velocities, arterial flow velocity profiles, and arterial volume flow from the raw RF data were originally developed and optimized in MATLAB. For portability and efficiency, the algorithms were translated into Watcom C, a 32-bit C compiler for personal computers.

For measurements of flow, velocity information was available from the RF data as long as the insonation angle was not perpendicular to the artery. In these cases, the insonation angle was determined from B-mode images of the artery, and was used to scale the measured flow-velocities and diameter changes. Doppler velocity was estimated from the RF data by: 1.) quadrature demodulation in the depth dimension, which was trivialized by setting the sampling frequency at four times the center frequency of the ultrasound. 2.) Lowpass filtering in the depth dimension

[2]The consistent phase relationship was necessary for accurate "time of flight" and Doppler information.

with a four-point moving average filter. This filter had a convenient zero at the location of the undesired sideband. 3.) Integration in the depth dimension over a ~0.7mm pulse gate. 4.) Highpass filtering in the time dimension with a third order Chebychev type II infinite impulse response filter, implemented in a direct form II structure [120]. This "wall filter" had stopband attenuation of 50dB and a cutoff velocity of 0.015m/sec. Therefore, filter coefficients varied depending on the pulse repetition frequency of the RF data. 5.) Mean Doppler frequencies for blood velocity measurements were determined by the complex autocorrelation technique [95], which estimates the centroid of the Doppler spectrum from the first lag of the complex autocorrelation of the time series. The signal to noise ratio of the mean Doppler frequencies could be improved by averaging over multiple pulse gates in the depth dimension [85, 86]. 6.) The estimated mean flow velocity was accepted or set to zero based upon a combination of the energy of the spectrum, the variance of the spectrum, the derivative of the arterial diameter signal (see below), and the prior value of mean flow velocity.

Arterial volume flow was determined by integrating the mean flow velocities across the profile of the artery under the assumption of cylindrical flow symmetry. Flow volume and mean flow velocity were stored along with the arterial diameter signal. Doppler velocity information was displayed graphically by either 1.) Calculation of the Doppler spectra by Radix-8 fast-Fourier transform [26] of 64-point windows of the time series data, or 2.) Color coding of the mean flow velocities versus depth in the artery and versus time of the measurement.

For diameter tracking, a temporally-decimated version of the RF data set, containing approximately 100 RF lines of data per second, was graphically displayed. The decimation factor was chosen to allow sufficient temporal density of RF lines to avoid tracking errors due to aliasing in the tracking algorithms. The user designated the location of the near and far walls of the artery at the beginning of the data set. The near and far walls were tracked using either the zero-crossing method of Hokan-

son [87], the Doppler method of Hoeks [84] (where mean velocity was estimated via the complex autocorrelation technique of Kasai et al. [95], using a tracking window of 0.3mm in depth and 60ms in time), the correlation interpolation method of de Jong [47](using the same tracking window), or a novel hybrid algorithm. The hybrid algorithm determined each successive tissue location by both the Hokanson and de Jong methods, and selected the de Jong result in the presence of RF transition regions (described below) and the Hokanson result otherwise. The wall trackings and the corresponding diameter measurements were then superimposed onto the RF data for user inspection.

For qualitative assessment of the methods, approximately 50 data sets containing at least 26 Megabytes of digitized RF data were acquired from the carotid, brachial and radial arteries, with insonation angles of 70° to 90° relative to the artery.

2.2 RESULTS AND DISCUSSION

The RF data acquired by the above methods had a similar format to M-mode ultrasound. The RF data, however, contained the phase information necessary for the majority of the tracking algorithms and for flow velocity measurements. Figure 2-1 compares a section of RF data to an M-mode image derived from the RF image by quadrature demodulation, lowpass filtering, and magnitude extraction.

Comparisons of the tracking results to the original RF data afforded new insight into the validity of echo-tracking applications. These comparisons raised two major concerns for the application of echo tracking to endothelium-dependent vasoreactivity (EDV) or arterial distensibility measurements: tracking drift and RF transition regions. Tracking drift is a concern primarily for EDV measurements, due to their long duration. The endothelial-derived change in arterial diameter must be measured with a resolution of at least 100μm. For our implementation, the tracking algorithm could therefore accumulate no more than 50μm of error for each wall location in

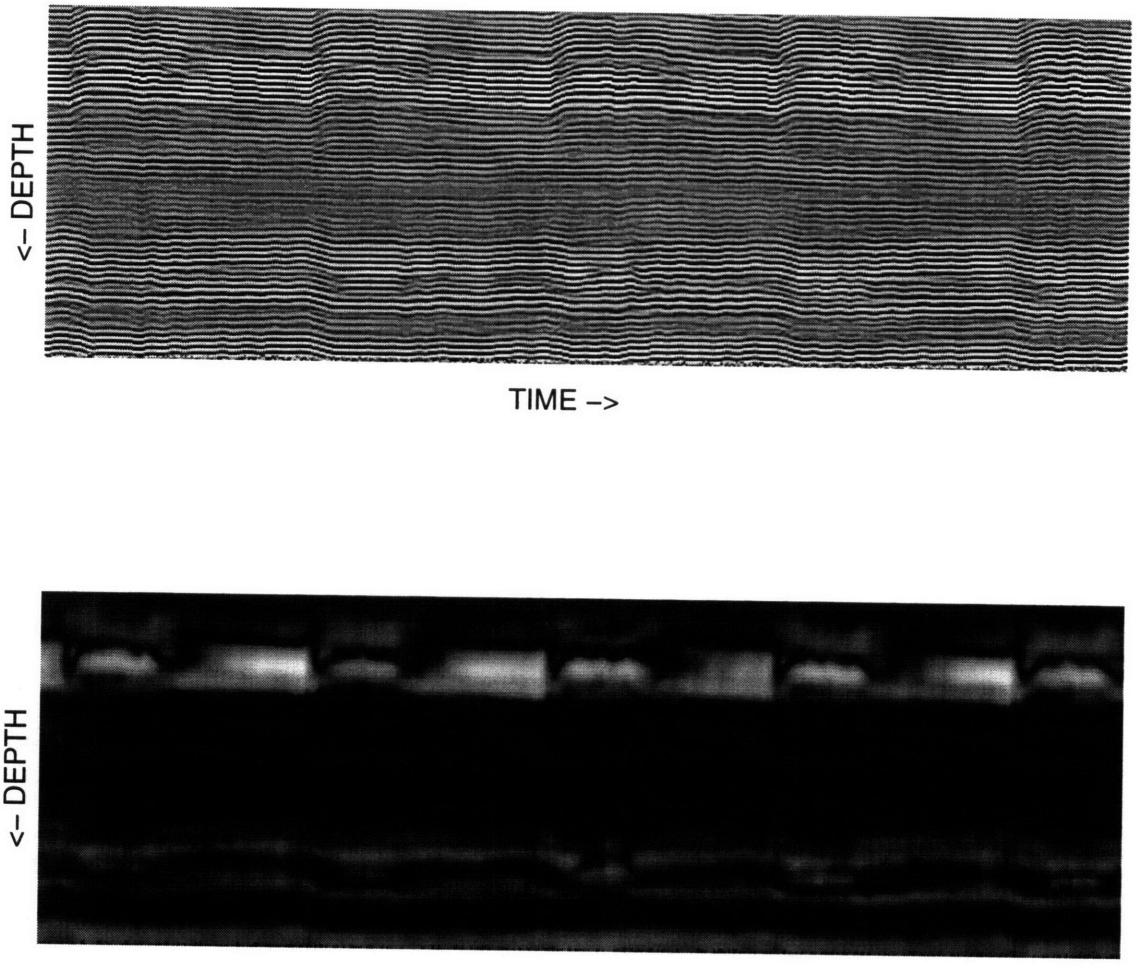

Figure 2-1: **Top:** RF image of the carotid artery, containing 4 complete cardiac cycles. **Bottom:** M-mode image derived from the RF image by quadrature demodulation, lowpass filtering, and magnitude extraction.

about 3000 position estimates over a 30 second duration. The Hoeks and de Jong methods could not meet this constraint. The Hoeks method tracks tissue position by integrating the estimated tissue velocities over time. This integration results in a drift as the errors of each position estimate are added. The de Jong method estimates the tissue movement in a series of RF lines by calculating 5 cross-correlation values, and selecting the maximum value of a model-based interpolation of the cross-correlation as the new tissue location. As only local RF lines are used in the correlation, the small error introduced by the interpolation slowly accumulates. In contrast, the zero-tracking method of Hokanson [87] has a long-term memory which prohibits the slow accumulation of error. For this reason, the Hokanson method was the default method in the hybrid algorithm.

The RF transition regions were defined as slow transitions (i.e., decorrelations) of successive RF lines. These RF transitions may have involved convergence or separation of neighboring tissue reflectors or insonation of a new series of tissue layers. Examples of RF transition regions are depicted by rectangles in Figure 2-2. The number of these transitions was greatly reduced by decreasing the gross movement of the tissue e.g., by switching from the carotid to the radial artery, by decreasing measurement duration, or by increasing the angle of insonation of the vessel towards the perpendicular. In the presence of these transitions, the true location of the desired tissue was unclear. The Hokanson method often produced abrupt changes at the RF transitions. Conversely, the de Jong method generally passed smoothly through the transitions. Therefore, the hybrid algorithm selected the Hokanson result in the absence of RF transitions and the de Jong result otherwise,[3] although neither result was free from error in the neighborhood of transitions.

The effect of the RF transition regions on the echo-tracking measurements is best demonstrated by examples. A rare example of a 30 second carotid measurement using

[3]RF transition regions were algorithmically defined as either 1.) locations where neighboring RF zero crossings were closer or further apart than given thresholds, or 2.) locations where the Hokanson tracking result and the de Jong tracking result differed by more than a threshold value.

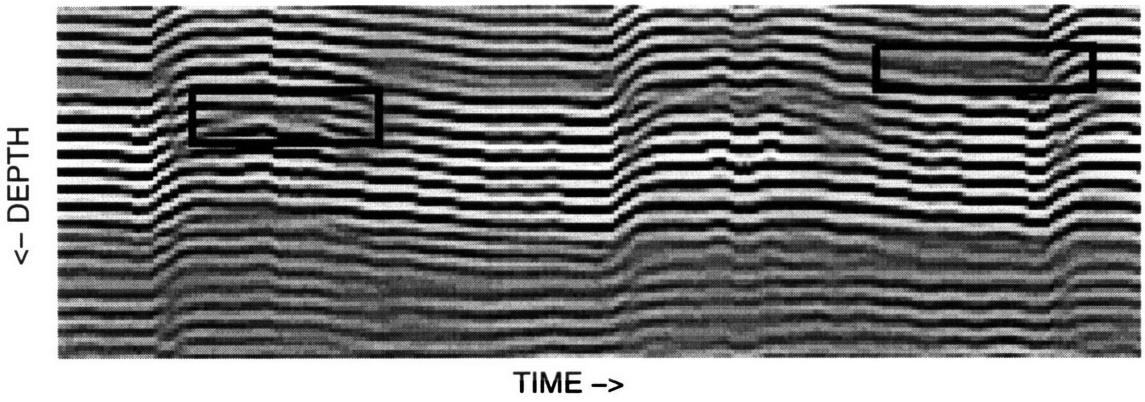

Figure 2-2: A portion of the RF image in the top of Figure 2-1, containing two cardiac cycles of the near wall. The left and right boxes highlight examples of RF transition regions.

a hand-held transducer where the tracking paths were free from RF transition regions is presented in Figure 2-3. This result was obtained from a 26 MByte RF data set, containing 60,000 RF lines acquired at 1,975 lines/second at an insonation angle of 80° with respect to the vessel. The pulse repetition frequency and the data storage requirement can be significantly reduced if the measurement of blood velocity is not required. The dashed line represents the diameter averaged over each cardiac cycle. The diameter plot demonstrates 0.5 mm diameter excursions during the cardiac cycle, but no significant long-term diameter changes. Figure 2-4 demonstrates the error introduced by RF transition regions. The diameter measurement in the top panel of Figure 2-4 was obtained from the same data as Figure 2-3, but the location of the near wall tracking was about 150μm deeper, yet still within the near wall. Direct comparison of the tracking results to the original RF data demonstrated numerous near wall tracking errors in the range of 15-20 seconds, due to RF transition regions. With the identification of these errors, the apparent vasoconstriction was ruled-out. This result is a strong argument against the use of long term (greater than several

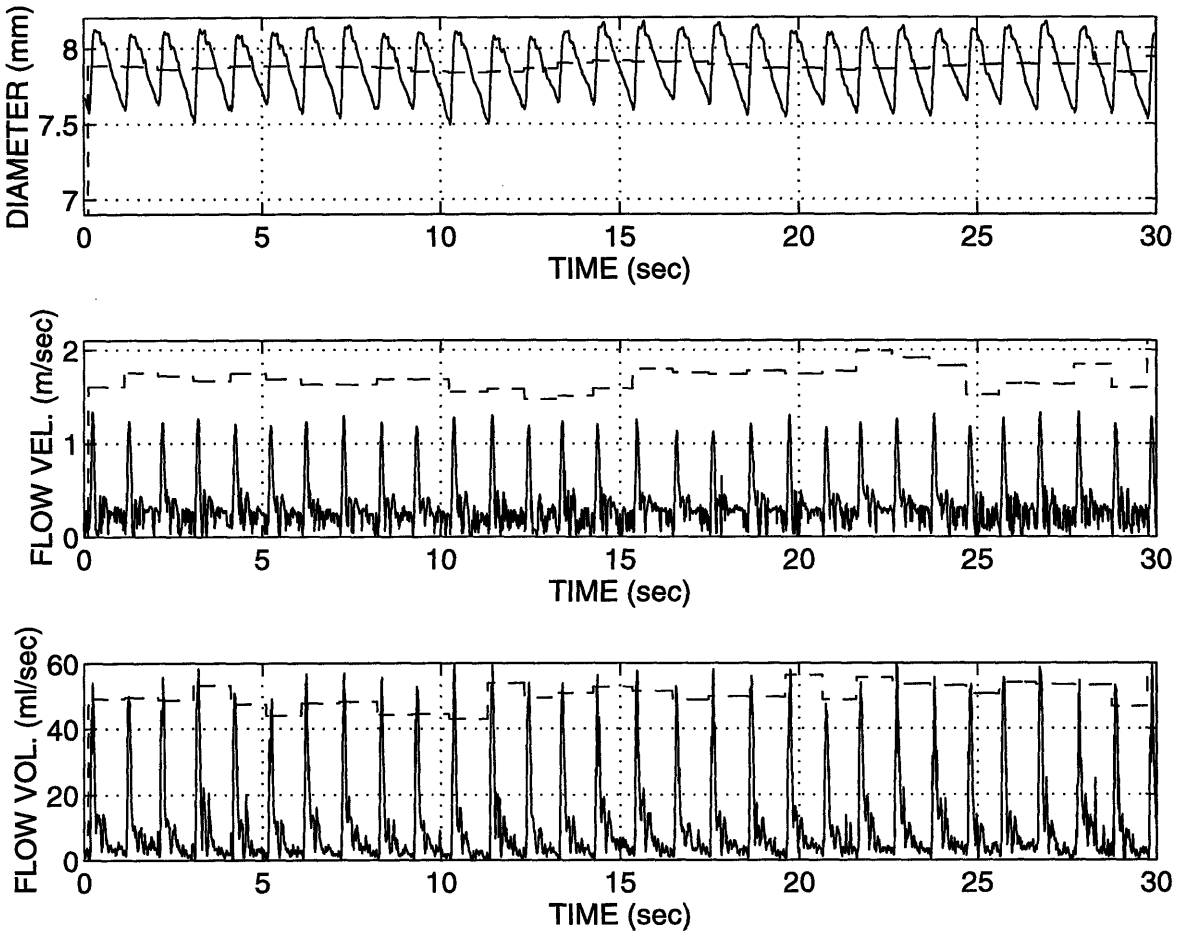

Figure 2-3: Echo-tracking and flow measurement from the carotid artery of a normal subject during rest. The dashed lines indicate the values averaged over each cardiac cycle. The average values for velocity and volume are multiplied by a factor of five for clarity. This diameter tracking was free from RF transition regions.

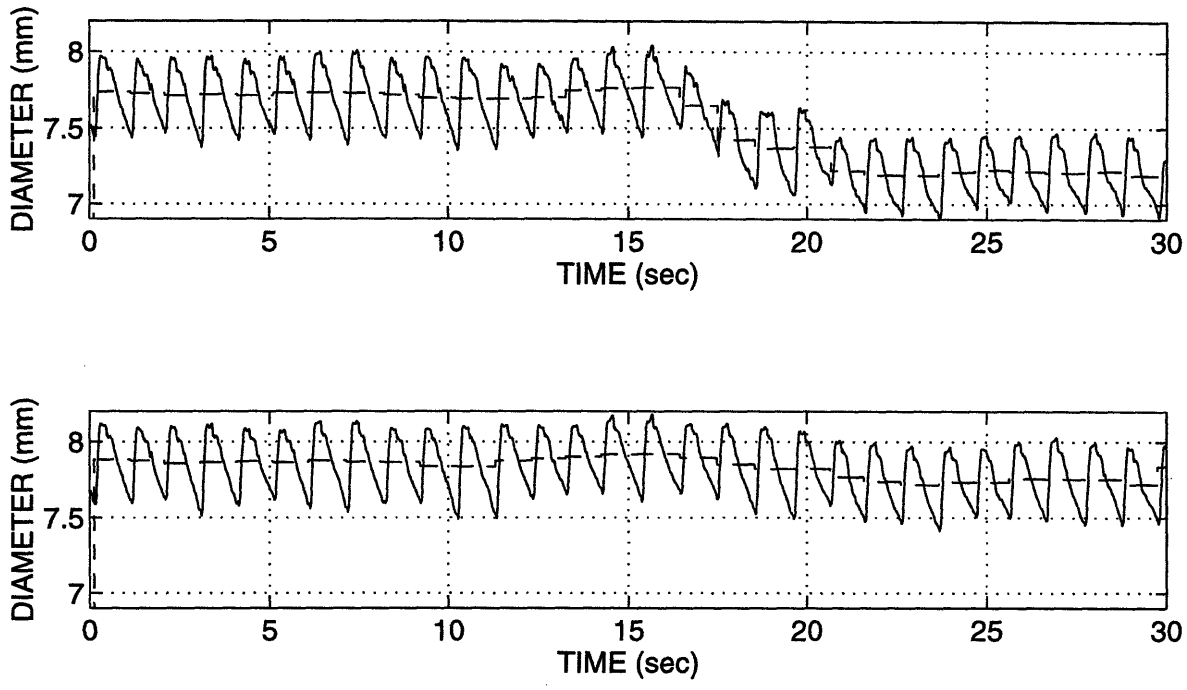

Figure 2-4: **Top:** Diameter tracking from the same data set as Figure 2-3, but the near wall tracking location was moved about 150 μm deeper, still within the limits of the near wall. Numerous near wall tracking errors, due to RF transition regions, were demonstrated in the range of 15-20 seconds when the near wall tracking was compared to the RF data. **Bottom:** Average diameter measurement from 11 near wall and 11 far wall tracking measurements. The 11 tracking locations for the near and far walls each span 575 μm, and the near wall locations include those used in **Top** and in Figure 2-3.

seconds) echo-tracking that does not carefully compare the path of tracking to the original RF data. Figure 2-4 (bottom) is the result of averaging 11 adjacent tracking results for each of the near and far walls. The 11 locations spanned a total of 0.575mm for each wall location, and the near wall locations included those selected for Figure 2-3 and for Figure 2-4 (top). The tracking error was less than that in the top panel of Figure 2-4, but still totaled about 100μm. Although the averaging of tracking results generally reduced the total tracking error, the tracking results also had to be compared to the original RF data to rule out any systematic tracking errors.

Echo-tracking methods are more robust for EDV measurement under favorable circumstances such as those used by Drexler et al. [51] and Joannides et al. [92]. First, their measurements were made on the radial artery, whose diameter excursions are typically 40μm (see Figure 2-5), compared to about 500μm for the carotid artery. Second, they used only perpendicular incidence angles, which reduced the likelihood of RF transition regions. Third, their algorithm was a discrete-time version of the Hokanson algorithm, which, as discussed above, is not subject to tracking drift errors. Fourth, inadvertent motions of the transducer were minimized during the measurements by mounting the transducer on a stereotactic positioning device. Fifth, the stimulus for EDV that was applied by Drexler was invasive (acetylcholine injected into the brachial artery) to reduce tissue motion and the noninvasive stimulus applied by Joannides (temporary wrist occlusion) was limited in duration to 3 minutes, also to reduce tissue motion. Finally, the results from individuals were averaged over subject populations. These methods considerably reduced the risk of tracking errors in the final results, although additional evidence for the validity of the measurements would have resulted from comparison of the tracking results to the original RF data, by checking for the presence of RF transition regions in the tracking paths. An alternative method of EDV measurement, based upon duplex ultrasound, is discussed in Chapter 3 (based upon Stadler et al. [152]).

The short-term nature of arterial distensibility measurements reduce the likelihood of tracking errors. However, RF transition regions may still occur, and must be avoided in the tracking path. The RF transition regions may also introduce variability into the distensibility measurements by causing variation in the measured diameter excursions for different initial tracking locations. The top panel of Figure 2-6 is an example of a short-term echo-tracking measurement from the carotid artery. Two diameter measurements from the same RF data, but with different initial near-wall tracking locations are shown. The excursions of the arterial wall are dependent upon the tracking location. The bottom of Figure 2-6 shows the corresponding RF data

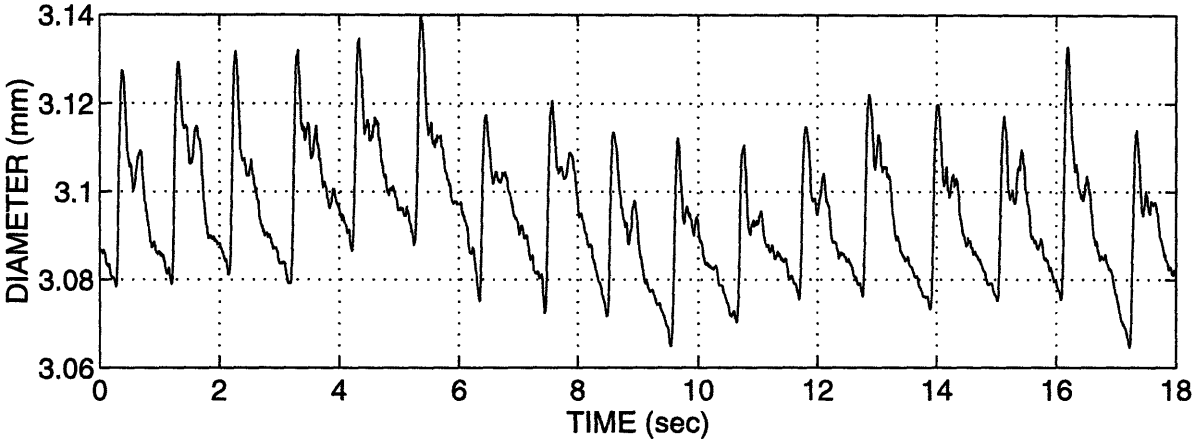

Figure 2-5: Echo tracking of the radial artery, demonstrating the small diameter excursions (about 40μm) and the resolution of echo-tracking methods. The axial resolution of the 3.7 MHz transducer that was used for this measurement is no better than 300μm.

from the near wall. The tissues closer to the lumen (deeper) appear to be less dynamic than those further from the lumen. The true pulsatile diameter changes are uncertain. These results demonstrate a potential source of variability in measurements of arterial distensibility. This variability can be reduced by averaging the results from several tracking locations within the RF data set or by averaging over groups of subjects to determine population differences.

Finally, measurement of arterial distensibility by estimation of the pulse propagation velocity is theoretically minimally affected by either the RF transition regions or the tracking drift. These measurements are concerned only with the timing of the maximum arterial distension, not the absolute degree of distension. The measurements require simultaneous diameter measurements from two locations along the artery. The mechanical-scanning transducer on our SONOS 100 did not permit such measurements.

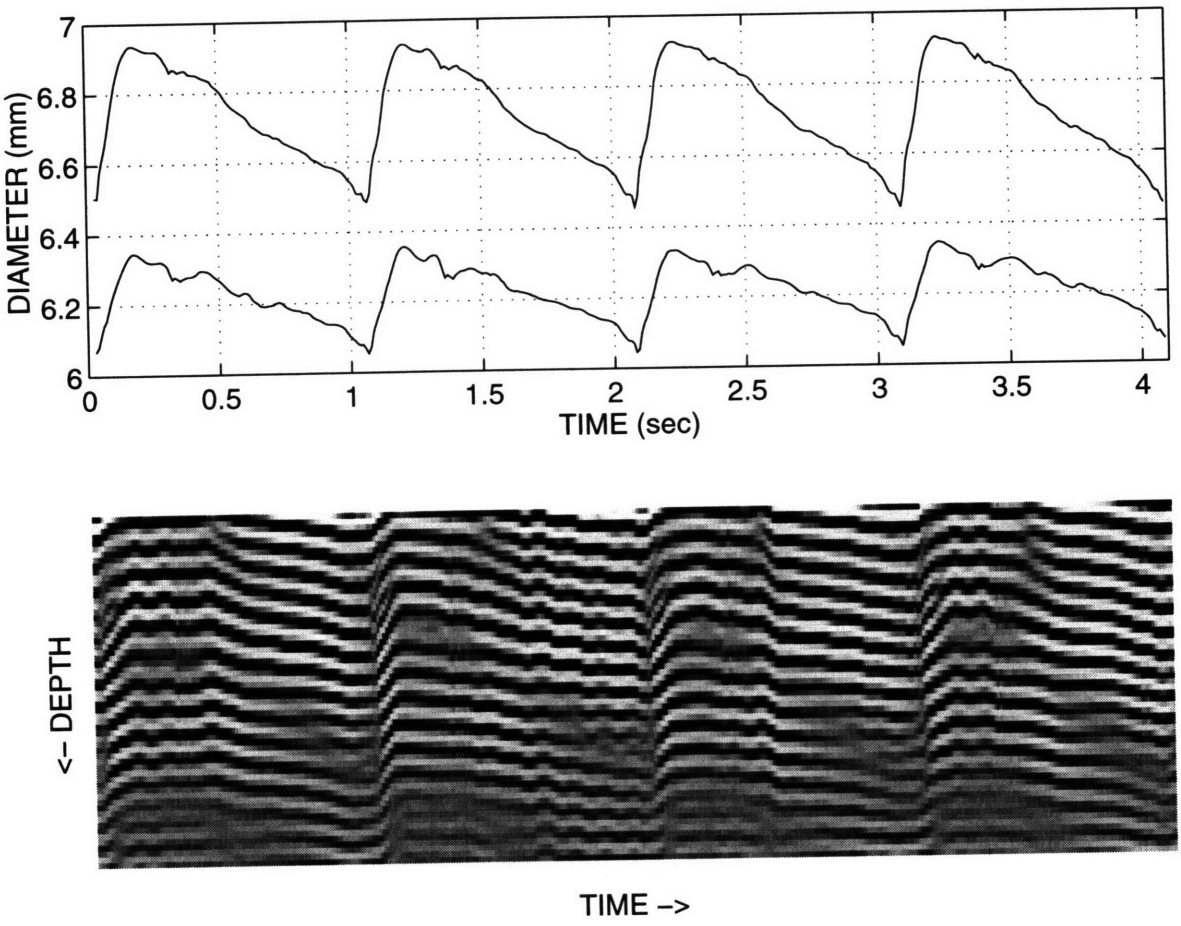

Figure 2-6: **Top:** Measurement of the diameter excursions of the carotid artery in a resting subject. The two trackings are from different initial locations in the same RF data set. **Bottom:** The RF data of the near wall. The systolic (upward) excursions of the near wall vary with depth, resulting in uncertainty of the true diameter changes.

2.3 CONCLUSIONS

The echo-tracking system described in this paper, like that of Brands et al. [23] and unlike many others, involved digitization of the radio-frequency ultrasound of the entire experiment, followed by off-line determination of motion. Measurements with this system demonstrated two potential concerns for echo-tracking measurements: tracking drift and RF transition regions. As a result of these sources of error, the output of any echo-tracking algorithm should be validated by direct comparison to the original RF data. In general, the prevalence of RF transition regions precludes successful application of these methods to routine measurements of EDV. The failure of echo-tracking methods stems from their ability to measure motion in only a single dimension (along the direction of insonation); the typical 3-dimensional motion of objects results in tracking errors.

The RF transition regions were also shown to be a potential source of variability in arterial distensibility measurements via the diameter/pressure relationship. The application of echo tracking to measurement of arterial distensibility via the pulse wave velocity should be unaffected by tracking drift or RF transition regions as the results are indifferent to the absolute diameter excursions.

Chapter 3

Methods II: Arterial Diameter from B-Mode Images

The measurement of arterial diameter is a central component of the ultrasonic assessment of endothelium-dependent vasoreactivity (EDV) and arterial distensibility. Ultrasonic assessment of EDV involves measuring the changes in arterial diameter in response to certain pharmacologic stimuli or changes in arterial wall shear stress. A common method of ultrasonic assessment of arterial distensibility is to determine the relationship between arterial diameter and blood pressure. The most common non-invasive sources of arterial diameter information are B-mode images and ultrasonic echo tracking. In Chapter 2 we investigated the use of echo tracking for EDV and arterial distensibility measurements. In this Chapter, we present and evaluate new methods for arterial diameter measurement and tracking from B-mode images.

3.1 METHODS

3.1.1 Theoretical Considerations

The accuracy of arterial diameter measurements from B-mode images is determined primarily by the process of image acquisition and secondarily by the diameter measurement algorithm used. Image acquisition depends on the skill of the operator and the desired representation of the artery in the image. A logical imaging plane for the measurement of arterial diameter is parallel with the artery and passes through the centerline, representing the artery as a rectangle or curved rectangle (See Figure 3-1). This plane (which we will refer to as "longitudinal") contains the most arterial wall information, but diameter measurements made from longitudinal planes are likely to be underestimated due to deviations of the imaging plane about the centerline. To avoid the underestimation, the operator can scan through the artery, searching for a combination of: 1.) the largest representation of the artery, 2.) the plane with the strongest specular echoes on the near and far walls signifying perpendicular incidence to the arterial walls, 3.) the plane with the best "7 zone" representation of the arterial structure (i.e., the plane with 4 echo zones created by the media/adventitia and lumen/intima interfaces of both the near and far arterial walls, separated by 3 anechoic zones [173]). However, even with these methods in mind, errors in diameter measurement are possible; for example, lateral movements of the imaging plane a distance of 10% of the arterial diameter (0.4 mm for a medium-sized, 4 mm vessel) in either direction off-center result in a 2% error in the diameter measurement. Furthermore, there is no way to prove that the image was acquired through the center of the artery.

The imaging plane perpendicular to the artery represents the artery in circular cross-section (Figure 3-2). This imaging plane contains the least arterial wall information as only the specular echoes from the top and bottom of the vessel can be used to estimate the diameter of the artery. However, diameter estimates from the perpen-

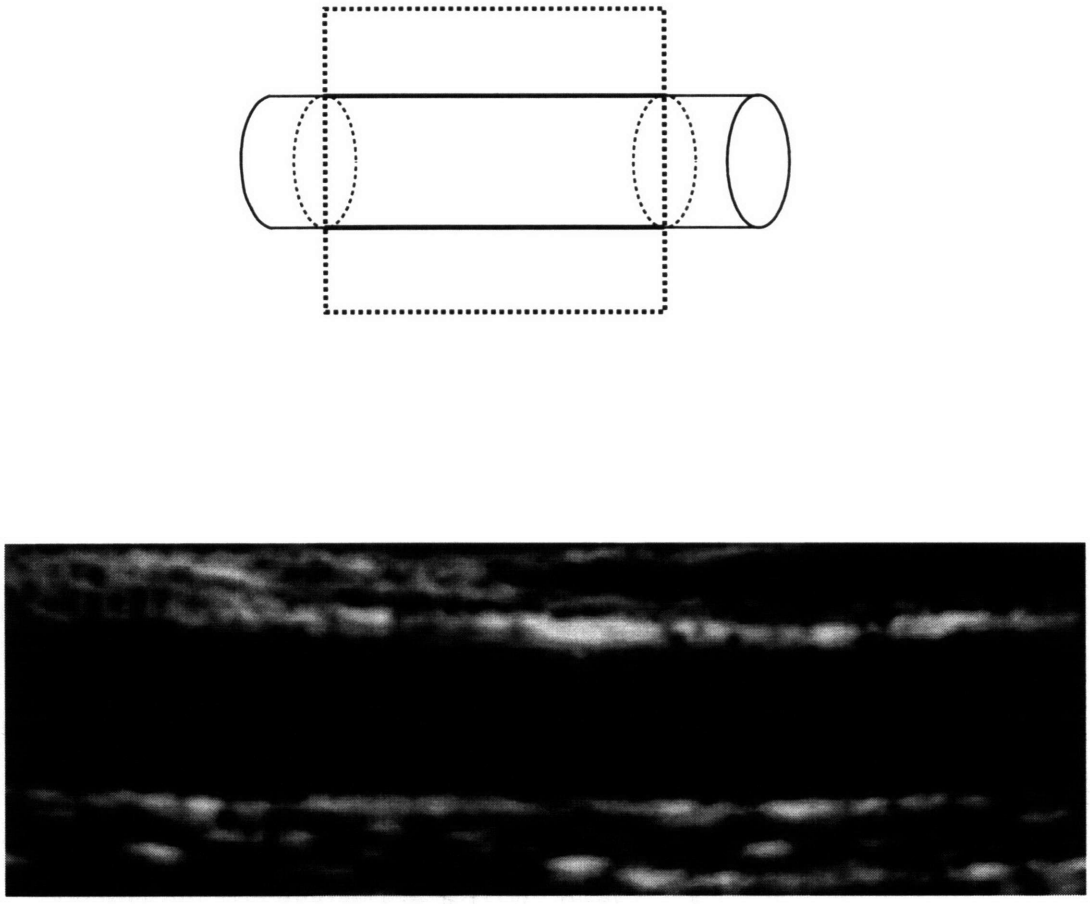

Figure 3-1: **Top:** A diagram of the longitudinal imaging plane. **Bottom:** A longitudinal B-mode image of the brachial artery. This plane contains the most edge information but the resulting diameter measurements are sensitive to transducer location errors as the plane of measurement is likely to be off the centerline of the artery.

dicular imaging plane are not affected by transducer position errors as the artery will always be represented by an ellipse whose minor axis is equivalent to the diameter of the artery.

As a compromise of the longitudinal and perpendicular imaging planes, we introduce the "skew" plane, which is produced by locating the imaging plane rotated slightly (about 10°) off-axis of the artery (cf. Figure 3-3). A cylindrical artery then appears in theory as a long ellipse, a moderate amount of arterial wall information is available, and transducer position errors will not result in a bias of the diameter measurement as the imaging plane always passes through the center of the artery. As the variance of the optimal diameter estimate is inversely proportional to the available arterial wall (edge) information in the image, the angle of the skew rotation is a concern. The maximum possible edge information is constrained by the span of the artery that the transducer can insonate. As the image is rotated off the center of the artery, the available edge information decreases until it reaches its minimum in the perpendicular plane. A simple theoretical model for the dependence of edge information (and therefore the accuracy of the estimate) on the angle of rotation (θ) relative to the axis of the artery is

$$I \propto \begin{cases} \frac{d}{\sin(\theta)}, & I < I_{max} \\ I_{max}, & \text{otherwise} \end{cases}, \tag{3.1}$$

where I is the edge information, d is the diameter of the artery, and I_{max} is the maximum possible edge information. Therefore, the angle of skew rotation should be relatively small ($< 20°$).[1]

A secondary determinant of measurement accuracy is the diameter measurement

[1]A second reason for selecting small skew rotation is the error introduced into Doppler velocity estimates. The angle between the diameter of blood flow and the diameter of insonation, which is used to scale the velocity, is more difficult to determine when the blood is flowing into and out of the plane of the image (*i.e.*, in the skew plane). The angle can be estimated from the appearance of the artery in the image; however, the overall error in velocity will be less than 1.5% when the angle of the skew rotation is less than 10°.

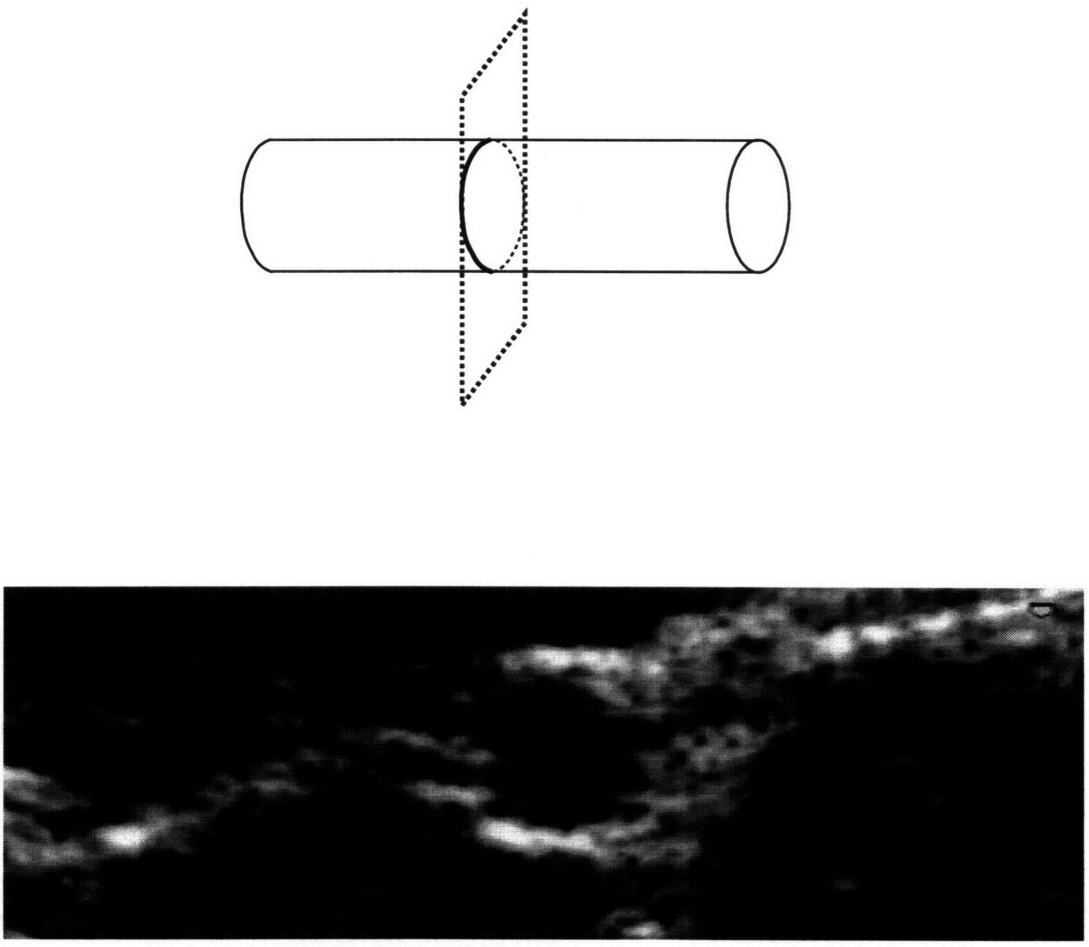

Figure 3-2: **Top:** A diagram of the perpendicular imaging plane. **Bottom:** A perpendicular image of the brachial artery. This plane contains the least edge information but diameter measurements are insensitive to transducer location errors.

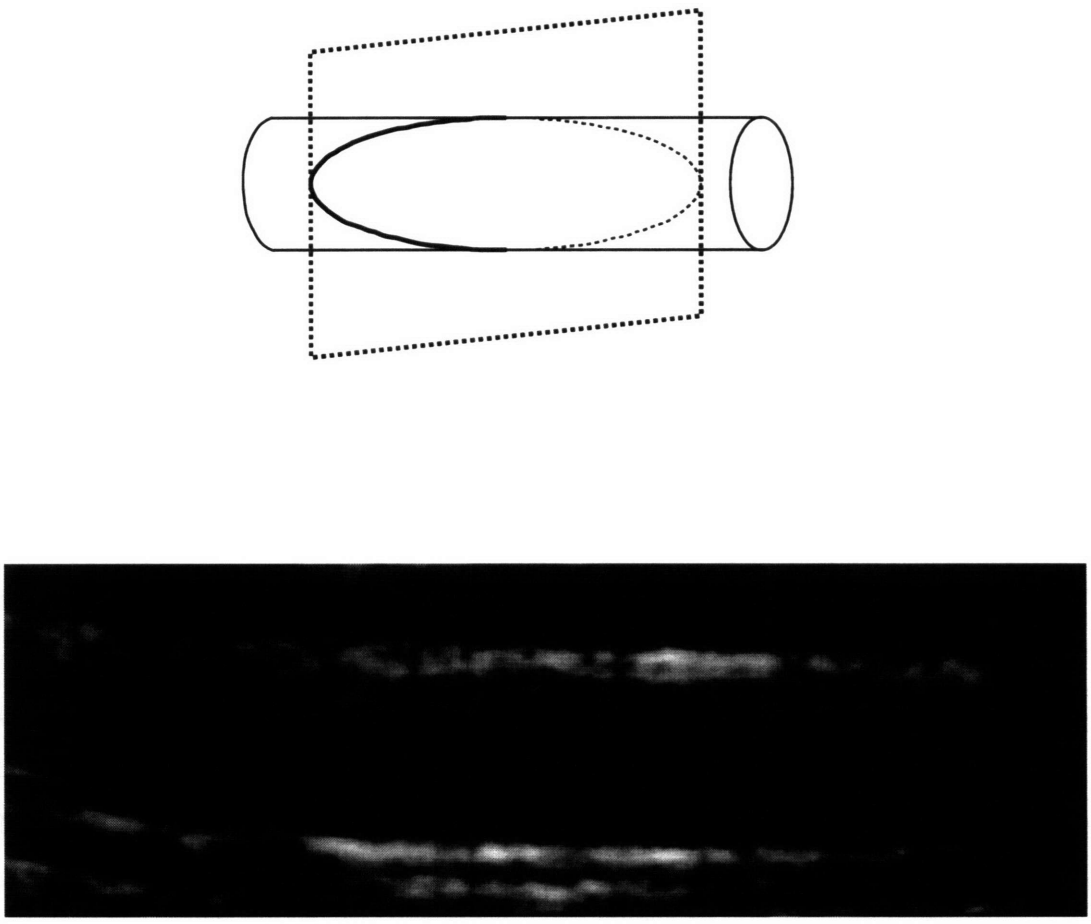

Figure 3-3: **Top:** A diagram of the skew imaging plane. **Bottom:** A skew image of the brachial artery. This plane contains a moderate amount of edge information and is relatively insensitive to transducer location errors.

algorithm. The most readily available and simplest B-mode diameter measurements are made with ultrasonic calipers (i.e. manual measurement in a single location). The performance of these estimates suffers from the use of a small fraction of the available edge information. The best estimate of a parameter must make use of all of the available information and *a-priori* knowledge. For the measurement of arterial diameter from B-mode images, the available information is the echoes from the arterial walls. The *a-priori* knowledge includes the expected representation of the artery in the image and the expected structure of the arterial echoes. The expected representation of the artery depends upon the imaging plane and the presence of pathological change. In an anatomically normal artery, an image in a longitudinal plane will theoretically show two parallel lines (Figure 3-1) while an image in a skew plane will theoretically show an elliptical representation (Figure 3-3). These strong constraints on vessel shape facilitate the incorporation of all of the edge information into a single, model-based estimate of diameter. In the presence of gross arterial pathology, the diameter becomes a localized estimate and the representation of the artery can only be constrained with regard to edge smoothness. The second item of *a-priori* knowledge, the structure of the arterial echoes, should ideally follow the "7 zone" representation detailed by Wendelhag et al. [173]. In this case, the diameter should be estimated from the leading edges of echo zones 3 and 5. In reality, the 7 zone appearance is difficult to achieve, especially for smaller arteries and lower frequency transducers. Under these circumstances, the leading edges of the available wall echoes can be used to measure the diameter. The location of the trailing edge of an echo is not anatomical as it depends on the angle of insonation, the presence of reverberation, and the gain and contrast settings of the ultrasound system [173]. Measurements from trailing edges of echoes should therefore be avoided except perhaps in the case of a diameter tracking measurement (i.e. measurement of the changes in diameter) where the system parameters and the localization of the artery in the image are constant.

We have incorporated the above design considerations into two algorithms for

arterial diameter measurement from B-mode images. Both algorithms require extraction of arterial wall edge information as a preliminary step. We therefore begin with a description of the common edge detection scheme. The edge detection method is similar to those for quantitative coronary angiography [106, 131] and ultrasonic intima-media thickness measurement [143].

The user first selects several points in proximity to the edges of the near and far walls on a digitized B-mode image. The computer fits a spline containing a user-defined number of points (typically 100) to each set of preliminary edge points (see Figure 3-4). The direction perpendicular to each spline point is calculated. The image is then interpolated in the perpendicular direction for a user-defined distance (typically, the image intensities along a distance of 6 image pixels in either direction are interpolated to create a 120 point perpendicular line). The interpolation is produced by a normalized weighting of the intensity values of the four adjacent pixels, based upon the relative distances to each pixel, followed by lowpass filtering of the interpolated line. The lowpass filter is a seven point Parks-McClellan FIR filter [113]. The location along the interpolated line with the largest weighted sum of the first derivative ($I'(l)$) and second derivative ($I''(l)$) (specifically, $\left(I'(l) + \frac{I'(l)_{max}}{I''(l)_{max}} I''(l)\right)_{max}$, where $_{max}$ indicates the maximum value) is chosen as the best local edge point. This derivative-based edge detector is widely used in quantitative coronary angiography [106, 131].

The edge-detection process is repeated for each spline point of the near and far walls. The same weighted sum of the derivatives used to find each edge point is also used to weight the least squares model fit to the edge points, as described below.

The edge points extracted by the above procedure are then used in a model-based estimation of the diameter (see Figure 3-5). For arteries with normal anatomy imaged in the longitudinal plane, the model should include a parallel course for the two edges. An appropriate model for arteries whose edges are nearly horizontal in the image is a pair of parabolas with the same curvatures but different vertices. The N_n near

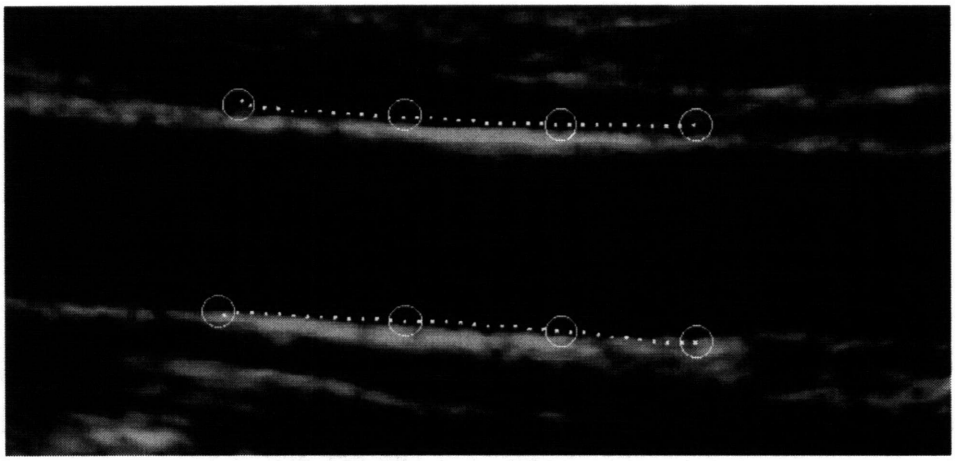

Figure 3-4: A demonstration of the first step of the automated edge-detection process. The circles indicate the location of the user-defined preliminary edge points. The circles are connected by spline interpolations, represented by dotted lines. The algorithm searches in directions that are locally perpendicular to each spline, over a distance represented by the diameter of the circles, for the best edge.

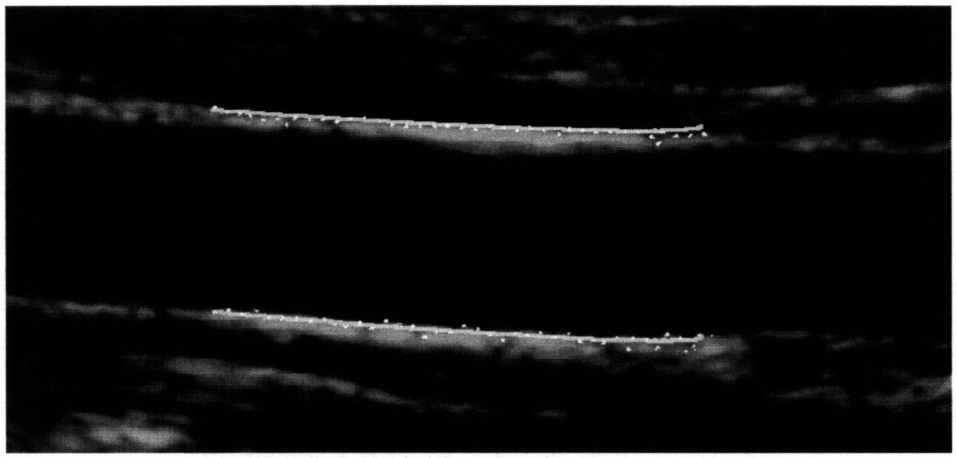

Figure 3-5: A demonstration of the second step of the automated edge-detection process. Each point of the near wall and far wall splines is adjusted to the location of the best edge. A model of the arterial representation in the image, a pair of parabolas in this case, is then applied to the edge points using a weighted least-square error approach. The arterial diameter is then estimated from the model fit.

edge points with image coordinates (x_{ni}, y_{ni}), $i = 1, \ldots, N_n$ and the N_f far edge points with image coordinates (x_{fj}, y_{fj}), $j = 1, \ldots, N_f$ should satisfy the system of equations for a pair of parabolas:

$$\begin{aligned} y_{ni} &= ax_{ni}^2 + b_n x_{ni} + c_n, \quad i = 1, \ldots, N_n \\ y_{fj} &= ax_{fj}^2 + b_f x_{fj} + c_f, \quad j = 1, \ldots, N_f. \end{aligned} \tag{3.2}$$

Thus, the curvature parameter a is associated with both sets of edge points but the parameters b and c (which determine the vertex of the parabola) are independent for the near and far wall edge points. This model does not constrain the two walls to a parallel course but good images will always produce nearly parallel results. For convenience, the overall system of equations for all data points can be represented by $\underline{y} = \mathbf{C}\underline{\theta}$ where

$$\underline{y} = \begin{pmatrix} y_{n1} \\ y_{n2} \\ \vdots \\ y_{nN_n} \\ \hline y_{f1} \\ \vdots \\ y_{fN_f} \end{pmatrix}, \qquad \mathbf{C} = \left(\begin{array}{ccccc} x_{n1}^2 & x_{n1} & 0 & 1 & 0 \\ x_{n2}^2 & x_{n2} & 0 & 1 & 0 \\ \vdots & \vdots & \vdots & \vdots & \vdots \\ x_{nN_n}^2 & x_{nN_n} & 0 & 1 & 0 \\ \hline x_{f1}^2 & 0 & x_{f1} & 0 & 1 \\ \vdots & \vdots & \vdots & \vdots & \vdots \\ x_{fN_f}^2 & 0 & x_{fN_f} & 0 & 1 \end{array}\right),$$

and $\underline{\theta}$ is the model parameter vector, $\underline{\theta} = [a\ b_n\ b_f\ c_n\ c_f]^T$ (^{T} signifies transpose). The system of equations (2) is generally inconsistent so $\underline{\theta}$ must be solved for in a least-squares sense. The standard weighted least squares formula [156]

$$\hat{\underline{\theta}} = \left(\mathbf{C}^T\mathbf{W}\mathbf{C}\right)^{-1}\mathbf{C}^T\mathbf{W}\underline{y}, \tag{3.3}$$

can therefore be used to fit the model to the edge points. The diagonal weighting

matrix **W** contains the squares of the weighted sums of the image intensity derivatives, i.e. $\left[\left(I'(l) + \frac{I'(l)_{max}}{I''(l)_{max}} I''(l)\right)_{max}\right]^2$, of the edge points. The weights represent the "strength" of the edges. Thus, weaker edge points contribute less to the model fit. Finally, the diameter estimate is obtained by averaging the distances between the parabolas in many locations because no simple geometrical distance relationship between the two parabolas is available.

For straight sections of arteries with normal anatomy imaged in the skew plane, the arterial representation is expected to be elliptical. The general conic section is represented by

$$ax^2 + bxy + cy^2 + dx + ey + f = 0, \tag{3.4}$$

where, for ellipses, $b^2 - 4ac < 0$. The parameters of the conic section must be normalized or otherwise constrained in order for Equation 4 to be uniquely solved. Bookstein [19] has solved the problem of fitting a conic section to scattered data points in a manner that is invariant to the equiform group of transformations of the Euclidean plane: rotations, translations, and changes of scale of the data points. The method minimized the sum of the squared error subject to the constraint $a^2 + \frac{1}{2}b + c^2 = 2$. He also proved that the scatter points do not contribute equally to minimum mean-square solutions to Equation 4. For example, scatter points near the minor axis of an ellipse were more heavily weighted than scatter points near the major axis. Safee-Rad et al. [135] proposed a solution that normalized the contributions of the scatter points. For our application, we preferred that the edge points near the minor axis of the ellipse contribute more to the model fit than other edge points because these points represent the strong, specular echoes at the center of the artery.

A simplified algorithm, but one whose results are not invariant to the Euclidian group is obtained by the constraint $f \equiv 1$ (i.e. normalization with respect to f). The x and y coordinates of the edge points should then satisfy the following system of

equations:

$$ax_{ni}^2 + bx_{ni}y_{ni} + cy_{ni}^2 + dx_{ni} + ey_{ni} = -1, \quad i = 1, \ldots, N_n$$
$$ax_{fj}^2 + bx_{fj}y_{fj} + cy_{fj}^2 + dx_{fj} + ey_{fj} = -1, \quad j = 1, \ldots, N_f. \tag{3.5}$$

For convenience, the equations for all of the data points can be represented in the form $\mathbf{C}\underline{\theta} = \underline{-1}$ where

$$\mathbf{C} = \begin{pmatrix} x_{n1}^2 & x_{n1}y_{n1} & y_{n1}^2 & x_{n1} & y_{n1} \\ \vdots & \vdots & \vdots & \vdots & \vdots \\ x_{nN_n}^2 & x_{nN_n}y_{nN_n} & y_{nN_n}^2 & x_{nN_n} & y_{nN_n} \\ \hline x_{f1}^2 & x_{f1}y_{f1} & y_{f1}^2 & x_{f1} & y_{f1} \\ \vdots & \vdots & \vdots & \vdots & \vdots \\ x_{fN_f}^2 & x_{fN_f}y_{fN_f} & y_{fN_f}^2 & x_{fN_f} & y_{fN_f} \end{pmatrix}, \quad \underline{\theta} = \begin{pmatrix} a \\ b \\ c \\ d \\ e \end{pmatrix},$$

and $\underline{-1}$ is a $N_n + N_f$ column vector. This system of equations is also generally inconsistent and estimates of $\underline{\theta}$ ($\underline{\hat{\theta}}$) are obtained in a weighted least squares sense from Equation 3 (by replacing $\underline{y}$ with $\underline{-1}$). The diameter estimate (the minor axis of the ellipse) is then obtained from the vector of parameter estimates as

$$D = 2\sqrt{\left(\frac{2(1-F_s)}{\hat{b}^2 - 4\hat{a}\hat{c}}\right)\left((\hat{c}+\hat{a}) - \sqrt{(\hat{c}-\hat{a})^2 + \hat{b}^2}\right)}, \tag{3.6}$$

where

$$F_s = \frac{\hat{b}\hat{d}\hat{e} - \hat{a}\hat{e}^2 - \hat{c}\hat{d}^2}{\hat{b}^2 - 4\hat{a}\hat{c}}. \tag{3.7}$$

On a typical diameter measurement from a B-mode image using a skew imaging plane, the Bookstein algorithm and the simplified algorithm above produce diameter estimates that differ by no more than 0.05%. The difference in estimates of 0.05% is a small discrepancy compared to the anticipated accuracy of the diameter measurement ($\sim$ 1%). Therefore, the simple algorithm is preferred.

3.1.2 Implementation

The parabola and ellipse diameter estimation algorithms were incorporated into a system for arterial diameter measurement and tracking from B-mode images. A Hewlett Packard SONOS 100 scanner with a 10 MHz transducer was used to acquire B-mode images. The video output of the SONOS was interfaced to a personal computer with a Data Translation DT-55LC frame-grabber card (Data Translation, Marlboro, Massachusetts) which captured NTSC frames directly from the ultrasonic imager or from super VHS video at a resolution of 640 by 480 pixels and a 256 element gray scale. Custom software then applied the edge detection and model-based diameter estimation techniques to the images.

By continuously acquiring end-diastolic (electrocardiogram-gated) B-mode images, this system was also used to track changes in arterial diameter. The parabola or ellipse model was applied to each image in the time series. The locations of the user-defined preliminary edge points were reused when appropriate. The preliminary edge points were moved as a group if the artery moved translationally in the image.

3.1.3 Performance Assessment

The performance of instantaneous diameter and diameter-tracking measurements from B-mode images was assessed by empirical measurements of the bias and variance of the estimators. Bias measurements were conducted on a phantom consisting of a solid block of plexiglass with a 5.06 mm lumen, filled with physiological saline solution. Plexiglas was chosen because it is sonoluminescent and saline solution was chosen because its acoustic propagation velocity is similar to that of blood (1520 to 1530 m/s for 5% saline compared to 1540 to 1560 m/s for whole blood; [72]. Bias measurements of the caliper and parabolic model estimators were conducted on 10 longitudinal B-mode images of the phantom. Parabolic and elliptical model bias measurements were also conducted from 10 skew (10° off-center) B-mode images. Each

type of diameter measurement was repeated 10 times by the same observer and the average value of the 10 measurements on the 10 images was determined as an estimate of the bias.

Variance was measured from in-vivo B-mode images of the brachial artery. To measure the "spatial variance" (i.e., the variance due to independent, repeated measurements on the same image), a total of 10 longitudinal and 10 skew images of the brachial artery were acquired from 10 different subjects. The images were randomly presented to a blinded observer who measured the diameter in longitudinal planes via the caliper and parabolic model methods, and in skew planes via the parabolic and elliptical models. The measurements were repeated 10 times on each image. The observer was blinded to previous results and was unaware of the purpose of the study. The sample variance of the 10 measurements on each image was computed. The average sample variance over the 10 images for each type of measurement was determined as an estimate of the spatial variance.

The "temporal variance" (i.e., the variance due to the use of identical preliminary edge points on a time series of electrocardiogram-gated images) was measured by acquiring a time series of 15 images over 28 seconds (one image every 2 seconds) in both the skew and longitudinal planes from each of 20 resting subjects. Because the subjects were resting, the arterial diameter was expected to remain constant throughout the 28 second measurement. The ultrasonic transducer was hand-held. As mentioned above, the user-defined preliminary edge points for the first image in each series were reused for each successive image. The sample variance over the 15 images in the series was calculated and was averaged over the 20 subjects for each method to estimate the temporal variance. The caliper method was not included in this study.

To validate the theoretical relationship between the angle of the skew image and the amount of available arterial wall information (Equation 1), empirical measurements were conducted on the plexiglass phantom. B-mode images of the phantom

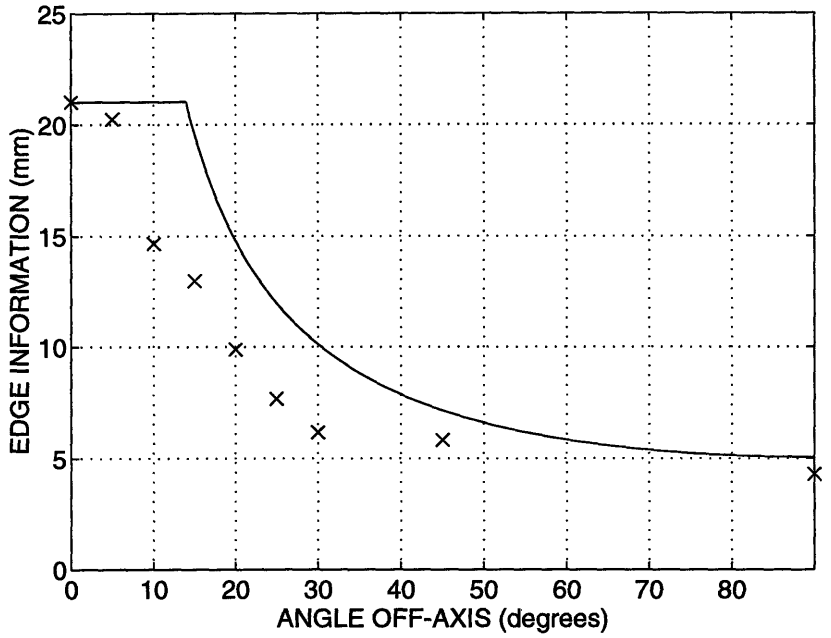

Figure 3-6: The theoretical (-) and measured (x) dependence of available arterial edge information on the angle of rotation of the skew image off-axis of the artery. The ordinate of the curve depends on the transducer and the diameter of the artery but the general shape of the curve is invariant.

were acquired at various angles of rotation off-center. The average length of the available echoes from the near and far walls was measured to quantify the available edge information.

3.2 RESULTS

Table 1 contains the results of the performance assessment of the measurement algorithms. The bias measurements are listed in column 3. All of the biases are less than 100 μm. The measurements of spatial variance are listed in column 4. The spatial variance of the caliper method is twice as large as that of the elliptical method and five times as large as either of the parabolic methods. Column 5 contains the temporal variance results, which are similar to the spatial variance results. Figure 3-6 compares the theoretical (cf. Equation 1) and empirical dependence of edge information on image angle.

3.3 DISCUSSION

3.3.1 Estimator Performance Comparisons

All of the biases in the third column of Table 1 are less than 100 μm, and are all within 50 μm of each other. Bias is relatively unimportant for the measurement of changes in diameter. Therefore, these biases are insignificant for EDV or arterial distensibility measurements.

From the variance measurements in the fourth and fifth columns of Table 1, we can conclude that the parabolic model-based diameter estimator has the best performance. The large spatial variance of the caliper method reflects its minimal utilization of arterial wall information. The relatively poor performance of the elliptical model in the skew plane is consistent with visual interpretation of model performance. As demonstrated by Figure 3-3, the empirical representation of the brachial artery in the skew plane is typically not elliptical.

The temporal variances in diameter (Column 5) were similar to the spatial variances in diameter (Column 4). This result suggests that reusing the initial preliminary edge points in a time series of images reduces the temporal variance. The variability of the true diameter in a time series of gated images in a resting subject should result in a greater sample variance than that of repeated measurements of the same image. By reusing the preliminary edge points, this effect may be reduced.

The variance results of Table 1 were measured entirely on the brachial artery. In our experience, skew planes of the brachial artery do not have an elliptical appearance. The best conic section fit to data from the brachial artery was often a hyperbola (i.e. $b^2 - 4ac > 0$). In these cases, the preliminary edge points were reselected. The elliptical model may be more appropriate for other arteries such as the carotid. In general, the human eye is an excellent judge of model fit for a given image.

3.3.2 Imaging Planes

The quantitative comparisons in Table 1 demonstrate equivalent performances for the parabolic model in the skew and longitudinal planes. These comparisons are for single images or for a time series of images in resting subjects (i.e. limited motion). In our experience with EDV measurements, the application of noninvasive stimuli such as reactive hyperemia often results in large translational motions of the artery. This type of motion is difficult to elicit in a reproducible fashion for quantitative comparisons of the imaging planes. However, the diameter estimates from the skew plane are theoretically less sensitive to translational motions of the artery. Also, the skew plane facilitates feedback of translational motions of the artery. In the longitudinal plane, motions of the artery orthogonal to the plane are ambiguous, thereby impeding compensatory motions by the operator. Translational motions of the artery in the skew plane are unambiguous. In reality, true longitudinal planes like that shown in Figure 3-1 are difficult to achieve but ultrasound operators should be cognizant of the potential for bias associated with longitudinal planes. In the measurements in our laboratory, we search for the best longitudinal plane, then rotate about 10° off axis. Figure 3-6 suggests that large rotations are detrimental to the estimator performance. The ordinate of Figure 3-6 depends upon the transducer and the diameter of the artery, but the general shape of the curve is invariant. The empirical edge information is less than the theoretical because the entire length of the arterial cross section does not produce strong echoes.

3.3.3 Resolution

B-mode resolution is an important issue for diameter measurements. The resolution of the image increases with higher frequencies and bandwidths of insonation, but the penetration depth decreases. Higher energy pulses can be used to increase the penetration, but safety standards and finite-amplitude effects will eventually dictate

the available resolution for a given imaging situation. A common resolution pitfall occurs with measurements made from paused NTSC, PAL, or SECAM video cassette recorders (VCRs). For these standards, each frame is composed of two fields, which are stored sequentially on the tape. When the VCR is paused, the head stops on a single field, thus presenting a frame composed of duplicate fields. Therefore, any measurement made on a paused image has half of the available resolution in the vertical direction. Fortunately, most modern ultrasound systems contain the equivalent of a frame-grabber which digitizes both fields of a frame before pausing the VCR. If this feature is not available, the image can be digitized with an external frame-grabber while the VCR is playing or a VCR with a digital frame memory (such as the Panasonic AG-7355) can be used. In general, the best method is to avoid entirely measurements from a VCR as the analog storage will result in image degradation.

3.4 CONCLUSIONS

We have proposed improvements to the two fundamental determinants of B-mode diameter-measurement accuracy: image selection and the diameter estimation algorithm. The skew imaging plane was introduced as an alternative to the common longitudinal imaging plane. The accuracy of diameter tracking measurements from these two planes was shown to be equivalent in studies with limited translational motion of the artery. However, the skew plane is theoretically less sensitive to translational motions of the artery and it facilitates compensatory motions by the ultrasound operator through its unambiguous representation of translational arterial motions. The theoretical and empirical relationships between the angle of rotation of the skew plane and the performance of diameter estimators mandate small angles of rotation for best performance. Two new algorithms for diameter estimation were developed. The parabolic model-based diameter estimate outperformed the elliptical model-based diameter estimate and standard caliper estimates.

Table 2-1: Performance of B-mode diameter estimators.

PLANE	METHOD	BIAS*	SPATIAL VAR.†‡	TEMPORAL VAR.§†
LONG.	CALIPER	92 μm	0.0139 mm^2	—
LONG.	PARABOLIC	64 μm	0.0028 mm^2	0.0032 mm^2
SKEW	PARABOLIC	41 μm	0.0027 mm^2	0.0032 mm^2
SKEW	ELLIPTICAL	52 μm	0.0072 mm^2	0.0045 mm^2

* Bias measurements were conducted on a 5.06 mm cylindrical plexiglass phantom filled with physiological saline.
† Variance measurements were conducted on B-mode images of the brachial artery.
‡ "Spatial Variance" refers to measurements with independently-chosen preliminary edge points on the same image.
§ "Temporal Variance" refers to measurements on a time series of images using equivalent preliminary edge points.

Chapter 4

Methods III: Measurement of Vasoreactivity After Temporary Forearm Ischemia

In Chapter 3, we defined new methods for measurement of arterial diameter from B-mode images. The work was motivated by that of Celermajer et al. [29], who described a simple and convenient method for noninvasive measurement of peripheral artery vasoreactivity and used the method to demonstrate abnormal vasoreactivity in groups of subjects with atherosclerosis or risk factors for the disease [29, 30, 31, 32, 68, 150]. This method involved caliper-based measurements of arterial diameter at two times: before and after release of a 5-minute forearm vascular occlusion. Our immediate goal is to incorporate the new methods from Chapter 3 into a system for measuring the temporal behavior of peripheral arterial vasoreactivity, thus enabling us for the first time to characterize the normal vascular response to temporary forearm ischemia, and eventually allowing us to describe specific abnormalities in vasoreactivity associated with atherosclerosis and its risk factors.

In this Chapter, we describe a system that is capable of simultaneously obtaining high resolution measurements over time of microvascular (resistance arteriole)

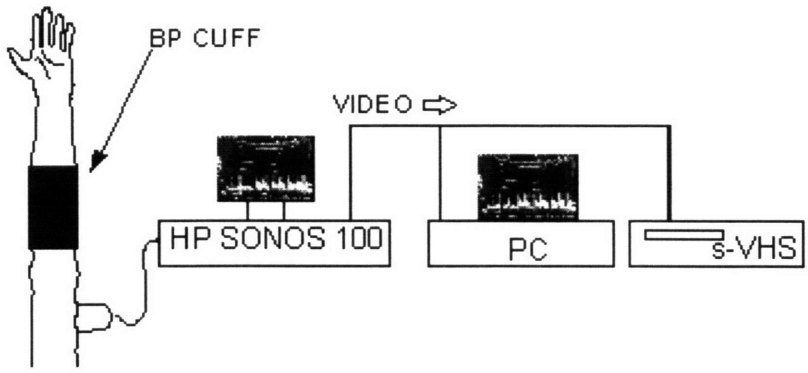

Figure 4-1: A schematic diagram of the vasoreactivity measurement system. A blood pressure cuff is placed around the forearm, distal to the antecubital fossa, and inflated to 200mmHg for 5 minutes. B-mode images are digitized directly from the video output of the ultrasound system and are also stored on super-VHS videotape for archiving.

and conduit artery vasoreactivity. The time series measurements allow extraction of multiple parameters of vasoreactivity. We characterize normal vasoreactivity after temporary forearm ischemia, determine the normal values of vasoreactivity parameters, and estimate the reproducibility of these parameters.

4.1 METHODS

4.1.1 Measurement Technique

A Hewlett-Packard SONOS 100 duplex ultrasound imaging system was used to measure brachial arterial diameter with a 10 MHz, mechanical-scanning transducer, and brachial blood flow velocity with a 3.5 MHz transducer (Figure 4-1). The brachial artery was insonated in a duplex mode which acquired B-mode images at every other R-wave of the electrocardiogram (i.e., end diastole) and standard pulsed Doppler

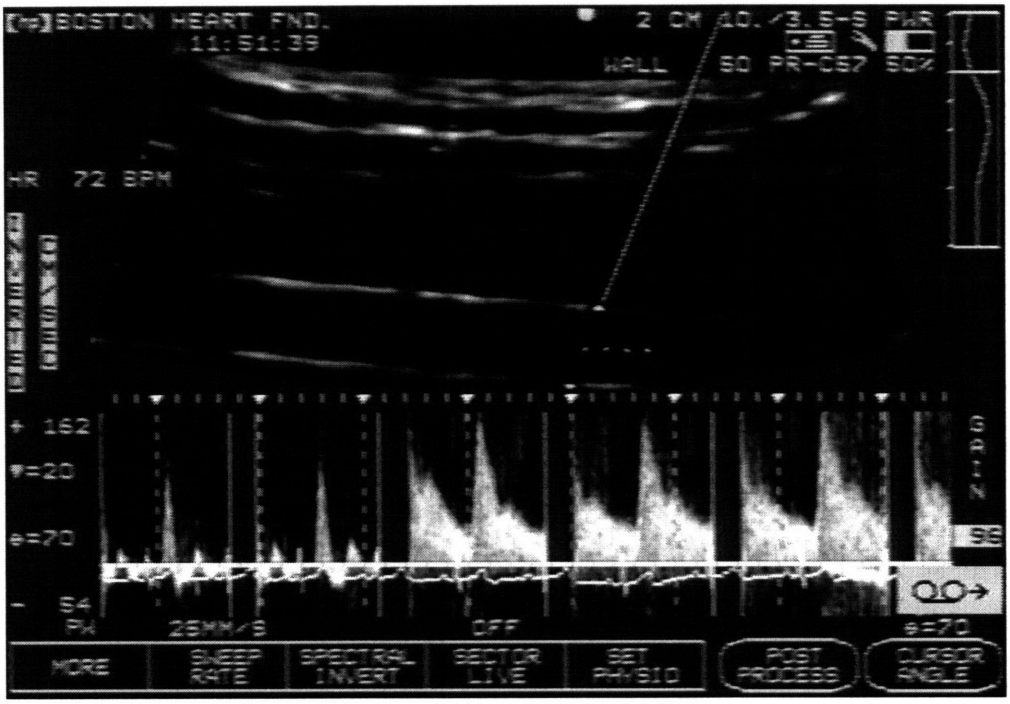

Figure 4-2: An example of the duplex imaging mode, demonstrating an end-diastolic, B-mode image of the brachial artery and pulsed-Doppler measurement of arterial flow velocity. The flow velocity tracing demonstrates the onset of reactive hyperemia after release of a 5-minute forearm vascular occlusion. Flow velocity and B-mode images are acquired during alternate cardiac cycles.

blood flow data between B-mode images. All images were digitized directly from the video output of the SONOS by a frame grabber (Data Translation DT55-LC) at a resolution of 640 by 480 pixels and 256 shades of gray, and were stored on a 80486-based personal computer. The images were also stored on super-VHS videotape for archiving.

Subjects remained seated during the measurements and rested for at least 5 minutes with an uninflated blood pressure cuff around the forearm, prior to initiation of the study (Figure 4-1). The diameter and flow velocity of the brachial artery were then measured 5-10 cm proximal to the antecubital fossa to establish baseline values. Next, the forearm cuff was inflated to 200 mmHg or 50 mmHg above the measured

systolic pressure, whichever was greater, for the desired duration. Brachial image acquisition and flow velocity measurement, at the same location as at baseline, began approximately 15 seconds prior to release of the cuff and continued for 100-180 seconds afterwards. Images of the artery were acquired in skew planes (i.e., planes rotated about 10° off center of the arterial axis). An example of the duplex imaging mode, showing the skew imaging plane and the increase in flow velocity after release of the cuff is shown in Figure 4-2. In Chapter 3, we showed that the skew plane for arterial diameter measurements was superior to the more common longitudinal (long axis) plane because diameter estimates from the skew plane are less sensitive to translational motions of the artery. Also, unintentional motions of the transducer or the subject are readily detected in the skew image, making correction easier.

The arterial diameter was measured from the B-mode images with a parabolic model-based estimation algorithm as described in Chapter 3 and in [152]. The diameter was measured from each end-diastolic image in the time series to determine the temporal behavior of the arterial diameter. The corresponding arterial flow velocities were measured from the video archive, by averaging the maximum flow velocities throughout a cardiac cycle.

4.1.2 Subjects

Measurements of post-ischemic hyperemia and brachial artery diameter were acquired from a total of 31 subjects, 14 females and 17 males, of average age 37.6 $\pm$ 2.4 years (mean $\pm$ SEM). None of the subjects had overt cardiovascular disease. Risk factors for atherosclerosis were not determined; the subjects were intended to represent the general population without significant atherosclerosis. None of the subjects were smokers or were taking vasoactive drugs, such as beta blockers, calcium channel blockers, nitrates, or ACE inhibitors. Caffeine was prohibited for four hours prior to the measurements. All subjects gave informed consent and the study was approved by the M.I.T. Committee on the Use of Humans as Experimental Subjects.

4.1.3 Vasoreactivity Measurements

1.) Initially, two measurements of hyperemic response and arterial diameter were conducted on each of 16 subjects (7 females and 9 males, average age 31.2 ± 2.7 years). The forearm occlusion times for these measurements varied from 5 to 5.5 minutes and the second measurement on each subject was acquired between 1 and 47 days (mean 13 days) after the first measurement. From the resulting diameter and flow-velocity data, physiological parameters were extracted to determine their variability. The parameters included the maximum increase in flow velocity after the release of the cuff, representing the stimulus for flow-mediated dilation, the half-time of decay of the hyperemic response ($t_{1/2}$), the time of onset of brachial artery vasodilation after release of the cuff (t_0), the maximum and mean brachial artery diameter change (ΔD), and the time to maximum diameter change (t_D), all representing the arterial response to increased flow. The parameters were extracted by an automated algorithm which first smoothed the diameter time series with a lowpass filter.

2.) Because there was considerable variability in repeated measurements of the response parameters, we conducted additional measurements to determine the variability of the response under identical stimuli. The measurements included: a.) two measurements made on different days on each of 11 subjects, with identical occlusion conditions, to determine the variability of the hyperemic response and b.) acquisition of two measurements on different days from each of 11 subjects, with similar peak hyperemic responses, to determine the variability of $t_{1/2}, t_0$, the maximum and mean ΔD, and t_D.

3.) From a total of 101 measurements on 31 subjects (including both of the above groups), the three measurements (from different subjects) which demonstrated the largest percent brachial artery dilation were averaged. Similarly, the three measurements which demonstrated the smallest percent arterial dilation were averaged. These averages were then contrasted to explore the two extremes in vasoreactivity.

4.) To investigate the effects of rapidly repeated cuff inflation, measurements of

hyperemic responses and changes in brachial artery diameter were repeated with an interval of only 10 minutes between the release of the first 5-minute occlusion and the onset of the second 5-minute occlusion, in 6 subjects. All of the cuff inflations were completed (i.e., circulation was stopped) within 2 seconds. The skin temperature of the palm and the antecubital fossa (ACF) was measured before each occlusion by an infrared pyrometer (Omega OS-613, Stamford, Connecticut).

5.) The influence of the rate of occlusion (i.e., the time between venous and arterial occlusion) and the temperature of the forearm on the hyperemic response was also studied in the same 6 subjects. To study the influence of the rate of occlusion, two measurements of hyperemic response were conducted on each subject with a 10 minute interval between the end of the first 5-minute occlusion and the beginning of the second 5-minute occlusion. The first cuff inflation was completed within 2 seconds while the second inflation included an initial 10 second period at 50 mmHg cuff pressure before the cuff was inflated to 200 mmHg. To study the influence of forearm temperature on the hyperemia, measurements were repeated after a 15-minute interval, during which the forearm (not including the palm or the ACF) was warmed with a heating pad. Cuff inflation for this temperature study was rapid (within 2 seconds) and was maintained for 5 minutes. The skin temperature of the palm and ACF was determined before each of these measurements by the infrared pyrometer.

6.) To determine the effects of reactive hyperemia on skin temperature, the temperature of the palm and ACF was measured before, and 3 minutes after, a 5-minute cuff occlusion for a total of 42 measurements of hyperemic response in 10 subjects. The mean results for each subject were then averaged so that each of the 10 subjects contributed equally to the overall mean.

7.) Finally, because changes in arterial diameter may have resulted from changes in arterial pressure, the latter was monitored from 10 seconds before to 80 seconds after the release of 5-minute occlusions. A total of 35 measurements on 15 subjects

were conducted with a Finapres photoplethysmograph (Ohmeda, Louisville, Colorado, [176]) to measure the blood pressure in the index finger of the contralateral arm. During the measurements, the subjects were seated and remained motionless, with the involved index finger located at the level of the heart. The blood pressure signal from the Finapres was digitized at 500 samples per second and 12 bits of resolution, and stored on a personal computer. Custom software was used to demarcate the cardiac cycles and compute the mean blood pressure for each cycle in each measurement. The mean results for each subject were averaged so that each of the 15 subjects contributed equally to the overall mean.

4.2 RESULTS

1.) An example measurement of the forearm microvascular and brachial artery response to temporary forearm ischemia is presented in Figure 4-3. The mean and the SEM of the measurements from 16 subjects are presented in Figure 4-4. For this figure, the diameters were normalized by the pre-release values before they were averaged. The mean diameter decreased by approximately 1.5% during the first 20 seconds after release of the occlusion, then increased over the range of 20 to 60 seconds post-release and peaked at approximately 6.5% dilation. The mean flow velocity in the brachial artery before the forearm occlusion was 29.8 cm/sec. During occlusion, the mean flow velocity decreased to 13.9 cm/sec, or 47% of the pre-occlusion velocity. After release of the occlusion, the velocity rapidly increased and peaked at 12 seconds post-release at a maximum of 135.3 cm/sec, or 454% of the pre-occlusion flow, then returned to pre-occlusion values in an exponential fashion. The second column of Table 4-1 contains the mean response parameters for these measurements. Because the percent flow-mediated dilation of an artery is known to be inversely proportional to the baseline diameter [5, 29, 32], both the absolute dilation and the percent dilation are reported. Since the time course of the vasoactive response varied among subjects,

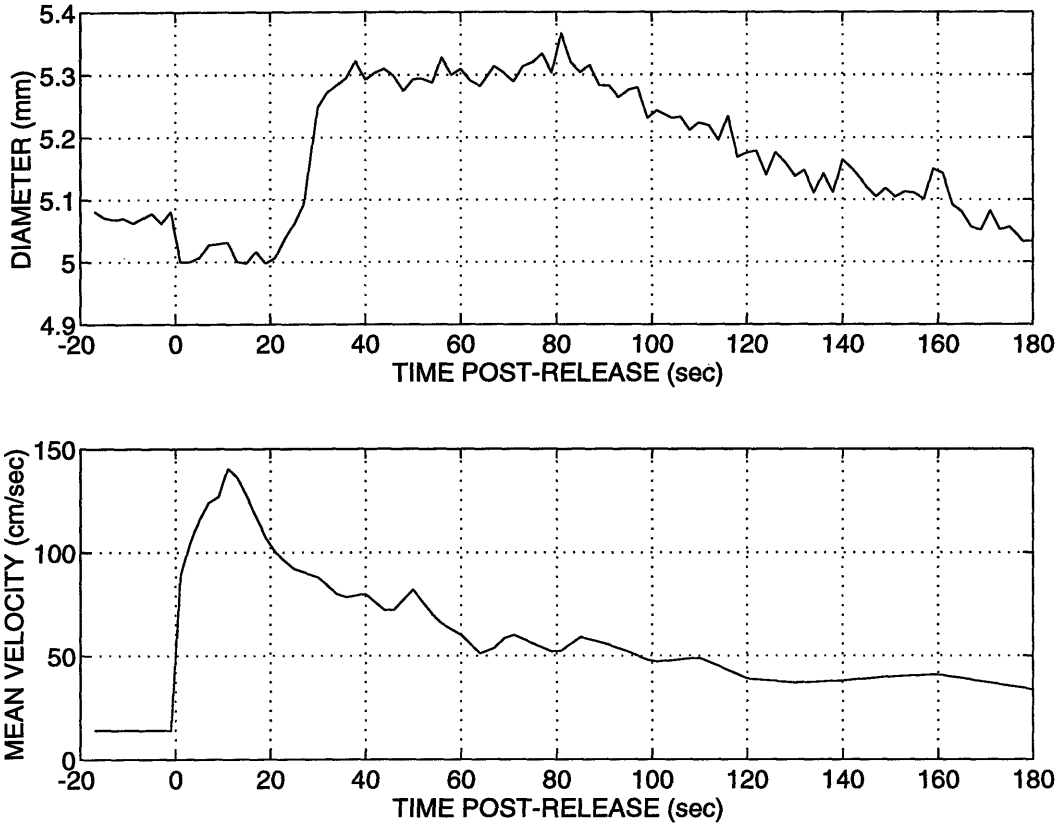

Figure 4-3: The response of the brachial artery to reactive hyperemia induced by a five minute occlusion of the forearm. The diameter was measured from end-diastolic B-mode images acquired in the skew plane using the parabola model. The flow was measured by standard pulse Doppler, and averaged over each cardiac cycle. The increased arterial wall shear stress results in a dilation of about 0.25 mm which persists for 2 minutes.

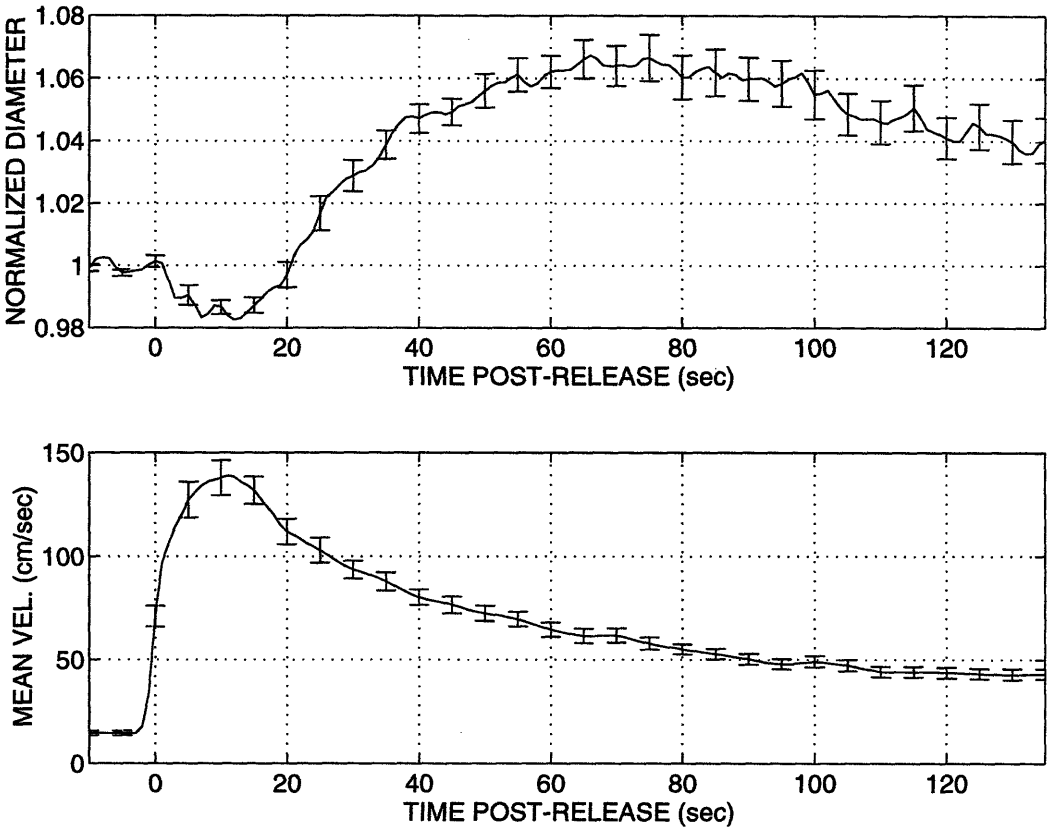

Figure 4-4: The mean and SEM of 32 measurements of brachial artery diameter and hyperemia from 16 subjects. The forearm vascular occlusion was released at time zero. **Top:** The mean of the normalized diameter measurements, representing the conduit artery vasoreactivity. **Bottom:** The mean flow velocity, which is related to microvascular vasoreactivity and comprises the stimulus for conduit artery vasoreactivity.

the mean of parameters from individual measurements in Table 4-1 is not equal to the parameters of the mean measurement shown in Figure 4-4. The third column of Table 4-1 lists the standard deviation of the response parameters for measurements of the 16 subjects. For example, the standard deviation of the maximum and mean percent ΔD for individuals in this group was 3.2% and 2.9%, respectively. As a measure of the stimulus variability, the standard deviation of individual measurements of the peak increase in flow velocity after cuff release (σ_s) was 30.7 cm/sec. The peak increase in flow velocity after cuff release was typically in the range of 100 to 150 cm/sec.

2a.) In pairs of measurements acquired on separate days on 11 subjects, complete cuff occlusion was produced within 2 seconds and the two occlusion times differed by an average of only 5 seconds (range 0 to 11 seconds). Under this constrained ischemic stimulus, σ_s was 26.0 cm/sec.

2b.) In pairs of measurements acquired on separate days from a second set of 11 subjects, the peak post-release increases in flow velocity between repeat measurements were within 10% of each other. Under these conditions, σ_s was 5.9 cm/sec and the standard deviation for individual measurements of the maximum and mean percent ΔD were 1.8 and 1.7%, respectively (see Table 4-1, Column 4). For 8 of these 11 pairs, the peak post-release increases in flow velocity between repeat measurements were within 5% of each other. Under these conditions, σ_s was 3.9 cm/sec and the standard deviation of the maximum and mean ΔD was 1.2 and 1.1%, respectively (see Table 4-1, Column 5). By removing the variability of the vasoreactivity parameters that resulted from stimulus variability, a combination of the inherent variability of the parameters and the variability of the measurement technique is reported in Column 5 of Table 4-1.

3.) Insight into the range of subject variability in the response to temporary forearm ischemia was obtained by contrasting measurements with opposite extremes in brachial arterial response. Figure 4-5 contrasts the mean of measurements from 3

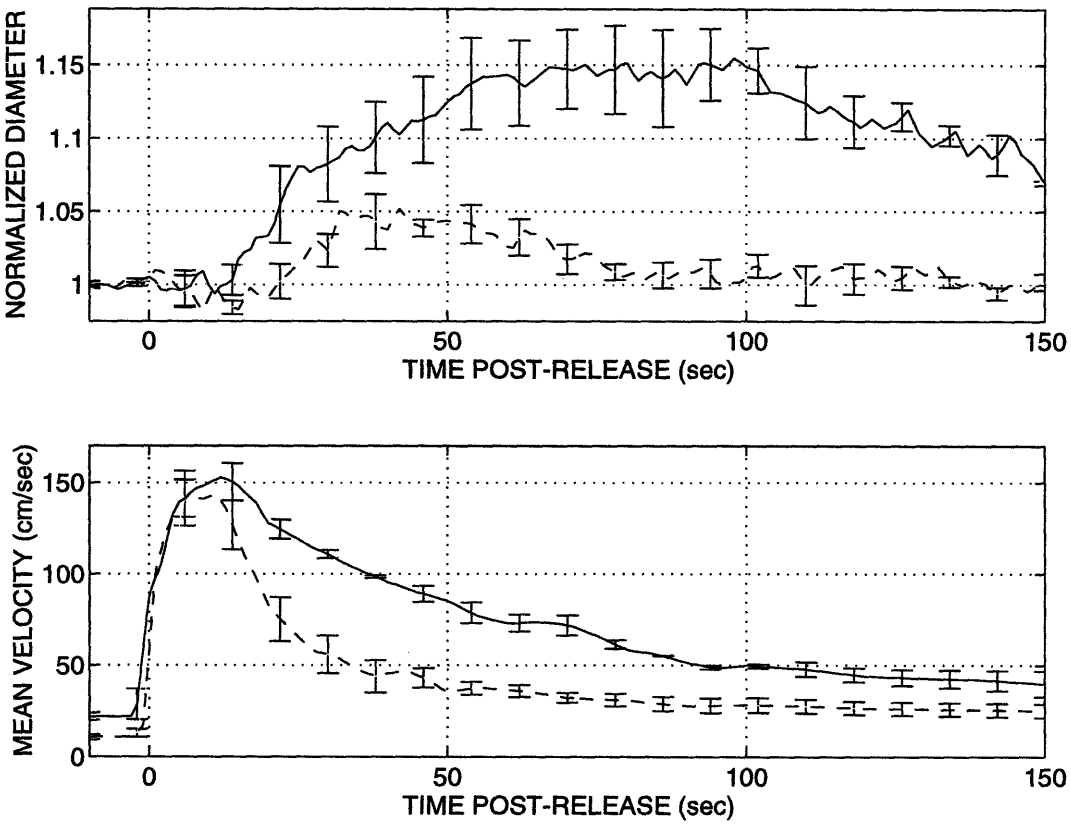

Figure 4-5: A comparison of the mean of the three measurements with the smallest post-release arterial dilation (dashed lines) with the mean of the three measurements with the largest post-release arterial dilation (solid lines). The time of onset of brachial arterial dilation, the extent and duration of dilation, and the duration of the hyperemic response are markedly different whereas the early hyperemic responses are similar. The bars indicate SEM.

subjects that demonstrated the smallest percent arterial dilation and the mean of measurements from 3 subjects that demonstrated the largest percent arterial dilation. The smallest brachial artery responses peaked at 3.8% dilation at 49 seconds post-release and returned to baseline by 80 seconds post-release. In contrast, the largest brachial artery responses peaked at 14.8% dilation at 97 seconds post-release and the vessels remained dilated for at least 3 minutes post-release. The largest responses were associated with longer duration of hyperemia; the half-time for the exponential return of the post-release flow velocity to baseline values (i.e., $t_{1/2}$) was 15.0 seconds for subjects with the smallest responses compared to 34.0 seconds for subjects with the largest responses. In addition, the subjects with the largest brachial responses exhibited earlier onset of arterial dilation, which virtually eliminated the characteristic decrease in diameter immediately after the release of the occlusion. The time of onset of dilation was independent of the magnitude of the hyperemic response for the two groups. The response parameters listed in Table 4-1 are the five parameters which best differentiate the two groups.

4.) A comparison of repeat measurements with 10 minutes between the release of the first occlusion and the onset of the second occlusion is presented in Figure 4-6. Each curve represents the mean of measurements from 6 subjects. The maximum ΔD and the peak increase in flow velocity after cuff release were significantly different in the repeat measurements ($p = 0.047$, from the Wilcoxon signed-rank test). The average palm temperature before the second occlusion was 0.5°C higher than before the first occlusion ($p = 0.031$).

5.) Figure 4-7 demonstrates the influence of the rate of occlusion and the temperature of the forearm on the degree of reactive hyperemia. Each response curve is the mean of 6 subjects. Slower onset of cuff occlusion resulted in significantly decreased hyperemic response compared with that of controls ($p = 0.031$ for the areas under the curves).

The area under the flow velocity curves and the peak post-release velocity increase were significantly greater for the warmed forearms compared with the controls ($p =$

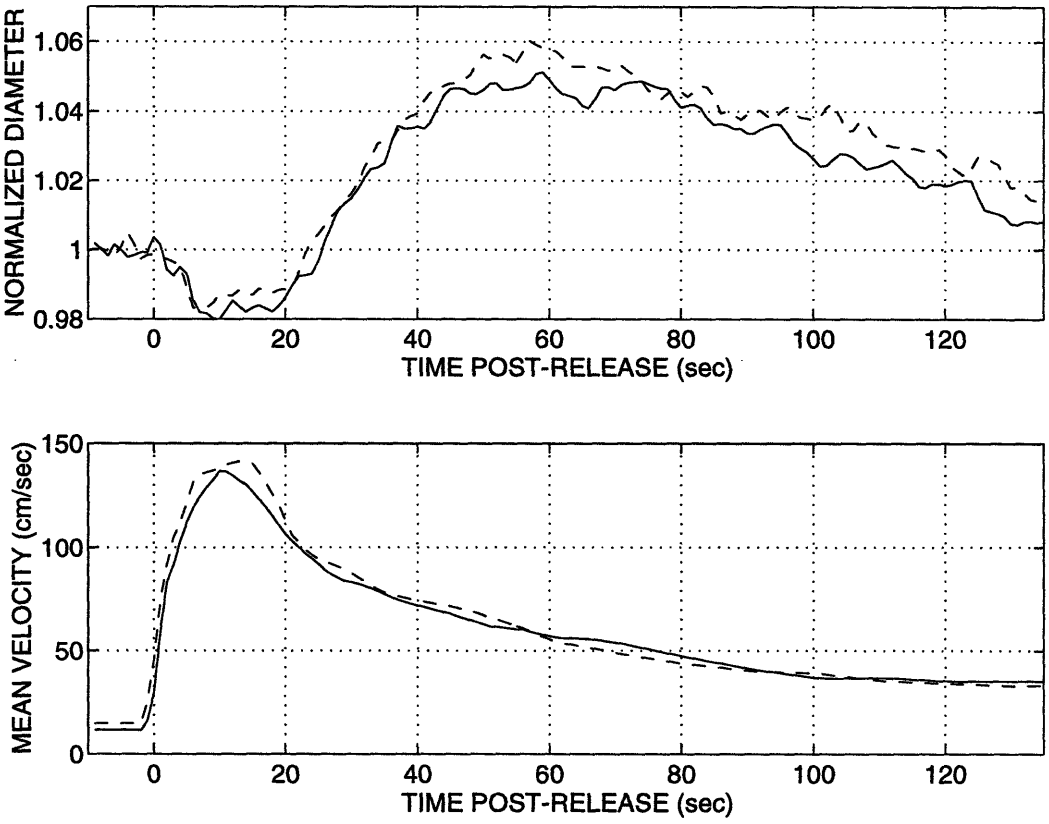

Figure 4-6: A comparison of measurements repeated with a 10 minute interval between the first cuff release and the second cuff inflation. Each response curve is the mean of 6 subjects. The second occlusion resulted in a slightly larger hyperemic response and brachial artery dilation (dashed line) than those from the first occlusion (solid line), perhaps because the mean palm temperature was 0.5°C warmer before the second cuff inflation ($p = 0.031$).

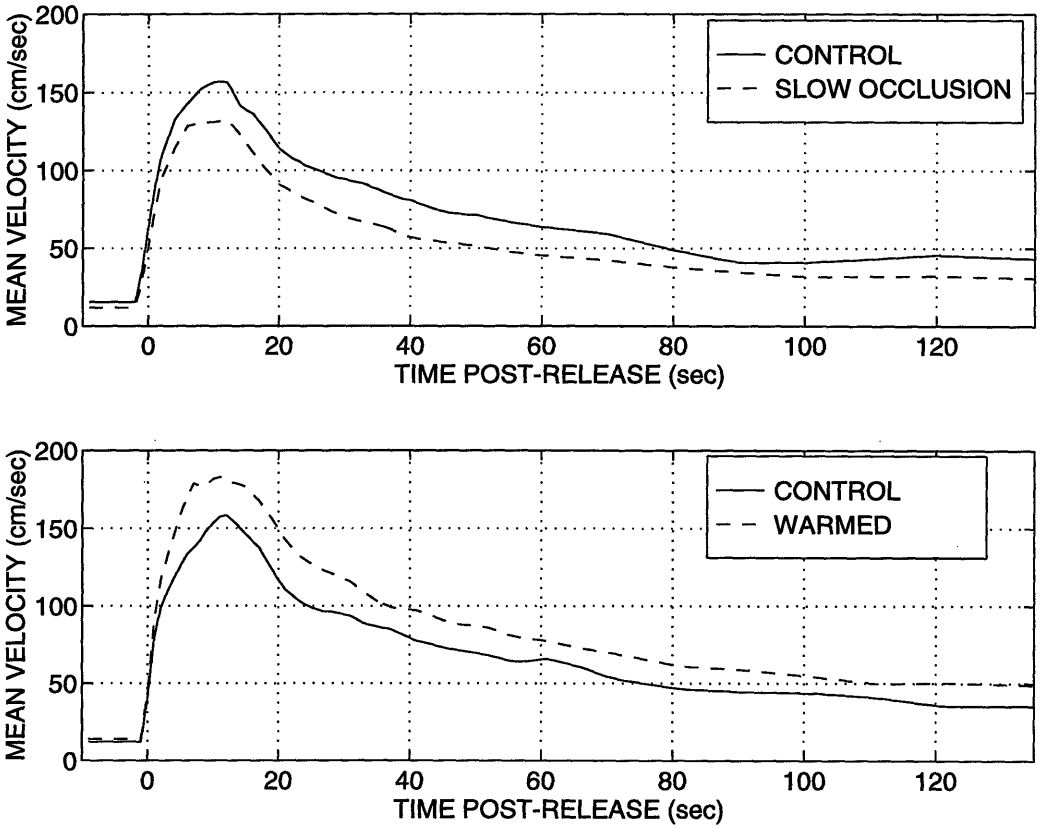

Figure 4-7: Variation in hyperemic response with change in rate of forearm vascular occlusion and forearm warming. Each curve is the mean of 6 subjects. **Top:** The solid line is the hyperemic response after 5-minute vascular occlusion which was produced within 2 seconds and the dashed line is the hyperemic response after 5-minute occlusion where the cuff pressure was held at 50 mmHg for 10 seconds during cuff inflation. The slow-onset occlusion began 10 minutes after release of the control occlusion. **Bottom:** Five-minute vascular occlusion of the warmed forearm resulted in larger peak hyperemic response (dashed line) than that of the unwarmed control (solid line). The second (warmed) occlusion began 15 minutes after the release of the control occlusion.

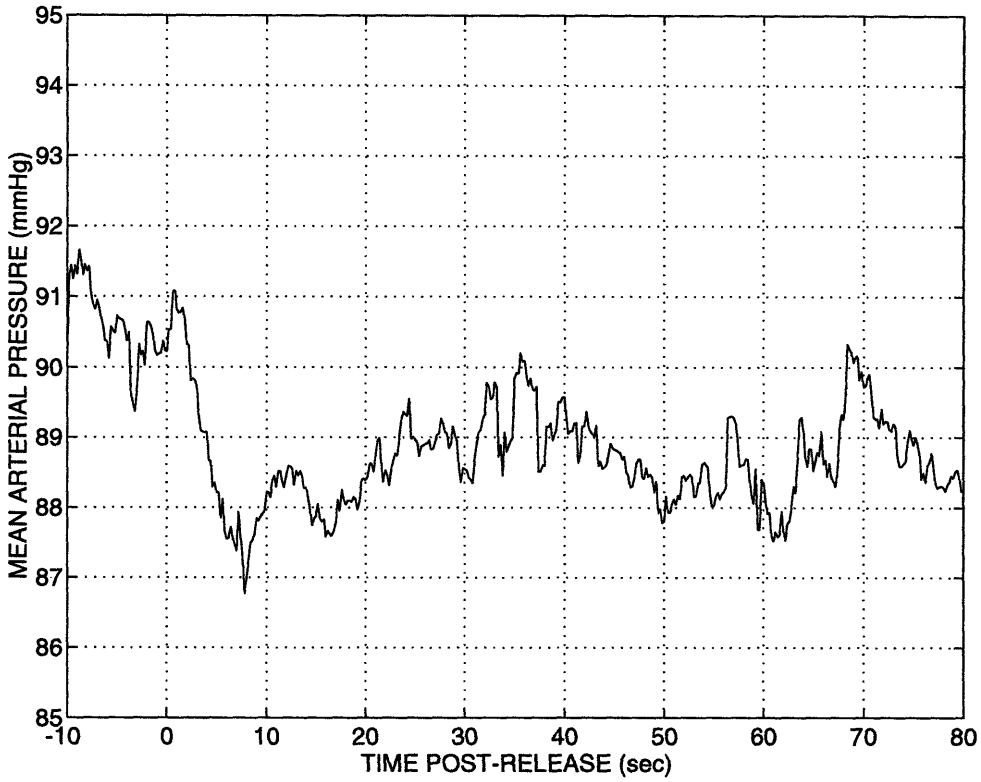

Figure 4-8: The mean arterial blood pressure of 15 subjects measured in the index finger with a photoplethysmograph. The forearm vascular occlusion of the contralateral arm was released at time zero.

0.016 for both comparisons). The average pre-occlusion flow velocity increased from 21.1 cm/sec to 36.8 cm/sec as a result of the warming ($p = 0.031$), while the average palm temperature increased by 0.95°C during the forearm warming ($p = 0.047$).

6.) The average skin temperature of the palm and ACF at three minutes post-release were 0.55°C ($p < 0.005$) and 0.16°C ($p = 0.5$) warmer than the pre-occlusion temperatures, respectively.

7.) The mean of the blood pressure measurements in the index finger of the contralateral arm is presented in Figure 4-8. The mean blood pressure pre-release was 90.6 mmHg. After cuff deflation, the mean pressure dropped by about 3 mmHg, then leveled off at approximately 88.5 mmHg. Intervention analysis [22] with a first-order autoregressive model of the mean pressure showed a significant decrease in pressure after cuff release ($p < 0.001$).

4.3 DISCUSSION

We have employed a new technique to characterize brachial artery and forearm microvascular vasoreactivity in response to temporary occlusion of the forearm vasculature. With this technique, we measured brachial flow velocity and end-diastolic diameter continuously, rather than at a few individual time points as in previous studies [8, 29, 104]. We have proposed five response parameters to quantify the observed vasoreactivity, determined the reproducibility of these parameters for measurements repeated on separate days, and examined the variability of the response with rapidly-repeated measurements.

4.3.1 Characterization of the Observed Vasoreactivity

Noninvasive measurements of flow-dependent dilation with the resolution shown in Figure 4-4 have not, to our knowledge been published. However, invasive studies in animal models have demonstrated similar behavior [63, 96, 128, 149]. In particular, Koller and Kaley [96] reported an initial decrease in arterial diameter when the blood velocity was suddenly increased in rat cremaster muscle arterioles, similar to that shown in Figures 4-4, 4-5, and 4-6. We offer three potential explanations for the initial decrease in diameter. First, Figure 4-8 demonstrates a maximum decrease in central arterial pressure of about 3 mmHg upon release of cuff occlusion. Second, the reduction of peripheral resistance in the ischemic forearm on release of the cuff results in a proximal displacement of the pressure gradient along the brachial artery. Therefore, the measured section of brachial artery experiences a reduction in intraluminal pressure after the release of the cuff. Finally, the increase in flow velocity after the release of the cuff results in an increase in the dynamic component of the arterial pressure and a decrease in the lateral component of the arterial pressure (i.e., the Bernoulli effect [13]). Koller and Kaley [96] also demonstrated a 5.8 to 15 second delay between a step increase in velocity and the initiation of dilation in rat arterioles.

Smiesko et al. [149] observed a delay averaging 7.7 seconds in rat arterioles, and Fujii et al. [63] reported an average delay of 13 seconds in the rat basilar artery. From Table 4-1, the mean delay for dilation of the brachial artery in humans is approximately 28 seconds. However, it is difficult to determine exactly when flow-mediated dilation begins because the initial decrease in diameter and the slower flow-mediated dilation response partially overlap.

After cuff release, the average arterial blood pressure drops and remains below the pre-release level during the entire period of increasing arterial diameter (Figure 4-8). This decrease in arterial pressure post-release probably decreases the conduit artery diameter and the observed arterial dilation slightly. However, the small change in arterial pressure upon cuff release is unlikely to contribute significantly to the observed diameter changes. The results of pressure measurements from other studies were similar to ours. Anderson and Mark [3] measured an average 1 mmHg decrease in pressure post-release and Joannides et al. [92] measured an average 3 mmHg decrease in pressure at the point of peak hyperemic flow and an average 1 mmHg decrease in pressure at the point of peak arterial dilation.

4.3.2 Role of NOMED in the Observed Vasoreactivity

The association between atherosclerosis and abnormal nitric-oxide-mediated endothelium-dependent dilation (NOMED) warrants an investigation of the contribution of NOMED to the observed vasoreactivity. Although this was not addressed experimentally in the present work, other laboratories have examined the contribution of NOMED to vasoreactivity comparable to that reported here. Recent studies [92, 158, 172] have established the role of NOMED in the hyperemic response to temporary ischemia. These studies demonstrated that the ratio of peak post-release blood flow to baseline blood flow was unchanged when the production of nitric oxide (NO) was inhibited. However, the studies also demonstrated a significant decrease in the effective duration of the reactive hyperemia upon inhibition of NO production. From these results, we

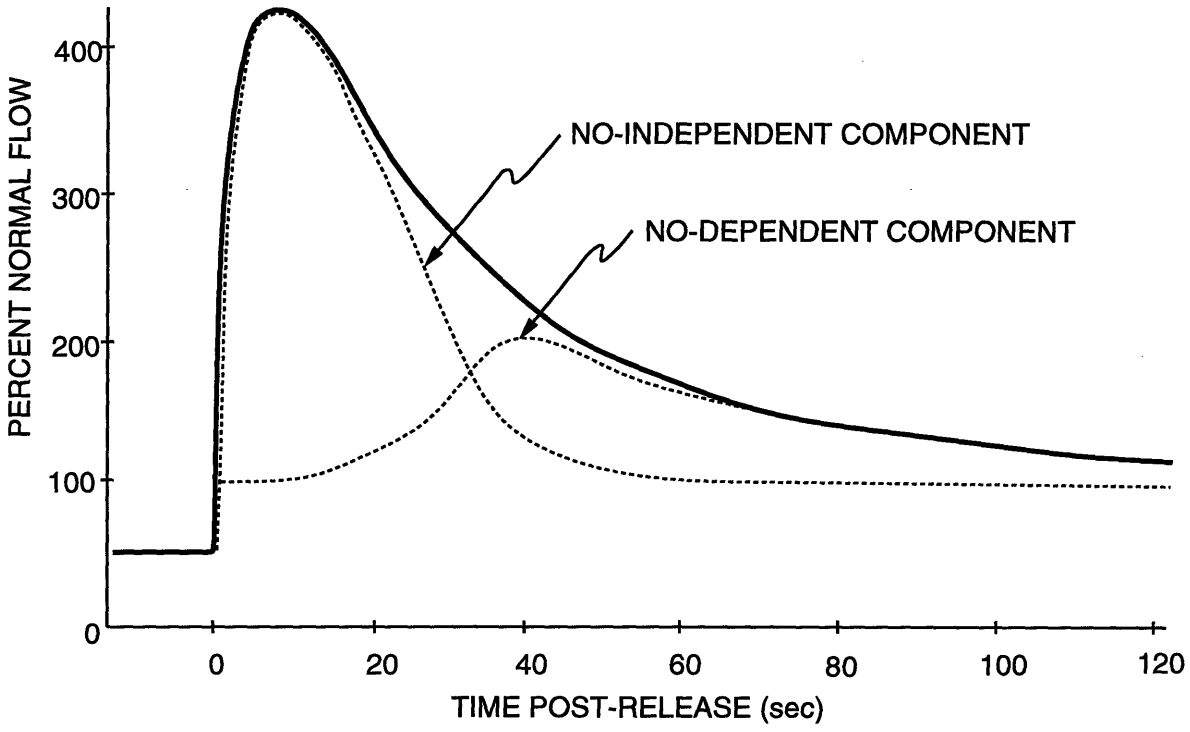

Figure 4-9: A proposed model for the separation of the reactive hyperemic response into its nitric oxide-independent and nitric oxide-dependent components (see text for details).

have constructed a model (Figure 4-9) based upon the additive effects of the NO-independent and NO-dependent components of reactive hyperemia. We hypothesize that the NO-independent, initial dilation of the resistance arterioles is due to direct relaxation of vascular smooth muscle cells by tissue hypoxia and/or by accumulation of vasodilatory metabolites such as lactate. As this stimulus for direct relaxation is rapidly removed by the early hyperemic response, the NO-independent portion of the hyperemic response is relatively brief. The NO-dependent portion of the hyperemic response, representing microvascular NOMED, occurs later and is responsible for prolonging the hyperemic response. Several studies have associated abnormalities in microvascular NOMED with atherosclerosis by demonstrating paradoxical vasoconstriction to the endothelium-dependent vasodilator acetylcholine [142, 180, 184] and abnormal microvascular flow-mediated dilation [99] in atherosclerotic humans or in animal models. The role of NOMED in the duration of post-ischemic reactive hyperemia, but not in the initial peak hyperemic response [92, 158, 172], suggests that atherosclerosis should be associated with smaller values of the half-time for decay of reactive hyperemia (i.e., our parameter $t_{1/2}$). Figure 4-5 demonstrates markedly smaller $t_{1/2}$ for subjects with less flow-mediated dilation to the ischemic stimulus.

Several authors have shown in animals [82, 96, 108, 128, 149, 179] and in humans [3, 92, 110, 147] that NOMED is responsible for changes in arterial diameter in response to changes in arterial wall shear stress. Therefore, conduit artery NOMED is expressed by the relationship between the reactive hyperemia and the conduit artery dilation. Abnormal conduit artery NOMED has been associated with atherosclerosis or risk factors for atherosclerosis [117, 168, 183]. For a given flow stimulus, subjects with atherosclerosis or risk factors for the disease demonstrate less dilation of the conduit artery (i.e., smaller maximum and mean values of ΔD). The maximum and mean ΔD represent combinations of microvascular and conduit artery NOMED because conduit artery dilation depends upon the flow stimulus, which is enhanced by microvascular NOMED. For example, the difference in the extremes of the conduit

artery dilation shown in Figure 4-5 result from both the difference in flow stimuli and the difference in conduit artery NOMED. However, despite similar flow stimuli during the early hyperemic response, the arteries with greater NOMED (Figure 4-5, solid line) dilate much earlier than the arteries with less NOMED (Figure 4-5, dashed line). Therefore, we hypothesize that conduit artery NOMED may be characterized by the time of onset of dilation (t_0), as well as by the mean and maximum ΔD for a given, standardized flow stimulus. Finally, because the shear stress-induced dilation of the conduit artery occurs via a combination of microvascular and conduit artery NOMED, the time of peak dilation (t_D) may also represent a combination of microvascular and conduit artery NOMED.

4.3.3 Application to the Assessment of Atherosclerosis

Celermajer and associates [29, 30, 31, 32, 68, 150] have devised a convenient method to study the relationship between atherosclerosis or risk factors for the disease and abnormal peripheral artery vasoreactivity. They measured the percent diameter change of the brachial or femoral arteries, relative to the pre-occlusion diameter, at 45–60 seconds after the release of a 4 to 5 minute occlusion, and reported significant differences between groups of control subjects and subjects with known coronary artery disease or risk factors for atherosclerosis. Because arterial dilation after release of cuff occlusion was measured relative to the pre-occlusion diameter in Celermajer's work, any changes in arterial diameter during occlusion were superimposed on the post-ischemic response. In this chapter, we have focused on the vasoreactivity during and after the release of the occlusion, thereby avoiding the variability introduced by the inclusion of the changes during the low-flow occlusion period.

The promising results of multiple studies [8, 29, 30, 31, 32, 68, 104, 150] warrant the development of methods for noninvasively measuring peripheral artery vasoreactivity with sufficient sensitivity and specificity to classify individual subjects. The data presented here contribute to that goal. We have measured arterial diameter

and flow velocity continuously during and after the release of cuff occlusion, thereby increasing the information content of the measurement. The accuracy of the diameter measurements was improved with the use of a model-based diameter estimator [152]. We have also suggested the extraction of 5 parameters, rather than 1 as has been customary, from the observed vasoreactivity, thereby increasing the information available for classifying the results. Finally, we have determined the measurement accuracy of the vasoreactivity parameters, which suggests the degree of change in the vasoreactivity of an individual that can be detected by our methods.

The variability of the post-ischemic reactive hyperemia was a major contributor to the variability of the measured vasoreactivity parameters. Tight constraints on the rate and duration of cuff inflation for repeated measurements did not significantly reduce the variability of the hyperemic response (σ_s decreased from 30.7 to 26.0 cm/sec). This persistent variability in the flow stimulus is a result of our inability at present to control the ischemic stimulus. The duration of the occlusion certainly affects the ischemic stimulus; other factors which may affect the relationship between the ischemic stimulus and the hyperemic response include the temperature of the forearm, the rate of onset of arterial occlusion, pre-occlusion blood flow, postcibal status, emotional status, estrogen levels, caffeine intake, arginine intake [38], and use of cyclooxygenase inhibitors. If a single measurement does not achieve a desired flow stimulus goal, Figure 4-6 suggests that more than 10 minutes of rest are required before the measurement is repeated. Column 5 of Table 4-1 reports the variability of the vasoreactivity parameters when the contribution of the stimulus variability is minimized. These values represent a combination of the inherent variability in individuals and the variability of the measurement technique.

The ability of our methods to detect changes in vasoreactivity can be estimated by the standard deviation of the parameters in an individual, listed in the third, fourth and fifth columns of Table 4-1. For example, if the mean ΔD is measured on an individual subject before and after a therapeutic intervention, after the intervention

it is at least 2.6% larger than that before the intervention, and the flow stimuli for the two measurements are equivalent, one can conclude that the vasoreactivity improved significantly at the $p = 0.05$ level.[1] Measurement of the 5 vasoreactivity parameters should result in greater sensitivity than measurement of only the mean ΔD or the dilation at a given time after release of the cuff [29], although this conclusion must be experimentally validated.

In conclusion, we have characterized the vasoreactivity of the brachial artery and forearm microvasculature in response to temporary forearm ischemia. We have proposed 5 parameters of vasoreactivity, and determined the measurement accuracy of these parameters. These results may allow better assessment of vasoreactivity, as well as of response to therapy, in individual patients, without the need for intra-arterial injection of provocative pharmaceutical agents.

[1]This calculation is based on the standard deviation of 1.1% for measurements of the mean ΔD (and thus a standard deviation of 1.6% [$1.1 \times \sqrt{2}$] for the therapeutic change in the mean ΔD), and is valid under the assumption of normal distribution for individual measurements of the mean ΔD.

Table 4-1. The mean and standard deviation of proposed vasoreactivity parameters.

Response Parameter	**Mean** (n=16)	**St. Dev. for Individual Measurements*** $\sigma_s = 30.7$, n = 16	$\sigma_s = 5.9$, n = 11	$\sigma_s = 3.9$, n = 8
Max. ΔD †	0.29mm (7.3%)	0.11mm (3.2%)	0.07mm (1.8%)	0.04mm (1.2%)
Mean ΔD †	0.20mm (5.1%)	0.10mm (2.9%)	0.07mm (1.7%)	0.04mm (1.1%)
t_D‡	71.4 sec.	20.5 sec.	12.6 sec.	11.8 sec.
$t_{1/2}$§	31.3 sec.	11.3 sec.	7.3 sec.	10.3 sec.
t_0‖	27.9 sec.	7.0 sec.	8.8 sec.	10.0 sec.

FOOTNOTES:

* The standard deviation of measurements of the response parameters in an individual is related to the variability of the flow stimulus, which is quantified by the standard deviation of the peak hyperemic response in that subject (σ_s). Details of the measurement groups are given in the text.

† ΔD = the change in brachial arterial diameter (and percent change) during post-ischemic reactive hyperemia, relative to the diameter before release of the cuff. Mean ΔD is the mean diameter change for the first 100 seconds after the initiation of dilation (t_0).

‡ t_D = the time of the maximum change in diameter after the release of the cuff.

§ $t_{1/2}$ = the time after the peak hyperemic response for the velocity to return halfway to the pre-occlusion velocity.

‖ t_0 = the time after the release of the occlusion when dilation began.

Chapter 5

Methods IV: Extended Vasoreactivity Measurements

The methods of Chapter 4 resulted in high-resolution measurements of vasoreactivity after temporary forearm ischemia. However, we have not yet completely characterized the vasoreactivity that results from temporary inflation of a blood pressure cuff around the forearm. Our immediate goal is to extend the methods of Chapter 4 to include measurements of arterial diameter and flow velocity before, during, and after temporary forearm ischemia. This will allow direct comparison of our measurement accuracy and experimental results with the commonly-reported measurement of percent flow-mediated dilation relative to pre-occlusion diameter [5, 8, 29, 170]. Also, the extended measurements may provide additional diagnostic information. For example, Filitti et al. [60] demonstrated constriction of the brachial artery of hypercholesterolemic subjects during distal cuff inflation, but dilation or no diameter change in normal subjects during distal cuff inflation.[1] Complete characterization of the vasoreactivity will allow us to explore the full diagnostic potential of the technique.

[1]These findings are counterintuitive and worthy of further study. One would think that low flow would imply less NO release and arterial constriction in normal subjects, but little change in the already low NO status of hypercholesterolemic subjects. Sorting out this phenomenon may provide considerable insight into the mechanisms of vasoreactivity.

5.1 METHODS

For extended measurements of vasoreactivity, duplex ultrasound images of the brachial artery were acquired from 60 seconds before inflation of the blood pressure cuff, through 5 minutes of cuff inflation, and for at least 3 minutes after cuff release. The images were digitized and arterial diameter and flow velocity were measured from the images as described in Chapter 4. From each vasoreactivity measurement, a total of 8 parameters were automatically extracted: 1.) slope of diameter change during occlusion; 2.) time to onset of dilation; 3.) time to peak dilation; 4.) half-time of decay of hyperemia; 5.) maximum change in diameter relative to the pre-occlusion diameter; 6.) mean change in diameter relative to the pre-occlusion diameter; 7.) maximum change in diameter relative to the pre-release diameter; and 8.) mean change in diameter relative to pre-release diameter. These include the 5 parameters that were described in Chapter 4. The algorithm for computation of the parameters is described in Appendix A.

To characterize the normal vasoreactivity before, during and after temporary forearm ischemia, 2 extended vasoreactivity measurements were performed on each of 15 subjects (9 females and 6 males, average age 38.1 $\pm$ 3.6 years [Mean $\pm$ SEM]). The subjects were nonsmokers, normocholesterolemic, nonhypertensive, nondiabetic, and were free of significant family history of atherosclerosis (*i.e.,* stroke, myocardial infarction or revascularization procedure in at least one first degree relative before age 60). For this group of subjects, mean systolic blood pressure was 112.8 $\pm$ 3.2, mean diastolic pressure was 72.3 $\pm$ 2.1, mean total cholesterol was 187.6 $\pm$ 9.8, mean LDL was 106.8 $\pm$ 8.5, and mean HDL was 62.9 $\pm$ 3.5. The 8 vasoreactivity parameters described above were computed automatically from the diameter and flow velocity time series data and were entered into a computer database.

To estimate the measurement accuracy of the 8 vasoreactivity parameters, repeated measurements (on separate days) were collected from a total of 22 subjects. Four measurements were collected on each of 6 subjects, three measurements were

collected on each of 7 subjects, and two measurements were collected on each of 9 subjects. The 8 vasoreactivity parameters were extracted automatically from each measurement. The peak dilation relative to the pre-occlusion diameter was also estimated according to the technique of Celermajer et al. [29], for a comparison of measurement accuracy. The variance of each vasoreactivity parameter for measurements on individual subjects was estimated by averaging across subjects the variance of repeated measurements.

5.2 RESULTS

Figure 5-1 is the mean $\pm$ SEM extended vasoreactivity measurement from the 15 subjects with no risk factors for atherosclerosis. Table 5-1 contains the mean values of the vasoreactivity parameters for these subjects. Since the time course of the vasoactive response varied among subjects, the mean of parameters from individual measurements in Table 5-1 is not equal to the parameters of the mean measurement shown in Figure 5-1.

The third column of Table 5-1 lists the estimated standard deviations for individual measurements of the vasoreactivity parameters, obtained from repeated measurements on 22 subjects. Because the flow-mediated dilation of an artery expressed as a percent is known to be inversely proportional to the baseline diameter [5, 29], both absolute and percent dilation are reported. For example, the standard deviation of the peak dilation relative to the pre-occlusion diameter is 0.11mm (3.1%). For comparison, our estimate of the standard deviation of this parameter using the technique of Celermajer [29] is 0.16mm (4.7%). Statistical analysis of the ratio of these variances (using an F distribution with 21 and 21 degrees of freedom), revealed a p value of 0.047. Therefore, our technique has significantly greater accuracy than the technique used by Celermajer and others [8, 29, 170].

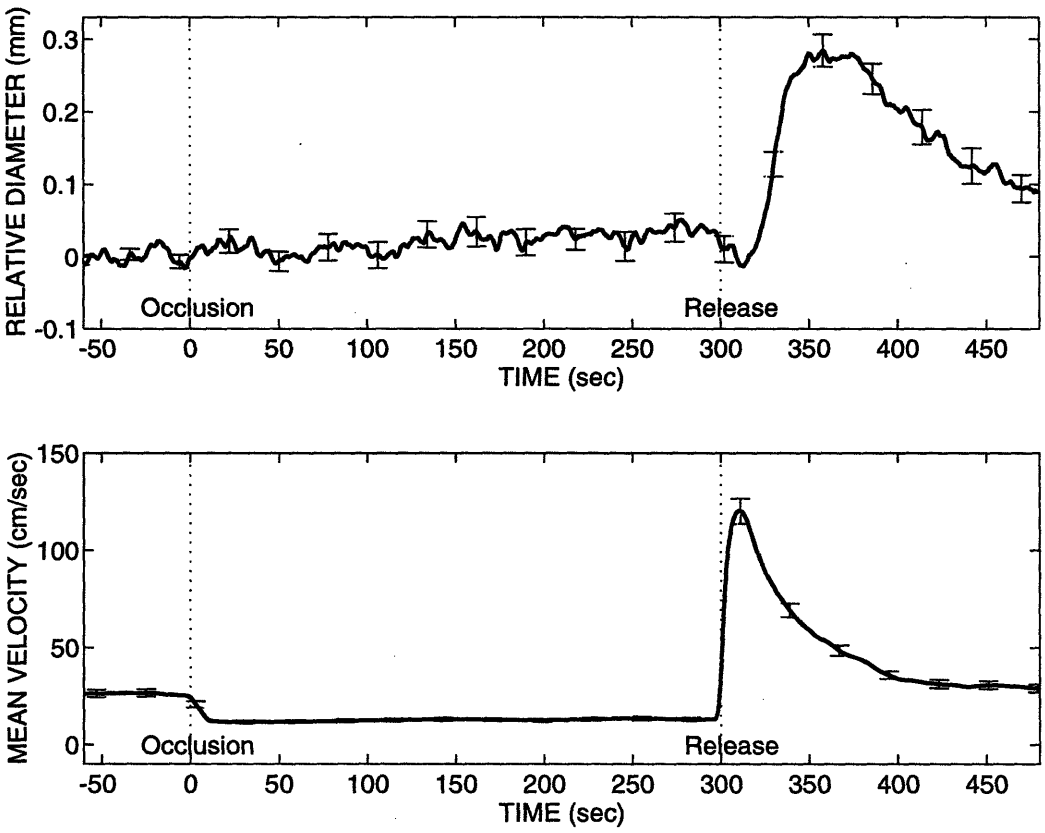

Figure 5-1: The mean and SEM of 30 measurements of brachial artery diameter and flow velocity from 15 subjects with no risk factors for atherosclerosis. The forearm vascular occlusion began at time zero and was released at 300 seconds.

5.3 DISCUSSION

The first major result of this chapter is characterization of normal vasoreactivity during and after temporary forearm ischemia. This characterization includes: 1.) demonstration of the normal diameter and flow-velocity time series (Figure 5-1), 2.) designation of 8 parameters of vasoreactivity and their normal values (Table 5-1, Column 2), and 3.) estimation of the measurement variability of these parameters within individuals (Table 5-1, Column 3). The latter can be used for power calculations in studies investigating therapeutic changes in vasoreactivity.

The peak flow-mediated dilation of the brachial artery relative to the pre-occlusion diameter (9.0%) is similar to that reported by Celermajer [32] for subjects with no risk factors for atherosclerosis. Also, the mean and standard deviation of the 5 parameters in Table 4-1 are very similar to those listed in Table 5-1. For comparison with Table 4-1, the standard deviation of the peak hyperemic response (σ_s) for the group of 22 subjects in this chapter was $\sigma_s = 23.8$ cm/sec.

The second major result in this chapter is the demonstration of significantly better measurement accuracy with our methods compared with that of the methods in common use. For measurement of the peak flow-mediated dilation relative to the pre-occlusion diameter, our method has a standard deviation of 0.11mm compared with 0.16mm for the commonly-used method ($p = 0.047$) [8, 29]. As demonstrated in Table 4-1, the majority of the variance in parameters of flow-mediated dilation is due to inherent variability in the flow stimulus. A second contribution to the variance is variability in an individual's response to a given flow stimulus. These contributions to measurement variance are equivalent for all methods of measurement. The remainder of the measurement variance is from the measurement system. Because the majority of the measurement variance is system-independent, and our system has significantly lower overall variance, the variance due to the measurement method must be markedly smaller for our system.

Overall, our method for vasoreactivity measurement has several advantages over

existing techniques. First, we measure arterial diameter from B-mode images digitized directly from the ultrasound scanner, rather than from images stored on videocasette. Second, arterial diameter is measured via the edge detection and diameter-estimation algorithms described in Chapter 3. Third, we image the artery in the skew plane rather than the commonly used longitudinal plane, because diameter estimates in the skew plane are less sensitive to translational motions of the artery. Also, unintentional motions of the transducer or the subject are unambiguously detected in the skew plane, which allows for easier correction. Fourth, The user-selected preliminary edge points can reused for subsequent images in the time series, or can be moved as a group to compensate for translational motion of the artery in the image. Therefore, measurement of the change in arterial diameter is automated and objective. Fifth, with the aid of fast automated diameter estimation, we measure end-diastolic arterial diameter every 3-4 seconds from one minute before the onset of vascular occlusion, through 5 minutes of occlusion and for 3 minutes after release of the occlusion. Other systems measure diameter at only two points: before and after the stimulus (Figure 5-1). We can therefore characterize the entire physiological response and report specific abnormalities during portions of the measurement. Sixth, we do not perturb the artery whose response is being measured, because the occlusion cuff is applied distal to the measurement location (Figure 4-1). Seventh, we measure arterial diameter and flow velocity simultaneously (Figure 5-1), thus additionally quantifying the flow stimulus for vasoreactivity and characterizing the microvascular, as well as macrovascular, vasoreactivity.

This completes the development and validation of new methodology for vasoreactivity measurement. We have shown that our methodology conveys additional accuracy for measurement of flow-mediated dilation, as necessary for individual specificity. We must now show that measurement of multiple vasoreactivity parameters conveys additional additional information of abnormal vascular physiology.

Table 5-1: Mean values of vasoreactivity parameters for 15 subjects with no risk factors for atherosclerosis and estimated standard deviation of vasoreactivity parameters for individual measurements.

	Mean	**Standard Dev.†**
Vasoreactivity Parameter	($n = 15$)	($n = 22$)
Half-Time of Decay of Hyperemia (sec)	27.1	9.2
Diameter Slope During Occlusion (μm/sec)	0.13	0.30
Time to Onset of Dilation (sec)	31.4	12.0
Time to Peak Dilation (sec)	70.2	16.7
ΔD Peak - Pre-Occlusion (mm, %)	0.33, 9.0%	0.11, 3.1%
ΔD Peak - Pre-Release (mm, %)	0.29, 7.9%	0.13, 3.5%
$\overline{\Delta D}$ Relative to Pre-Occlusion (mm, %)	0.23, 6.1%	0.09, 2.5%
$\overline{\Delta D}$ Relative to Pre-Release (mm, %)	0.19, 5.1%	0.11, 3.1%

ΔD = change in diameter. $\overline{\Delta D}$ = mean change in diameter.

† Standard deviation for individual measurements was estimated from measurements repeated on separate days on 22 subjects, including the 15 subjects used to estimate the mean parameter values.

Chapter 6

Methods V: Intima-Media Thickness Measurements

In 1986, Pignoli et al. [125] compared ultrasonic images of ex-vivo arterial wall to histologic sections, and concluded that the lumen/intima and media/adventitia interfaces in the arterial wall produce distinct echoes. They also concluded that accurate measurement of the intima plus media thickness was possible via transcutaneous ultrasound. The correlation between histology and ultrasound echo structure was later confirmed [173, 178]. Ultrasonic measurement of arterial intima-media thickness (IMT) is now widespread, and is commonly utilized to track progression of atherosclerosis and to assess therapeutic efficacy [15, 44, 89, 112, 132, 137, 175]. However, the majority of recent measurements are conducted manually, based upon subjective location of the edges by a human operator [89, 132, 137, 173]. We believe that the accuracy of IMT measurements can be vastly improved by automated computer algorithms. Improved accuracy of IMT measurements may lead to a powerful, noninvasive method for assessment of early atherosclerosis. This chapter describes a new system for measurement of IMT, and reports the measurement accuracy.

6.1 METHODS

In our system, the IMT of the common carotid artery is measured from B-mode ultrasound images acquired with a Hewlett-Packard SONOS 100 and a 10MHz mechanically-scanning peripheral vascular transducer. Subjects lay in the supine position with neck slightly extended and head resting against a wedge-shaped pillow to maintain head rotation at a consistent 45° angle. End-diastolic (i.e., ECG-gated) B-mode images of the common carotid artery are acquired in longitudinal (e.g., long axis) planes, with the carotid bulb as a reference point.[1] Gain and contrast controls are set to obtain the clearest visualization of the distal 1 cm of the far wall of the common carotid artery. An example B-mode image of the common carotid artery is shown in Figure 6-1. IMT is measured only on the far wall of the common carotid artery as measurements on the near wall are known to be less accurate [177, 178]. The end-diastolic images are digitized by a frame grabber (Data Translation DT55-LC, Marlboro, MA) at a resolution of 640 by 480 pixels and 256 shades of gray. The images are digitized directly from the scanner (rather than from videotape) and are stored in a Intel-based computer. Images are simultaneously archived on super VHS videotape.

The algorithm for measurement of IMT from B-mode images involves three steps: edge detection, smoothing of edge points, and measurement of distances between edges. The operator first calibrates the image by selecting a standard imaging depth or by designating a distance of one centimeter, based upon the depth indicators in the image. The operator next selects several preliminary points in proximity to the leading edges of the far wall lumen/intima and media/adventitia echo zones. The computer then connects a spline containing 100 points to each set of preliminary edge points. The direction perpendicular to the spline at each point is calculated. The image is then interpolated in the perpendicular direction over a restricted range (e.g., image intensities along a distance of 3 image pixels in either direction are interpolated

[1]The skew plane, introduced in Chapter 3 for vasoreactivity measurements, is unnecessary for this application because complete measurements are conducted on single images.

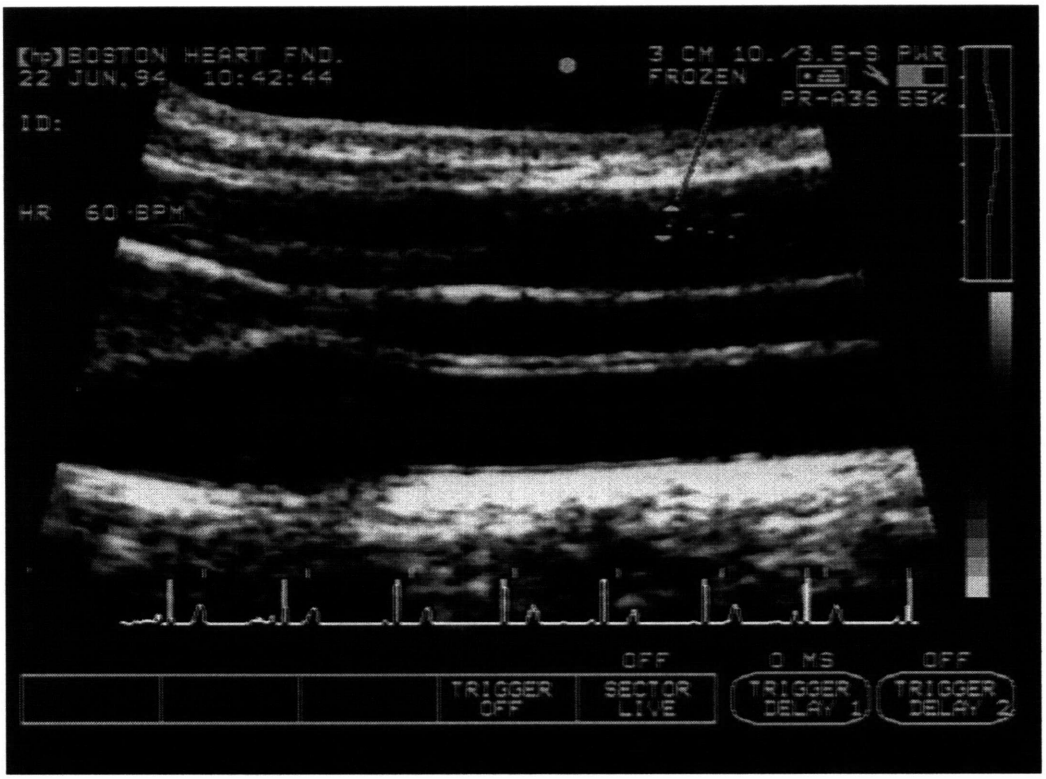

Figure 6-1: An example B-mode image of the common carotid artery (center of image) and carotid bulb (left of center). The intima-media thickness is the distance from leading edge to leading edge of the double line pattern at the far (deep) wall of the common carotid artery. This IMT measured 0.438mm. A similar double line pattern is present at the near wall of the artery. The two sets of double line patterns and the central anechoic lumen form the classic "7-zone" appearance described by Wendelhag [173].

to create a 100 point perpendicular line). The location along the interpolated line with the largest sum of first and second derivatives is chosen as the best local edge point. This process is repeated for each spline point of the two edges. Edge points that represent weak edges (e.g., points selected at edges with less than 20% of the maximum sum of the intensity derivatives of all edge points) are replaced by linear connections between the nearest strong edge points. The two sets of edge points are smoothed with a 7-point Parks McClellan lowpass filter [113]. A centerline is then constructed between the two sets of edge points and the distance between the two edges, the IMT, is determined in directions that are locally perpendicular to the centerline. At least 35 local IMT measurements along the edges are averaged to produce each final IMT value.

To estimate the variability of the measurement technique, bilateral IMT measurements were conducted on 15 subjects, and were repeated with a measurement interval of at least 1 day. The gain and contrast settings of the imaging system (as stored on each acquired image) were reproduced during acquisition of the follow-up images. The pair of digitized images of each artery were displayed simultaneously for IMT measurement. A technician who was blinded to measurement purpose was instructed to measure IMT on the pair of images at the same anatomical locations and over the same spans of the far wall of the distal common carotid artery.

6.2 RESULTS

Measurements of IMT were conducted unilaterally on 2 of the 15 subjects, because adequate images could only be obtained on one side. The standard deviation of individual IMT measurements was 51.3μm. The mean absolute difference between repeated measurements was 53.7μm. The correlation coefficient between the first and second IMT measurement was 0.80. Figure 6-2 compares the first and second IMT measurement on each of the 28 arteries.

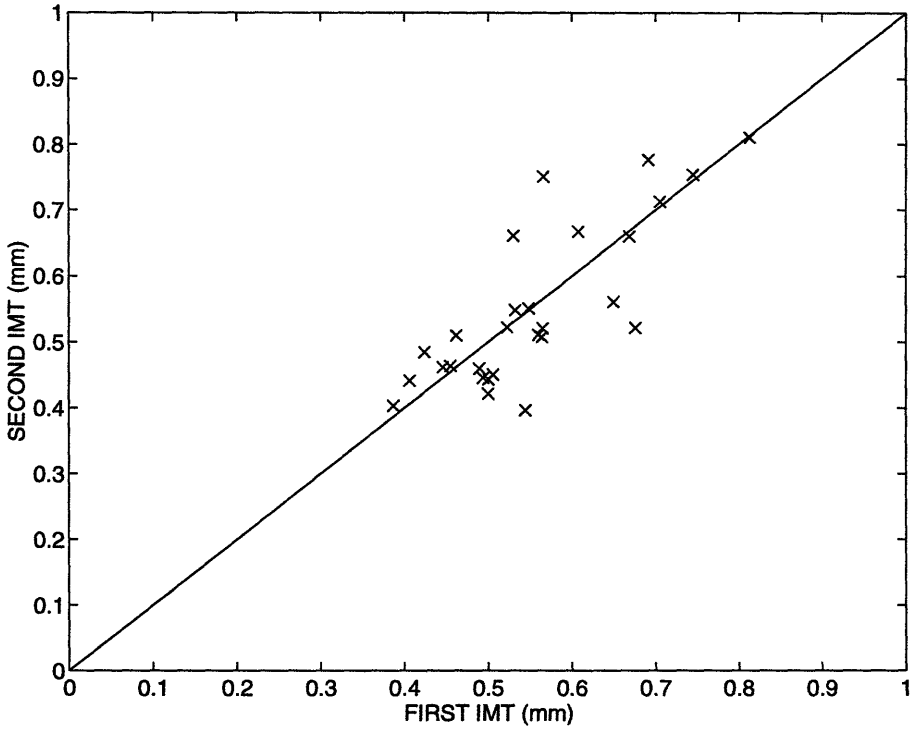

Figure 6-2: Reproducibility of IMT measurements on 15 subjects. The correlation coefficient between the first and second IMT measurement was 0.80.

6.3 DISCUSSION

The standard deviation of individual measurements from our system (51.3μm) is similar to that of the system described by Selzer et al. (45μm) [143], which is also based on automated edge-detection. Other systems which are based on manual edge location, rather than computerized edge detection, report standard deviations in the range of 80 to 110μm [12, 136, 173].

The high accuracy of IMT measurements reduces the number of subjects, and therefore the cost, of studies of therapeutic regression of atherosclerosis. For example, one study reported a significant reduction of IMT in 14 subjects with coronary artery disease treated for one year with colestipol and niacin [112]. An angiographic trial with comparable power would require hundreds of subjects treated for several years.

However, unlike measurements of vasoreactivity, the accuracy of IMT measurements is not sufficient to track therapeutic changes in individual subjects. The annual change in common carotid IMT in an average subject is estimated to be 10μm/year

[89]. The standard deviation (SD) of individual IMT measurements with our system is 51.3μm, which implies an SD of 72.5μm for measurement of change in IMT (i.e., the SD of the difference is $\sqrt{2} \times 51.3\mu$m). Thus, there is a low "signal-to-noise ratio" for measuring individual changes in IMT. In contrast, the typical range of IMT in adults is 400μm to 800μm [89], and our standard deviation for a single measurement is 51.3μm. Therefore, estimation of annual change in IMT by dividing the absolute IMT by the age of the subject improves the signal to noise ratio by a factor at least 50. However, we must then question the assumption of linear IMT progression with age. The ARIC study, which included 13,870 subjects of age 45 to 64 years [89] and the CLAS study [112], strongly support this assumption. Despite the use of a quadratic regression model for IMT versus age in the ARIC study, the IMT increased linearly in the common carotid artery over a 20 year span. The CLAS study initially modeled 4 years of progression in the placebo group (a group with prior bypass surgery) as a quadratic, but found no significant quadratic relation between time and IMT. A linear model was then adopted. The linear progression of IMT in these studies indicates that absolute IMT divided by subject age is a much more accurate estimator of annual growth rate than is measurement of annual differences. This method obviously excludes subjects participating in antiatherosclerotic therapy, whose age-related IMT progression does not reflect the current state of altered progression.

6.4 CONCLUSIONS

In conclusion, we have developed a system for measurement of carotid artery intima-media thickness, and have demonstrated comparable performance to a similar automated system. Automated IMT measurement techniques perform significantly better than subjective, manual methods. Although IMT measurements are not sufficiently sensitive to detect changes in individual subjects during typical study durations, the annual rate of progression of IMT in untreated subjects can be estimated by the ab-

solute IMT divided by subject age. The rate of change of IMT during therapeutic interventions can be measured in small subject groups over periods of at least one year.

Chapter 7

Vasoreactivity and IMT in HELP Subjects

In previous chapters, we focused on the design, construction and validation of new methods for noninvasive assessment of early atherosclerosis. In this and the following chapters, we will describe the application of the methods to small-scale clinical studies.

At the Boston Heart Foundation, we have the unusual opportunity to study vasoreactivity before and after Heparin-Induced Extracorporeal LDL Precipitation (HELP). HELP is a newly-approved method for treatment of severe drug- and diet-resistant hypercholesterolemia [9, 55, 139]. A single 2 hour HELP treatment reduces plasma LDL cholesterol, total cholesterol and apolipoprotein B by 50%, while HDL cholesterol and apolipoproteins A-I and A-II decrease by only 8 to 16% [100]. On average, weekly or biweekly HELP treatment produces a greater than 50% decrease in plasma LDL cholesterol, and a slight increase in HDL cholesterol [140]. HELP therapy has also been associated with angiographically-documented regression of coronary artery disease [138], reduction of carotid artery plaque volume [78], and reduction of xanthoma size [160, 186].

We studied 7 subjects with severe drug- and diet-resistant familial hypercholesterolemia (FH) who were on chronic HELP therapy, and compared them with 12 age-

and sex-matched control subjects. We measured brachial artery and forearm vasoreactivity in 6 of the HELP subjects and the control population, and carotid IMT over the course of 1 year in all 7 HELP subjects. We report here the effects of acute LDL lowering on peripheral vasoreactivity, compare HELP subject vasoreactivity with that of a population at low risk for atherosclerosis, and assess the absolute IMT and the rate of change of IMT in the HELP subjects during chronic therapy.

7.1 METHODS

7.1.1 Subjects

Every patient in the United States on chronic HELP therapy was studied, including 2 FH homozygotes and 5 FH heterozygotes. The subjects included 2 males, 2 premenopausal females, 2 post-menopausal females on estrogen/progesterone replacement, and 1 post-menopausal female on estrogen replacement only. Four of the HELP subjects had prior coronary artery bypass surgery; two of the latter also had unilateral carotid endarterectomy. For vasoreactivity measurements, 6 of the HELP subjects (mean age 40.7 $\pm$ 5.2 years) were compared with 12 age- and sex-matched control subjects (mean age 41.2 $\pm$ 4.0 years) that were normocholesterolemic, normotensive, nonsmokers, nondiabetic, and free of significant family history of atherosclerosis (See Table 7-1 for cholesterol levels and blood pressures). Four of the female control subjects were post-menopausal; one was on estrogen replacement and two were on estrogen/progesterone replacement. The seventh HELP subject, a post-menopausal female on estrogen/progesterone replacement, was consistently treated during the IMT study, but discontinued treatment before the subsequent vasoreactivity study because of poor venous access. One HELP subject was taking a calcium channel-blocker, which he did not take on treatment days. None of the other HELP or control subjects were taking calcium-channel blockers, beta blockers, ACE inhibitors, or long-acting nitrates, nor were they smokers. All subjects provided informed consent and

the study was approved by the Massachusetts Institute of Technology Committee on the Use of Humans as Experimental Subjects.

7.1.2 HELP Therapy

The HELP treatment procedure has been described in detail elsewhere [55, 139]. Briefly, the HELP machine separates plasma from cellular elements and precipitates LDL from plasma with an acid/heparin buffer. After continuous on-line filtration of the precipitated LDL, removal of heparin, and normalization of the pH, the blood is recombined, warmed, and returned to the patient. The 7 HELP subjects had been treated weekly ($n = 4$) or biweekly ($n = 3$) for periods of 3 to 5 years prior to the initiation of this study. Total cholesterol, triglycerides, HDL-cholesterol, and LDL-cholesterol were estimated before and after each HELP treatment [62, 76].

7.1.3 Intima-Media Thickness Measurements

The IMT of the distal common carotid artery (just proximal to the carotid bulb) was measured from B-mode ultrasound images as described in Chapter 6. At least 2 images were acquired from each carotid artery of the 7 HELP subjects at baseline and at each of 2 follow-up measurements, all by the same operator. The gain and contrast settings of the imaging system at baseline were reproduced during acquisition of follow-up images. The two sets of follow-up measurements were acquired unilaterally in one subject who had interim elective carotid endarterectomy. The first set of follow-up measurements was made between 238 and 330 days (mean 287 days) after baseline and the second set of follow-up measurements between 280 and 419 days (mean 344 days) after baseline. During the duration of this study, none of the HELP subjects experienced an interruption in therapy of more than 4 weeks. The three sets of images were used to conduct two measurements of annual change in IMT. For each measurement of change in IMT, the baseline and follow-up images with the best match of insonation angle and fiducial points were paired. Each pair of images was

then displayed simultaneously in random order and a technician who was blinded to chronological order and to measurement purpose conducted the IMT measurements. The technician was instructed to measure IMT on the pair of images at the same anatomical locations and over the same spans of the far wall of the distal common carotid artery.

To obtain mean annual IMT growth rates for the 7 HELP subjects, the change in IMT for each baseline/follow-up comparison was first converted to an annual change, based upon the interval between the baseline and follow-up studies. The 26 measurements of annual IMT change (2 measurements on each of 13 arteries) were then averaged. The standard deviation of individual IMT measurements was estimated from the two sets of follow-up images, and the standard deviation of the mean annual IMT change was estimated from the standard deviation of individual IMT measurements.[1]

7.1.4 Vasoreactivity Measurements

After completion of the IMT study, measurements of vasoreactivity were conducted on the brachial artery and the forearm microvasculature according to the methods of Chapter 5. Measurements of vasoreactivity were conducted immediately before and after HELP treatment. A total of 88 measurements of vasoreactivity were collected on the 6 HELP subjects over a period of 5 months: 46 pre-HELP and 42 post-HELP. In 4 cases, treatment was unsuccessful and post-HELP measurements were not obtained. Thirteen measurement pairs were not analyzed either because of extensive motion during the pre- or post-HELP measurement (i.e., subject motion or translational motion of the artery during cuff inflation/deflation), or technical error during

[1]The standard deviation of the mean IMT change was estimated from the variance of individual measurements, rather than directly from the measured change in IMT, so that the covariances between measurements could be accounted for. The covariance between contralateral measurements on the same subject and the covariance between the 2 estimates of annual IMT change for each artery were included in the calculation. The variance of individual measurements of IMT and the associated covariances were then followed through the process of calculating the mean annual IMT change.

acquisition. Of the remaining 29 pre-HELP/post-HELP measurement pairs, the 4 pairs from each of the 6 subjects with the closest match of pre-HELP and post-HELP peak hyperemic response were selected for inclusion in the study. Two measurements of vasoreactivity were acquired on separate days from each of the 12 matched controls. Quantitative comparisons of vasoreactivity were accomplished by algorithmic extraction of vasoreactivity parameters, including the diameter slope during vascular occlusion, time to onset of vasodilation after release of occlusion, half-time of decay of reactive hyperemia, and the mean, maximum, and time to maximum flow-mediated dilation of the brachial artery (as described in Chapter 5 and Appendix A).

7.1.5 Statistical Analysis

Single measurement parameters were compared with the Wilcoxon sign-rank test for paired data (i.e., pre-HELP compared with post-HELP) and Wilcoxon rank-sum test for unpaired data (i.e., pre-HELP compared with controls) [37]. Cholesterol levels and blood pressure were also compared by the appropriate Wilcoxon test; corrections to the resulting significance levels for multiple comparisons were obviated by the strong polarity of the significance levels. Vasoreactivity parameters were compared, and confidence intervals were determined by Hotelling's T^2 multivariate test for two samples or for paired data [115]. Statistical significance was assumed if a null hypothesis could be rejected at the 0.05 probability level.

7.2 RESULTS

Blood pressures and lipid data are displayed in Table 7-1. HELP therapy acutely normalized the plasma lipids and lipoproteins of the hypercholesterolemic subjects.

7.2.1 Intima-Media Thickness

The far wall of the distal common carotid artery was free of complex atherosclerotic plaques in all cases, thereby improving measurement accuracy. The average annual change in IMT for the HELP subjects, based upon 26 comparisons of the baseline images and two sets of follow-up images, was -3.0 $\pm$ 17.4 μm per year (mean $\pm$ SEM). The IMT measurements for these comparisons were obtained over an average span of 2.53 $\pm$ 0.09 mm of the distal common carotid artery. The overall mean IMT for the 7 HELP subjects was 582 $\pm$ 32 μm.

7.2.2 Vasoreactivity

The mean pre-HELP and post-HELP vasoreactivity measurements are presented in Figure 7-1. Table 7-2 compares the vasoreactivity parameters for the pre- and post-treatment measurements. Since the time course of the vasoactive response varied among subjects, the mean of parameters from individual measurements (Table 7-2) was not equal to the parameters that could be obtained from the mean measurement (Figure 7-1). The vasoreactivity parameters were not significantly changed immediately after HELP treatment. For the HELP subjects, the 95% confidence interval for the peak arterial dilation relative to the pre-occlusion diameter was 0.20mm (5.2%) to 0.41mm (10.9%).[2] The mean brachial artery diameter before cuff inflation was 3.89mm pre-HELP and 3.67mm post-HELP ($p = 0.0005$).

Figure 7-2 compares the mean pre-HELP vasoreactivity with that of the control subjects. The HELP subjects demonstrated less dilation of the brachial artery but a smaller average flow stimulus for dilation. Table 7-2 compares the vasoreactivity parameters of the HELP and control subjects. The vasoreactivity parameters of the HELP population were not significantly different from those of the control population.

[2]In this study, we preferentially report absolute diameter change, rather than percent diameter change, because smaller arteries are known to produce larger percent dilations than larger arteries [5, 29]. The bias for smaller arteries is reduced by reporting absolute diameter change.

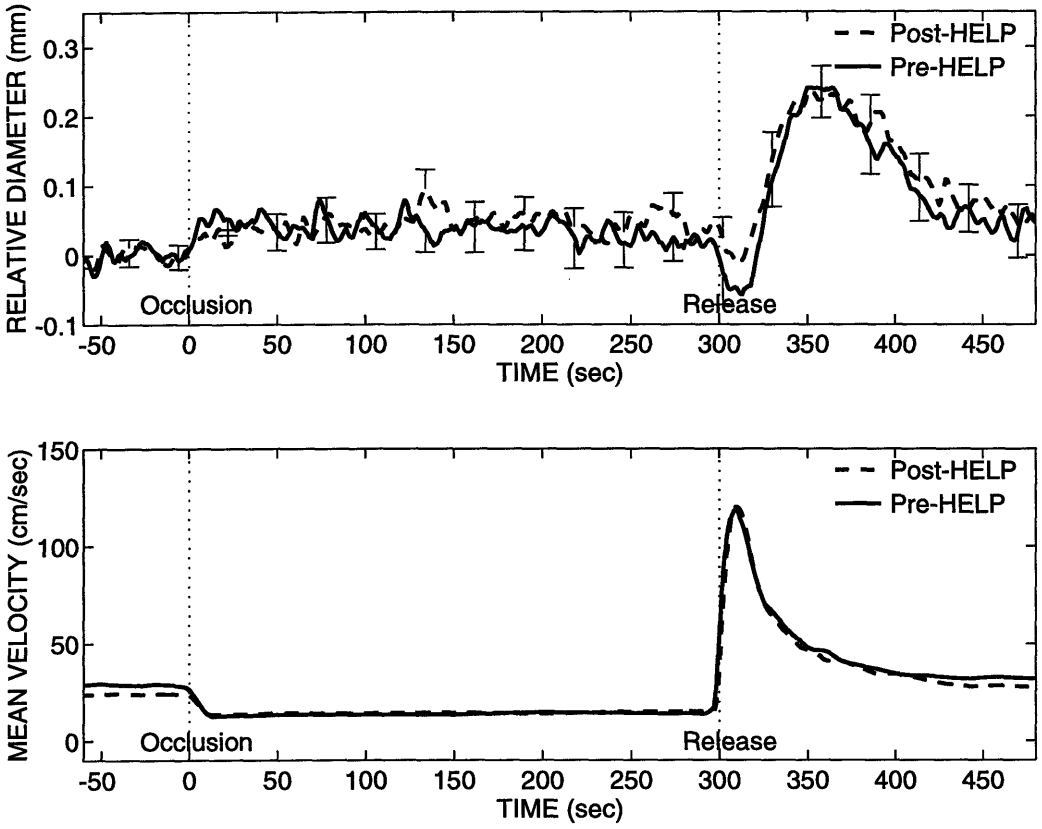

Figure 7-1: The mean of 24 pre-HELP and 24 post-HELP vasoreactivity measurements (4 pre/post pairs from each of 6 subjects). The error bars indicate representative values of the SEM. The SEM for the flow measurements was always less than 3 cm/sec.

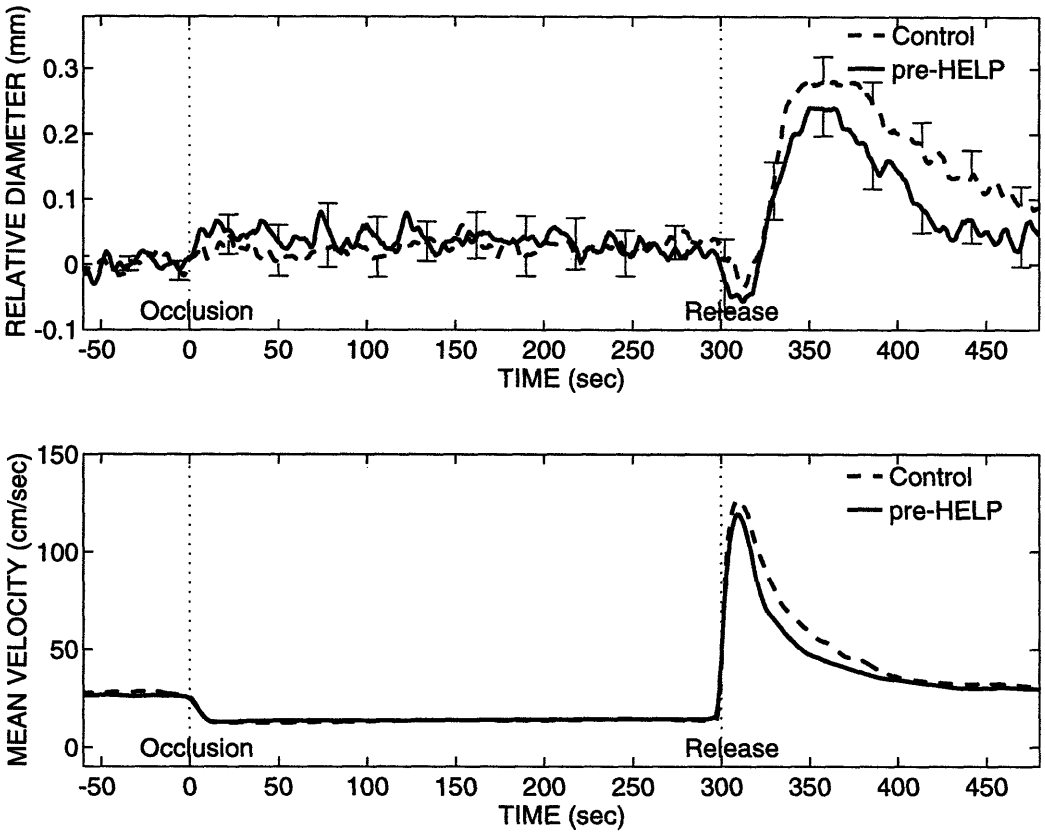

Figure 7-2: The mean of 24 pre-HELP measurements compared with that of 24 measurements from 12 age- and sex-matched control subjects. The HELP subjects demonstrate slightly less flow-mediated dilation and less peak hyperemic response than the control subjects. The error bars indicate representative values of the SEM. The SEM for the flow measurements was always less than 3 cm/sec.

The mean brachial artery diameter before cuff inflation was 3.56 mm for the control subjects (p = NS compared with pre-HELP).

The vasoreactivity of individual HELP subjects and changes in vasoreactivity immediately after HELP therapy were highly variable. One particular HELP subject ("**B**"), a woman with receptor-negative homozygous familial hypercholesterolemia who had been treated rigorously for 19 of her 28 years with plasmapheresis and HELP, consistently demonstrated changes in vasoreactivity immediately after HELP therapy. Figure 7-3 compares the mean $\pm$ SEM vasoreactivity of subject **B** with that of 3 age- and sex-matched control subjects.[3] The brachial arterial diameter of subject **B** decreased consistently during forearm cuff occlusion before treatment, but increased during cuff occlusion after treatment. The mean diameter slope during occlusion was -0.43μm/sec pre-HELP and $+0.14\mu$m/sec post-HELP, ($p = 0.016$), while the maximum arterial dilation relative to pre-occlusion diameter was 0.23mm pre-HELP and 0.39mm post-HELP, ($p = 0.016$). The post-HELP vasoreactivity of this subject was similar to that of 3 age- and sex- matched control subjects with low risk for atherosclerosis.

The mean vasoreactivity measurements of individual HELP subjects are displayed in Figure 7-4. A wide variation in vasoreactivity is evident.

7.3 DISCUSSION

Our results suggest that familial hypercholesterolemic (FH) patients treated regularly with HELP for acute reduction of LDL cholesterol have nearly normal peripheral artery vasoreactivity and lack of carotid IMT progression. All of our patients were already on chronic HELP therapy at the beginning of the study, which would be expected to maximize the normalization of their vasoreactivity and minimize sub-

[3]Two additional pre-HELP / post-HELP vasoreactivity measurements on subject **B** (for a total of 6) and two measurements from an additional (third) age- and sex-matched control subject were collected for Figure 7-3.

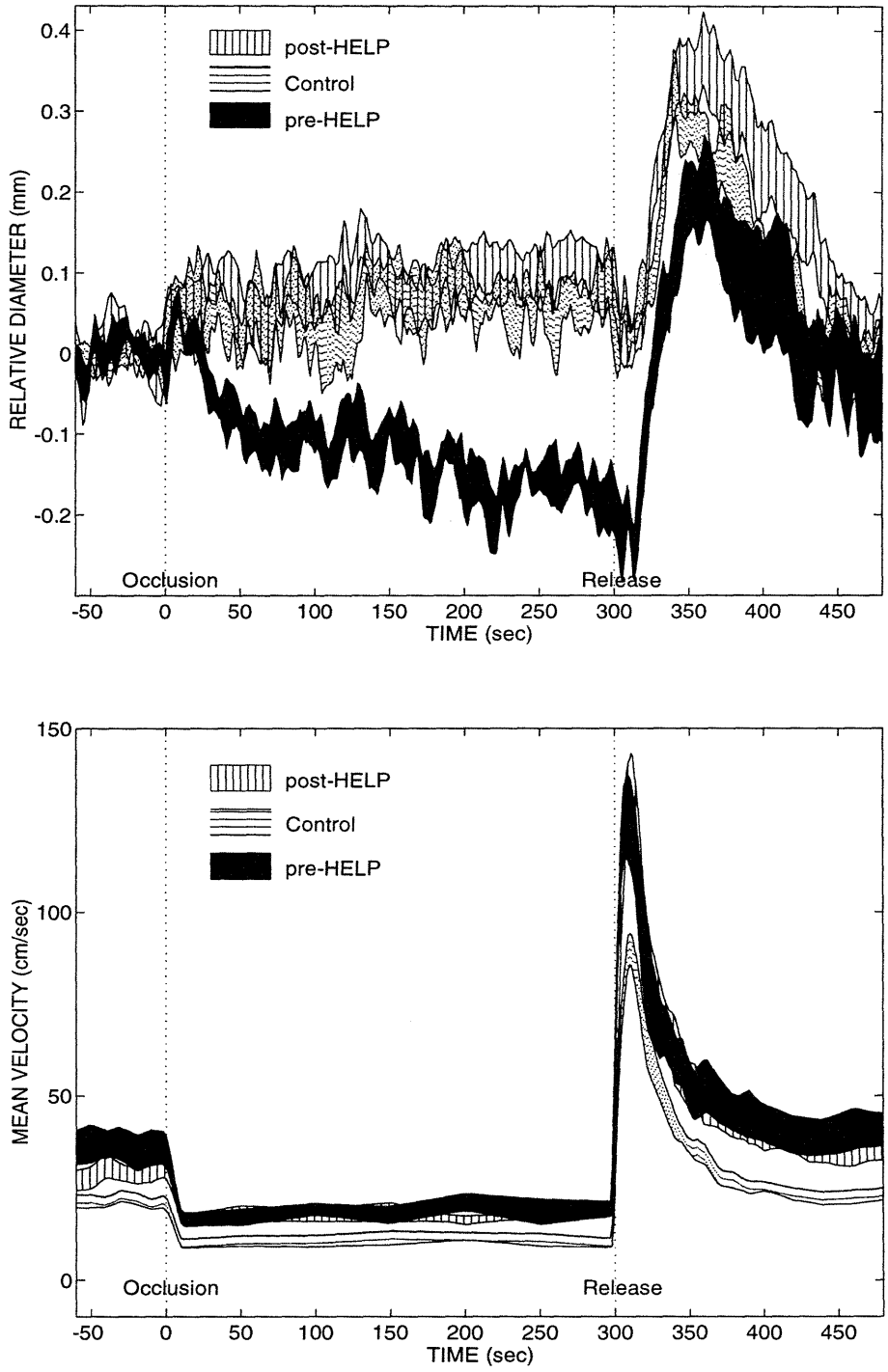

Figure 7-3: The mean ± SEM of 6 pre-HELP and 6 post-HELP vasoreactivity measurements of HELP subject **B**, compared with that of 6 measurements from 3 age- and sex-matched control subjects.

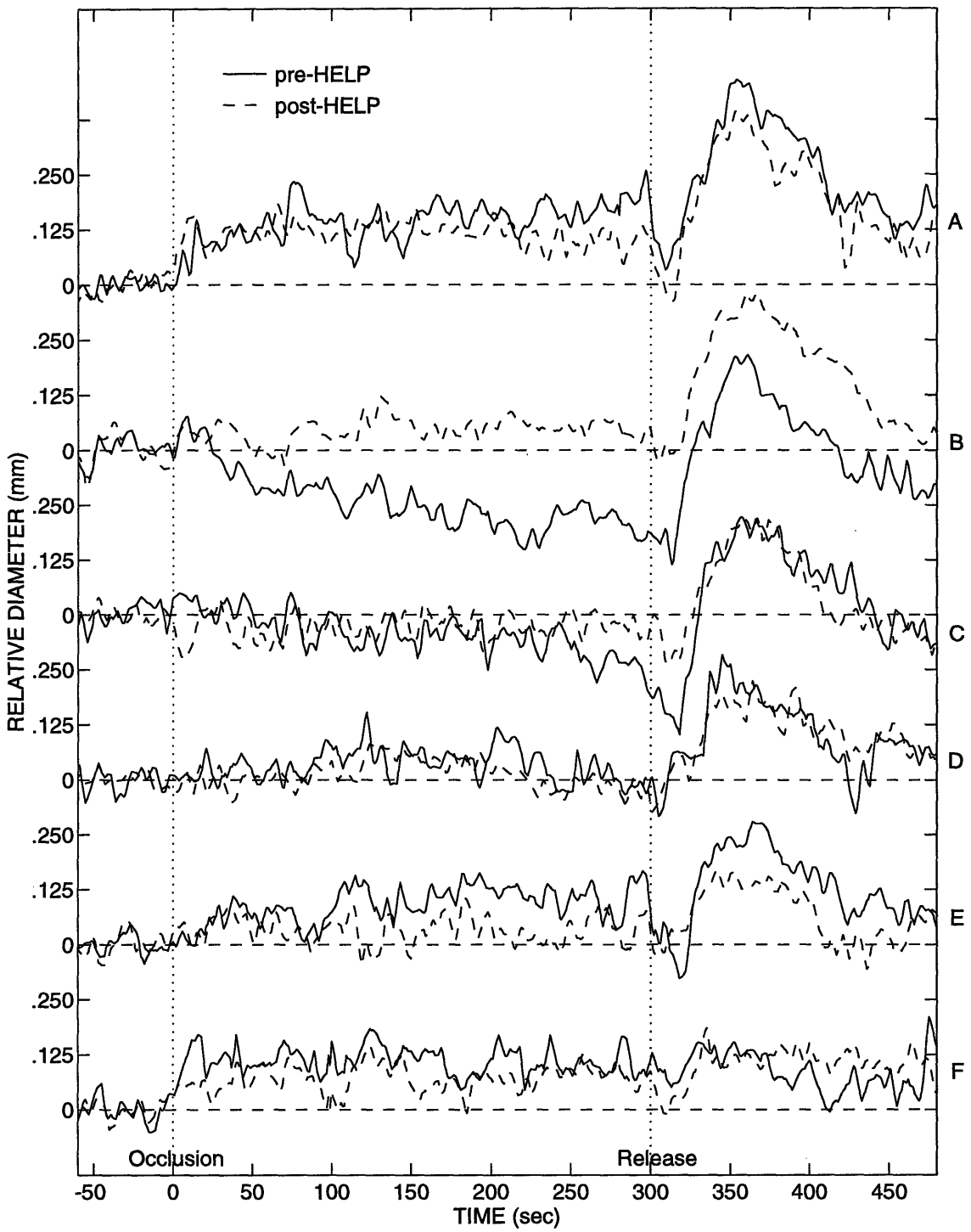

Figure 7-4: The mean of 4 pre-HELP and 4 post-HELP vasoreactivity measurements from each of the 6 HELP subjects.

sequent change in both vasoreactivity and carotid IMT. Given the severity of their disease, we deemed it unethical to remove the patients from treatment for the sake of "baseline data".

7.3.1 Vasoreactivity

Acute normalization of the plasma lipids with HELP treatment did not, on average, affect the brachial artery or forearm microvascular vasoreactivity (Figure 7-1 and Table 7-2). Only subject **B** showed a significant, acute change in vasoreactivity after HELP (Figure 7-3). Although hypercholesterolemia is associated with abnormal endothelial function [8, 29, 60, 150] and treatment of hypercholesterolemia is known to restore normal vasoreactivity [4, 54, 90, 107, 157, 163, 170], the time course of changes in vasoreactivity as a result of risk-factor modification remains an important research topic. Previous studies have shown that arterial wall LDL is in rapid equilibrium with plasma [25, 34], and that endothelial function is rapidly and reversibly inhibited by incubation with LDL ex-vivo [161]. To our knowledge, the most rapid in-vivo change in vasoreactivity was reported by Igarashi et al. [90] who demonstrated acute improvement in coronary microvascular endothelium-dependent vasoreactivity after LDL apheresis. We have previously suggested that the half-time of decay of hyperemia is a parameter of microvascular endothelium-dependent vasoreactivity in the periphery (Chapter 4 and [153]). In contrast to the results of Igarashi, this parameter did not improve immediately after HELP therapy (Table 7-2), conceivably because we used a different method of LDL apheresis, or more likely because our study used an ischemic stimulus in the forearm, whereas Igarashi used acetylcholine as a stimulus in the coronary microvasculature. Stroes et al. [157] demonstrated inhibition of nitric-oxide mediated vasoreactivity 2 weeks after cessation of lipid-lowering therapy in hypercholesterolemic subjects, and restoration of normal vasoreactivity 12 weeks after return to therapy. Vogel et al. [170] reported a significant improvement in brachial artery flow-mediated dilation (FMD) 2 weeks after initiation of cholesterol-lowering

therapy. Treasure et al. [163] showed no difference in coronary artery vasoreactivity between subjects with coronary artery disease who received either 80 mg/day lovastatin or placebo for 12 days. However, vasoreactivity was significantly different between the lovastatin and placebo groups after 5.5 months of therapy. The majority of published studies of therapeutic improvement in vasoreactivity compared the subjects' responses before and after at least 5 months of therapy.

The only significant difference between the groups of pre-HELP and post-HELP ultrasound studies was the baseline brachial artery diameter (3.89mm pre-HELP and 3.67mm post-HELP, $p = 0.0005$). We have observed a systematic decrease in forearm and palm skin temperature, but not core body temperature, after HELP therapy. These results suggest that HELP therapy causes mild temporary vasoconstriction of the periphery. The similarity of the mean pre-HELP and post-HELP vasoreactivity measurements (Figure 7-1) suggests that HELP treatment itself had no adverse effect on endothelial function.

Whereas Figure 7-1 shows no change in vasoreactivity with acute HELP treatment, Figure 7-2 and the vasoreactivity parameters in Table 7-2 suggest that on average, FH subjects treated chronically with HELP have nearly normal vasoreactivity. Previous studies have established strong correlations between coronary artery disease or plasma cholesterol and abnormal vasoreactivity. Celermajer et al. [29] reported 0% brachial artery FMD in subjects with coronary artery disease versus 11% FMD in normal subjects ($p < 0.001$). Leung et al. [107] reported a correlation of -0.64 between LDL and coronary artery dilation to acetylcholine. Sorensen et al. [150] and Arcaro et al. [8] reported correlations of -0.61 and -0.71, respectively, between total cholesterol and FMD of the femoral artery, whereas Celermajer et al. [32] reported a correlation of -0.21 between total cholesterol and FMD of the brachial artery. The established correlations between coronary artery disease or hypercholesterolemia and diminished FMD, together with the presence of coronary artery disease and the severe hypercholesterolemia of the HELP subjects, would predict profound abnormalities in

HELP subject FMD. However, the maximum brachial artery FMD of the HELP subjects immediately before treatment (0.30 mm) is similar to that of the control subjects (0.33 mm, p =NS), especially when one considers the smaller average flow stimulus of the HELP subjects. The 95% confidence interval for the maximum FMD of the HELP subjects is 0.20 mm (5.2%) to 0.41 mm (10.9%). Anderson et al. [5] considered abnormal FMD to be less than 3%. The maximum FMD of the control subjects (9.3%) is consistent with that reported by Celermajer et al. [32] for subjects with no risk factors for atherosclerosis.

The vasoreactivity of FH subjects under dietary and pharmacologic therapy has been investigated. Celermajer et al. [29] demonstrated that 10 children with FH (2 homozygous and 8 heterozygous) had significantly attenuated post-ischemic FMD of the femoral artery when compared with 16 normal children (0% versus 9%, $p < 0.001$). The vasodilation was profoundly abnormal in these FH subjects despite dietary and pharmacologic therapy (simvastatin and cholestyramine in the 2 homozygotes, diet and cholestyramine in 4 heterozygotes, and diet alone in the remaining 4 heterozygotes). In a separate study by Sorensen et al. [150], the femoral artery FMD of 30 children with FH was 1.2%, whereas that for 30 age- and sex-matched children with no known risk factors for atherosclerosis was 7.5%. This difference in vasoreactivity was also highly significant ($p < 0.0001$) despite dietary and pharmacologic treatment of the FH subjects (5 on HMG CoA reductase inhibitors, 7 on cholestyramine, and all on lipid-lowering diet). Both Celermajer and Sorensen report similar flow stimuli for the hypercholesterolemic and control populations. These results, together with the results of this paper suggest that HELP therapy may be superior to diet and pharmacologic therapies in normalizing vasoreactivity of FH subjects.

Proper interpretation of the acute and chronic effects of HELP therapy on vasoreactivity requires an investigation of individual responses. As shown in Figure 7-3, subject **B** demonstrated a dramatic and highly reproducible change in vasoreactivity immediately after HELP therapy. Filitti et al. [60] demonstrated brachial artery con-

striction during temporary forearm vascular occlusion in hypercholesterolemic subjects, but arterial dilation or no diameter change during distal occlusion in normal subjects. In HELP subject **B**, both the slope of arterial diameter during occlusion and the maximum post-release dilation relative to the pre-occlusion diameter increased significantly after treatment ($p = 0.016$).[4] We interpret these changes as an improvement in vasoreactivity because the vasoreactivity before treatment was consistent with that reported for hypercholesterolemic subjects [60, 150], whereas the vasoreactivity post-treatment was consistent with that of 3 age- and sex-matched control subjects with low risk for atherosclerosis. The observed changes in vasoreactivity in subject **B** were not observed in the other HELP subjects (see Figure 7-4). We hypothesize that the unusual behavior of subject **B** demonstrates an important genetic difference in arterial physiology.

The mean vasoreactivity measurements of individual HELP subjects (Figure 7-4) are highly variable. Three of the subjects (**A**, **B**, and **C**) have normal FMD, two subjects (**D** and **E**) have slightly below normal FMD, and one subject (**F**) has severely abnormal FMD. Subjects **D** and **E** are the two male subjects. The four female subjects are either pre-menopausal or are taking estrogen supplements. Estrogen is known both to protect endothelial function and to reduce risk for atherosclerosis [109]. The below average vasoreactivity of **D** and **E** may indicate increased sensitivity of the vascular endothelium to LDL in males. The abnormal FMD of subject **F** may be due in part to biweekly, rather than weekly, HELP therapy [101]. Also, subject **F** has Raynaud's phenomenon, a syndrome associated with high plasma levels of the potent vasoconstrictor endothelin [182]. The observed variation of vasoreactivity between

[4]One could argue that this subject demonstrated a larger flow-mediated dilation *pre-HELP* because the peak dilation relative to the pre-release diameter is greater pre-HELP. As a result of arterial constriction during the low-flow state, the dilation immediately after cuff release may be a combination of active flow-mediated dilation and passive return to pre-occlusion diameter. Therefore, interpretation of the peak dilation relative to the pre-release diameter, which has not been described prior to this work, is unclear. We discuss only the peak dilation relative to the pre-occlusion diameter, which is the commonly-reported parameter of peripheral vasoreactivity, and is known to decrease with hypercholesterolemia [29, 150].

HELP-subjects and the consistency of repeated measurements on a given subject are evidence of the individual specificity of our measurement technique.

The vast majority of peripheral arterial vasoreactivity measurements are still conducted with the original technique introduced by Celermajer et al. [29] to study groups of subjects. This technique measures arterial diameter only twice: once before inflation of a blood pressure cuff around the forearm or thigh, and again about 1 minute after release of a five-minute vascular occlusion. Measurement of arterial diameter at only two points precludes specification of abnormalities, may underestimate the peak dilation, and could lead to improper interpretation of the results. For example, in Figure 7-3, the 2 point measurement would not have detected the dramatic change in diameter slope during occlusion, which could lead to a misinterpretation of the subject's vasoreactivity. Because the role of the endothelium and nitric oxide is uncertain in the time-series vasoreactivity measurements presented here, we attempted to avoid using the term "endothelium-dependent dilation." The use of nitric-oxide synthase inhibitors in a similar study would be necessary to clarify this role.

7.3.2 Intima-Media Thickness

Our results indicate that HELP therapy may reduce IMT progression in the distal common carotid artery. The mean baseline common carotid IMT of the 7 HELP subjects, who had been treated weekly or biweekly for 3 to 5 years prior to this study, was 582 $\pm$ 32μm. The mean age of the HELP subjects was 40.7 $\pm$ 5.2 years. The ARIC study [89] reported a median common carotid IMT for 45 year old subjects of 540 to 620μm. The IMT of the HELP subjects, whose untreated plasma cholesterols are well above the 95th percentiles for their age, should have been, but were not, well above average for their age. Wendelhag et al. [174] demonstrated significantly increased common carotid IMT in subjects with FH, compared with matched normocholesterolemic subjects. The annual change in IMT of the HELP subjects (-3.0 $\pm$

17.4μm/year) suggests a trend toward regression or minimal progression. For comparison, Howard et al. [89] measured an increase in carotid IMT of 10μm/yr in a randomly selected population of 13,870 men and women aged 45-64 years. Mack et al. [112], Salonen et al. [137], and Crouse et al. [45] reported annual carotid IMT increases of 18, 28, and 46μm/year, respectively, in subjects with known coronary artery disease. The latter two values may be higher because the annual changes in maximum IMT, rather than mean IMT, were measured. Our results agree with those of Hennerici et al. [78] who reported regression of carotid plaque volume in some HELP patients in as little as 6 months and in all HELP patients within 12 months of treatment initiation.

7.4 CONCLUSIONS

- Subjects with severe familial hypercholesterolemia participating in HELP therapy had nearly normal peripheral artery vasoreactivity.
- On average, the vasoreactivity did not change immediately after HELP treatment, perhaps because vasoreactivity had been maximally normalized by at least 3 years of treatment prior to this study.
- One HELP subject consistently demonstrated a significant change in vasoreactivity after treatment. This may represent an important genetic difference in this subject. This result also suggests that our system can detect differences among individuals.
- The mean common carotid intima-media thickness in the HELP subjects, who had been treated for at least 3 years prior to this study, was equal to the medain value of an age-matched random population sample. The measured annual change of IMT in the HELP subjects suggested regression or mild progression.

Table 7-1: Blood pressure, plasma lipids, and lipoproteins (Mean ± SEM).

	pre-HELP	**post-HELP**	**Control**	p_1^*	p_2^{**}
Systolic BP (mmHg)	118.8±4.5	117.2±4.1	112.5±4.0	NS	NS
Diastolic BP (mmHg)	69.5±1.7	66.8±2.0	72.7±2.4	NS	NS
LDL-C (mg/dl)	309.8±48.4	93.1±16.7	103.5±9.4	$< .0001$	$< .0001$
HDL-C (mg/dl)	58.6±6.6	48.2±6.7	61.8±4.3	$< .0001$	NS
Trigly. (mg/dl)	181.5±41.1	92.3±24.4	94.8±11.8	$< .0001$	0.004
Total-C (mg/dl)	404.7±42.7	159.8±12.4	184.2±11.0	$< .0001$	$< .0001$

* Significance level for pre-HELP / post-HELP comparison.

** Significance level for pre-HELP / Control comparison.

NS = not significant

Table 7-2: Mean vasoreactivity parameters.

Vasoreactivity Parameter	**Pre-HELP**	**Post-HELP**	**Control**
Half-Time of Decay of Hyperemia (sec)	18.4	16.9	25.8
Diameter Slope During Occlusion (μm/sec)	-0.081	0.025	0.058
Time to Onset of Dilation (sec)	29.4	29.7	31.3
Time to Peak Dilation (sec)	60.3	66.8	70.0
ΔD (Peak - Pre-Occlusion) (mm, %)	0.301, 7.88%	0.303, 8.77%	0.330, 9.35%
ΔD (Peak - Pre-Release) (mm, %)	0.286, 7.45%	0.248, 6.92%	0.292, 8.32%
$\overline{\Delta D}$ Relative to Pre-Occlusion (mm, %)	0.176, 4.61%	0.187, 5.37%	0.225, 6.32%
$\overline{\Delta D}$ Relative to Pre-Release (mm, %)	0.161, 4.20%	0.132, 3.98%	0.188, 5.33%

ΔD = change in diameter. $\overline{\Delta D}$ = mean change in diameter.

There was no significant difference between the pre- and post-HELP or between the pre-HELP and control groups, by multivariate analysis.

Chapter 8

Plasma Homocysteine and Vasoreactivity

Elevated plasma homocysteine is now widely recognized as an independent risk factor for atherosclerosis [20, 35, 88, 133, 141]. There are two general types of hyperhomocysteinemia: fasting and post-methionine load (PML) [20]. Both forms of hyperhomocysteinemia may result from vitamin deficits or metabolic abnormalities, and both forms convey increased risk for atherosclerosis. Fasting hyperhomocysteinemia can result from low levels of vitamins B12 and folate, and from abnormalities in the enzymes cystathionine β-synthase and methylenetetrahydrofolate reductase [133]. For PML hyperhomocysteinemia, demethylation of ingested methionine in-vivo results in a temporary increase in plasma homocysteine; the extent of the increase varies widely among subjects. Low levels of vitamin B6 are thought to contribute to PML hyperhomocysteinemia [20].

Homocysteine is a highly reactive amino acid which may damage endothelial cells and impair the release of endothelium-derived relaxing factor [74, 155, 171]. Celermajer et al. [30] discovered abnormal brachial artery vasoreactivity in subjects with homozygous homocystinurea, a condition that results in extremely high plasma homocysteine levels and early atherosclerosis. Our technique of assessing vasoreactivity

is more accurate and provides more information than that of Celermajer. We may therefore be able to detect abnormal vasoreactivity in subjects with mildly elevated plasma homocysteine, and we may be able to characterize the abnormalities in vasoreactivity associated with hyperhomocysteinemia.

We hypothesized that acute increase in plasma homocysteine after ingestion of methionine may cause acute change in vasoreactivity. To test this hypothesis, we measured vasoreactivity before and after ingestion of 100 mg/kg methionine in 10 subjects. We show rapid but temporary inhibition of endothelium-dependent dilation in a subject with high fasting and PML plasma homocysteine levels, and a significant delay in PML endothelium-dependent dilation in the group of subjects.

8.1 METHODS

8.1.1 Subjects

Ten subjects were initially included in the study. One subject completed the study but was subsequently excluded due to discovery of hypercholesterolemia (LDL = 162mg/dl). The study of a second subject was not completed due to technical difficulty during data acquisition. The remaining 8 subjects (4 males and 4 females, average age 27.8 $\pm$ 2.1 [mean $\pm$ SEM] years) were normocholesterolemic, nonhypertensive, nonsmokers, nondiabetic, and were free of significant family history of premature atherosclerosis (Stroke, myocardial infarction or revascularization procedure in any first degree relative before age 60). The subjects had not taken multivitamin supplements for at least 6 weeks prior to the study. Plasma cholesterol, LDL, HDL and triglycerides were measured according to standard methods [62, 76]. Table 8-1 lists the blood pressures and cholesterol levels of the 8 subjects. All subjects provided informed consent and the study was approved by the Massachusetts Institute of Technology Committee on the Use of Humans as Experimental Subjects.

8.1.2 Measurement Protocol

Subjects fasted overnight before the study. On the morning of the study, resting blood pressure was measured, followed by insertion of a 21 gage Butterfly catheter into a right arm vein. Twenty cubic centimeters of blood was removed from the catheter for measurement of fasting plasma lipids and homocysteine. During the study, the catheter was constantly flushed with physiological saline drip at a rate of 30-40 cc/hr. After catheter insertion, the subjects rested quietly for at least 30 minutes. Brachial artery and forearm microvascular vasoreactivity were then measured twice according to the methods of Chapter 5, with at least a 20 minute interval between the end of the first measurement and the start of the second measurement. The subjects then ingested 100mg/kg of L-methionine (Aginomoto, Teaneck, NJ), mixed in 200cc of orange juice, and were offered a standardized snack low in methionine ($<$ 15mg). Two hours and four hours after the methionine load, 10cc of blood was removed from the catheter for homocysteine assay, and vasoreactivity measurements were repeated. Finally, common carotid intima-media thickness (IMT) was measured bilaterally according to the methods of Chapter 6, and the catheter was removed.

Measurement of total plasma homocysteine was performed by a modified method of that originally defined by Araki and Sako [7]. Measurement of brachial artery diameter for assessment of vasoreactivity was conducted by a observer who was blinded to plasma homocysteine levels and to the chronological order of the studies.

8.1.3 Statistical Analysis

Single parameters were compared with the Wilcoxon Sign-Rank test for paired data [37]. The relation between variables was assessed by linear regression analysis. Statistical significance was inferred at a p value <0.05.

8.2 RESULTS AND DISCUSSION

Mean ± SEM plasma homocysteine levels were 8.5±1.2 μmol/L at baseline, 20.2±2.6 μmol/L two hours PML, and 24.5±2.9 μmol/L four hours PML ($p < 0.01$ for all comparisons). One subject had mildly elevated fasting homocysteinemia (15.4 μmol/L, which was more than 2 standard deviations above the mean).[1]

The top panel of Figure 8-1 shows normal vasoreactivity at baseline, but rapid and temporary inhibition of flow-mediated dilation post methionine load (PML) in the subject with mild fasting hyperhomocysteinemia. Vasoreactivity was profoundly abnormal 2 hours PML, but returned to normal by the next day. To our knowledge, this is the fastest reported degradation in human vasoreactivity. The subject reported no symptoms during the study. Plasma homocysteine was 15.4μmol/L at baseline, 33.7μmol/L two hours PML, 38.4μmol/L four hours PML, and 20.7μmol/L twenty-six hours PML. The peak flow velocities were 137 cm/sec for the first baseline, 154 cm/sec for the second baseline, 135 cm/sec two hours PML, 177 cm/sec four hours PML, and 167 cm/sec twenty-six hours PML. Therefore, the observed changes in flow-mediated dilation PML cannot be attributed to changes in the flow stimulus. For comparison, the bottom panel of Figure 4 shows no change in the maximum brachial artery dilation in a normal subject after an equivalent dose of methionine. Plasma homocysteine in this subject was 8.1μmol/L at baseline, 15.3μmol/L two hours PML, and 18.3μmol/L four hours PML.

The mean±SEM of the 8 vasoreactivity parameters (defined in Appendix A) for the baseline and PML measurements are listed in Table 8-2. Because the subject with mild fasting hyperhomocysteinemia did not exhibit flow-mediated dilation PML, the time to onset of dilation and time to peak dilation were determined from the remaining 7 subjects. By comparing the mean of the two baseline measurements

[1] Although studies have demonstrated an incremental risk for atherosclerosis with increasing levels of fasting homocysteine, without a threshold effect [133], fasting homocysteine above 14 μmol/L is generally considered to be abnormal [133, 141].

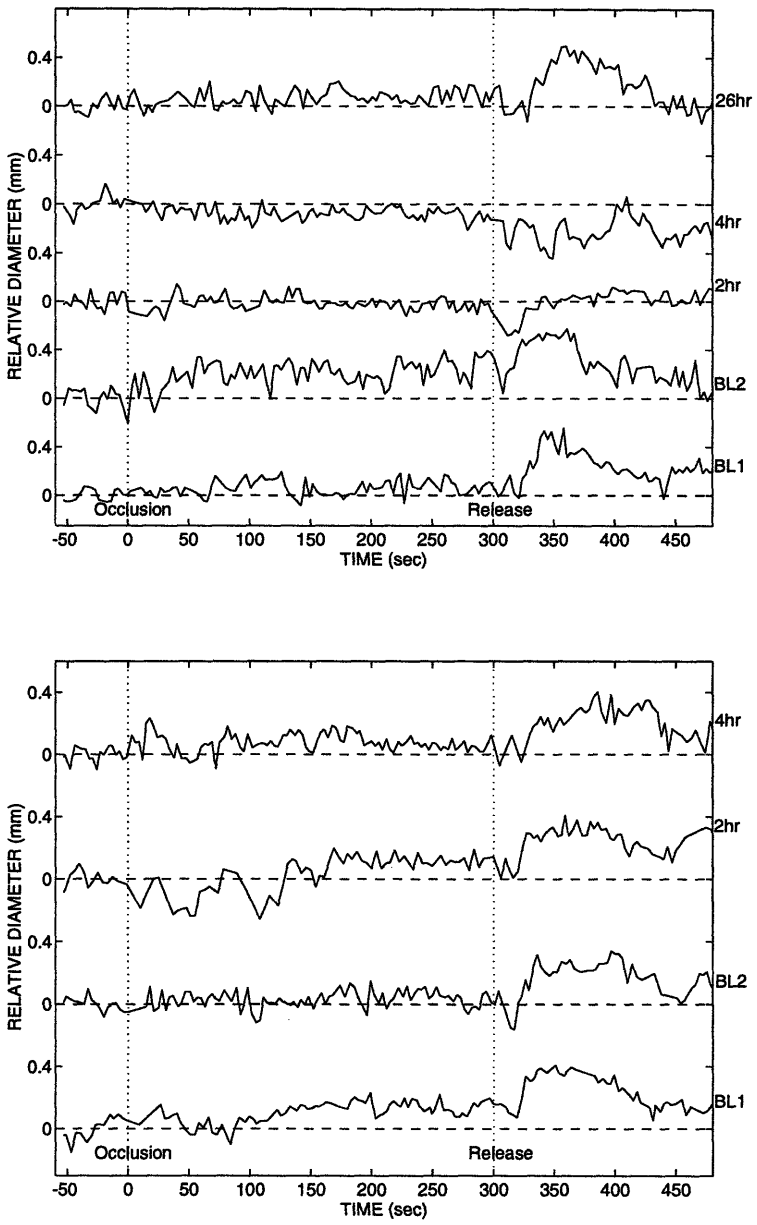

Figure 8-1: Changes in vasoreactivity post methionine load (PML), consisting of 100mg/kg of L-methionine in 200cc of orange juice. Two baseline (BL1 and BL2) measurements were acquired before loading and post-loading times are indicated. **Top:** This subject demonstrated a profound temporary loss of flow-mediated dilation PML. Plasma homocysteine was 15.4μmol/L at baseline, 33.7μmol/L two hours PML, 38.4μmol/L four hours PML, and 20.7μmol/L twenty-six hours PML. **Bottom:** The vaoreactivity of this subject was not affected by an equivalent dose of methionine. Plasma homocysteine in this subject was 8.1μmol/L at baseline, 15.3μmol/L two hours PML, and 18.3μmol/L four hours PML.

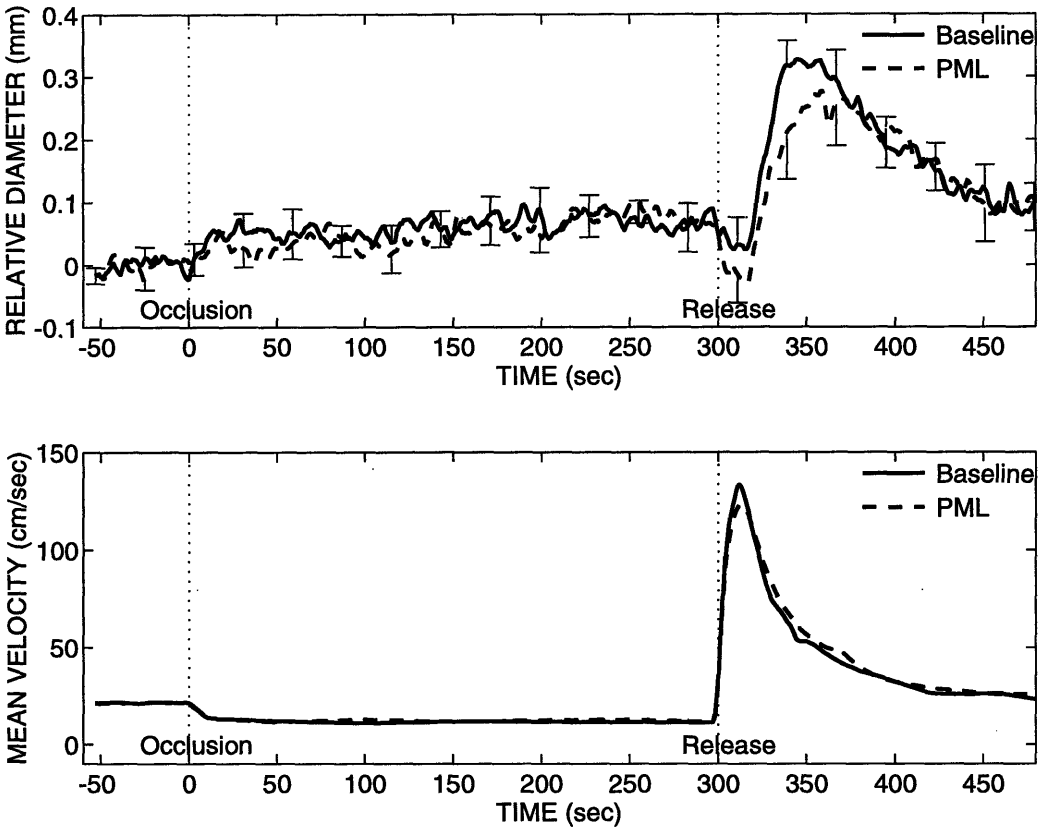

Figure 8-2: The mean of 16 baseline vasoreactivity measurements (2 measurements on each of 8 subjects) compared with the mean of 16 measurements PML (8 measurements 2 hours PML and 8 measurements 4 hours PML). The error bars indicate representative values of the SEM. The SEM for the flow measurements was always less than 7 cm/sec.

from each subject with the mean of the two PML measurements from each subject, the time to onset of dilation and the time to peak dilation were significantly delayed PML ($p = 0.039$ and $p = 0.016$, respectively). Other laboratories do not measure these two parameters. The delay in flow-mediated dilation may be attributed to either a decrease in the rate of production of NO or a decrease in response of the smooth muscle cells. These two categories of abnormalities could be differentiated by measuring the response to an exogenous form of NO at baseline and PML.

Figure 8-2 compares the mean of the baseline vasoreactivity measurements to the mean of the PML vasoreactivity measurements. Prior to release of the occlusion, the PML vasoreactivity was similar to the baseline vasoreactivity. After release of

occlusion, the brachial artery demonstrated a larger initial constriction PML and a delayed and diminished flow-mediated dilation. The decrease in peak flow-mediated dilation PML was almost entirely due to the subject with fasting hyperhomocysteinemia (whose vasoreactivity measurements are displayed at the top of Figure 8-1). Therefore, the average decrease in flow-mediated dilation PML was not statistically significant. The baseline and PML flow measurements were similar.

The mean common carotid IMT of the 8 subjects was 454±34 μm. No significant correlations were found between plasma homocysteine levels and IMT, IMT divided by subject age, or vasoreactivity parameters. The absence of significant correlations may be due to a lack of variability in homocysteine levels and vasoreactivity measurements: 7 subjects were normal and 1 subject was abnormal. A larger study containing subjects with a range of homocysteine levels and PML responses would be more appropriate for regression analysis.

Celermajer et al. [30] reported no correlation between flow-mediated dilation and plasma homocystine levels in subjects with homozygous homocystinurea. He reported a significant reduction in flow-mediated dilation in 9 children with homozygous homocystinurea, but normal flow-mediated dilation in the obligate heterozygous parents of the children. Fasting total plasma homocysteine in heterozygous homocystinurics averages 13.8±1.6 μmol/L [24], similar to that of our subject with mild fasting hyperhomocysteinemia. Therefore, the heterozygotes studied by Celermajer would probably behave similarly to our subject with hyperhomocysteinemia after methionine loading. The method used by Celermajer for assessing vasoreactivity, measurement of brachial artery diameter at two times, would probably misinterpret our discovery of a significant delay in flow mediated dilation PML as a decrease in flow-mediated dilation PML.

8.3 CONCLUSIONS

From this study, we conclude the following:

- Rapid increase in plasma homocysteine levels after methionine loading can acutely and temporarily inhibit flow-mediated vasodilation.
- Our technique appears to be sufficiently sensitive to assess individual differences in methionine/homocysteine metabolism.
- On average, acute increase in plasma homocysteine level after methionine loading resulted in a delay in the onset of and the time to peak flow-mediated dilation. The mechanism of this effect is not known.

Table 8-1: Blood pressure, plasma lipids, and lipoproteins (Mean ± SEM).

Systolic BP (mmHg)	111.8±3.6
Diastolic BP (mmHg)	73.3±1.9
LDL-C (mg/dl)	102.6±9.7
HDL-C (mg/dl)	60.9±3.4
Trigly. (mg/dl)	84.6±9.2
Total-C (mg/dl)	180.5±10.7

Table 8-2: Vasoreactivity parameters (Mean ± SEM).

Vasoreactivity Parameter	**Baseline**	**2hr PML**	**4hr PML**
Half-Time of Decay of Hyperemia (sec)	20.3±3.1	30.6±7.3	22.8±2.2
Diameter Slope During Occl. (μm/sec)	0.09±0.12	0.32±0.14	0.15±0.09
Time to Onset of Dilation (sec)†	23.2±1.9	33.9±4.9	31.3±1.5
Time to Peak Dilation (sec)†	54.0±5.7	70.8±5.9	65.3±5.9
ΔD (Peak - Pre-Occlusion) (mm)	0.360±0.039	0.338±0.061	0.295±0.056
ΔD (Peak - Pre-Release) (mm)	0.294±0.037	0.264±0.034	0.212±0.040
$\overline{\Delta D}$ Relative to Pre-Occlusion (mm)	0.247±0.040	0.244±0.060	0.192±0.059
$\overline{\Delta D}$ Relative to Pre-Release (mm)	0.179±0.038	0.169±0.026	0.110±0.043

† These parameters are reported for 7 subjects, because one subject did not exhibit flow-mediated dilation PML. These parameters are also significantly different PML compared with baseline.

ΔD = change in diameter. $\overline{\Delta D}$ = mean change in diameter.

Chapter 9

Vasoreactivity in Smokers

Cigarette smoking is the primary preventable risk factor for atherosclerosis. Previous studies have shown that smokers have a two- to fourfold greater risk of coronary artery disease than non-smokers, and increased risk of stroke and peripheral arterial occlusive disease [59, 164]. Although the causal relationship between smoking and atherosclerosis is strongly supported, the exact mechanisms by which smoking promotes atherosclerosis are unclear. Smoking is known to increase platelet activation and aggregation [14, 103], increase monocyte adherence to the endothelium [49], decrease production of prostacyclin [118], detrimentally modify the plasma lipid profile [42], and damage vascular endothelium [16, 97, 127]. The latter may be the most important pathologic effect of smoking on the vasculature, because endothelial damage can account for many of the other effects and is strongly associated with atherogenesis.

Endothelial damage can be assessed, in part, by measurement of vasoreactivity. Celermajer et al. demonstrated a dose-dependent decrease in flow-mediated dilation of the brachial artery in smokers [31] and in passive smokers [33]. Zeiher et al. demonstrated reduced flow-mediated dilation in the coronary arteries of smokers [185]. These studies were limited because they assessed flow-mediated dilation at only two time points (before and after the flow stimulus) and because they did not differentiate

between vasoreactivity immediately after smoking and vasoreactivity after several hours without smoking.

In this Chapter, we report the effects of smoking on time-series measurements of peripheral artery vasoreactivity. Measurements were conducted on 8 smokers, both immediately after smoking and after at least 2 hours without smoking, and on 8 control subjects with no risk factors for atherosclerosis. We demonstrate profound changes in vasoreactivity associated with withdrawal from smoking. This data may provide insight into the pathogenesis of smoking-induced atherosclerosis.

9.1 METHODS

9.1.1 Subjects

Eight current smokers (4 females and 4 males, of average age 39.5 $\pm$ 4.2 [mean $\pm$ SEM] years) and 8 non-smoking age-matched control subjects (5 females and 3 males, of average age 40.4 $\pm$ 4.3 years) were included in the study. The smokers had a mean smoking history of 18.8 pack years. All of the subjects were clinically well, and all were normocholesterolemic, normotensive, nondiabetic, and free of significant family history of atherosclerosis. None of the subjects were taking vasoactive medications such as calcium channel blockers, beta blockers, ACE inhibitors, or long-acting nitrates. All subjects provided informed consent and the study was approved by the Massachusetts Institute of Technology Committee on the Use of Humans as Experimental Subjects.

9.1.2 Measurements

A standard blood pressure measurement was acquired from each subject. Measurements of brachial artery and forearm microvascular vasoreactivity were conducted as described in Chapter 5. Two sets of vasoreactivity measurements were acquired from

the smokers: one measurement at least 2 hours after the most recent cigarette and a second measurement within 15 minutes after smoking one cigarette. Two vasoreactivity measurements were collected from each of the control subjects, and were subsequently averaged. Total plasma cholesterol, LDL, HDL, and triglycerides were then measured by standard techniques [62, 76]. Quantitative comparisons of vasoreactivity were accomplished by algorithmic extraction of the diameter slope during occlusion and the peak diameter change after cuff release, relative to the pre-occlusion and the pre-release diameters. The algorithm for extraction of these parameters is described in Appendix A.

9.1.3 Statistical Analysis

Descriptive data are reported as mean $\pm$ SEM. Measurement parameters were compared with the Wilcoxon sign-rank test for paired data (i.e., smokers pre-cigarette compared with post-cigarette) and Wilcoxon rank-sum test for unpaired data (i.e., smokers pre-cigarette compared with controls) [37]. Statistical significance was assumed if a null hypothesis could be rejected at the 0.05 probability level.

9.2 RESULTS

Figure 9-1 compares the vasoreactivity of the smokers pre-cigarette (i.e., after at least 2 hours without a cigarette) with that of the nonsmoking control subjects. The pre-cigarette smokers demonstrated marked constriction of the brachial artery during the low-flow state, and decreased dilation of the brachial artery after cuff release. Figure 9-2 compares the vasoreactivity of the smokers pre-cigarette with that immediately after smoking one cigarette. Smoking acutely returned the vasoreactivity of the smokers to or towards normal values.

Table 9-1 compares the age, blood pressure, pulse rate, plasma cholesterol, and vascular parameters of the three subject groups. The slope of arterial diameter dur-

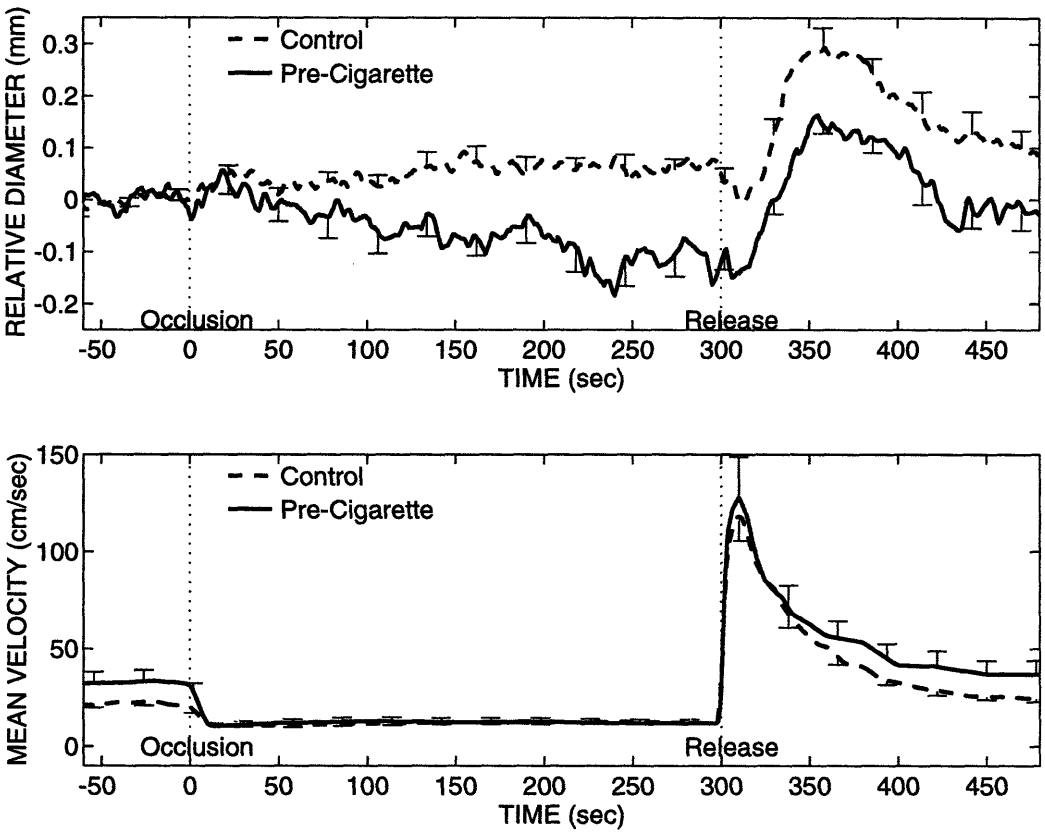

Figure 9-1: The mean of vasoreactivity measurements from 8 smokers who refrained from smoking for at least two hours, compared with measurements from 8 nonsmoking control subjects. The unilateral error bars indicate representative values of the SEM.

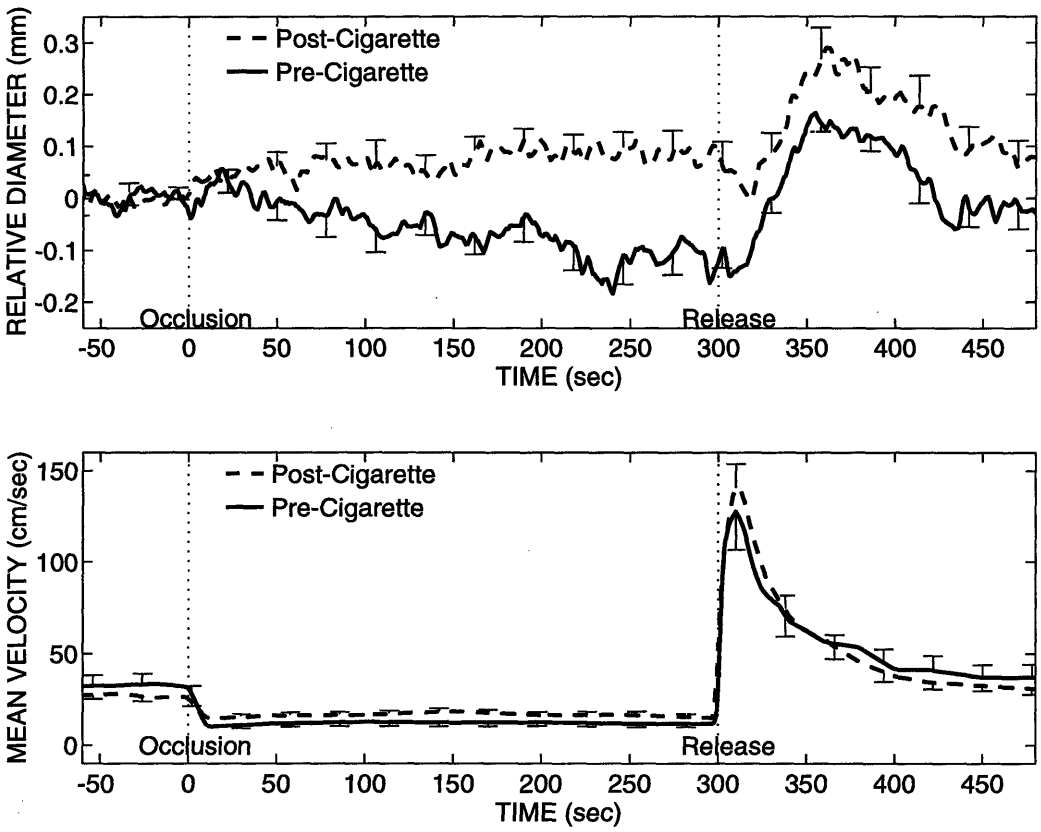

Figure 9-2: The mean of vasoreactivity measurements from 8 smokers before and after smoking a single cigarette. Before smoking, the subjects refrained from smoking for at least 2 hours. Compared with Figure 9-1, smoking acutely normalized the vasoreactivity of the chronic smokers. The unilateral error bars indicate representative values of the SEM.

ing the low-flow state and the maximum change in post-release diameter relative to pre-occlusion diameter were significantly smaller, whereas the baseline flow velocity and the pulse rate were significantly larger, in the pre-cigarette smokers compared with the nonsmoking control group. Comparison of the smokers before and after smoking one cigarette revealed a significant increase in the pulse rate, slope of arterial diameter during the occlusion, and the maximum change in post-release diameter relative to pre-occlusion diameter, while the baseline blood velocity in the brachial artery significantly decreased after smoking.

Figures 9-3 and 9-4 compare individual measurements of the baseline flow velocity, diameter slope during occlusion and peak dilation after cuff release. Figure 9-3 compares the pre-cigarette smokers with the nonsmoking control group and Figure 9-4 compares the smokers before and after smoking. Despite the small size of the groups, the smokers are distinct from the control subjects in these three parameters, and smoking one cigarette acutely changes each of the parameters to or toward normal values.

9.3 DISCUSSION

Our results demonstrate profound abnormalities in brachial artery vasoreactivity in smokers who temporarily refrain from smoking, and a return to or towards normal vasoreactivity immediately after smoking. Both the slope of the arterial diameter during the low-flow state and the peak arterial dilation relative to the pre-occlusion diameter increased significantly to or towards normal values after smoking. These results are somewhat counterintuitive; one might expect the acute effects of smoking to be detrimental to vasoreactivity, because smoking is associated acutely with myocardial ischemia and angina.

Celermajer et al. reported a reduction in "flow-mediated dilation" of the brachial artery in smokers [31] and passive smokers [33]. These measurements were based

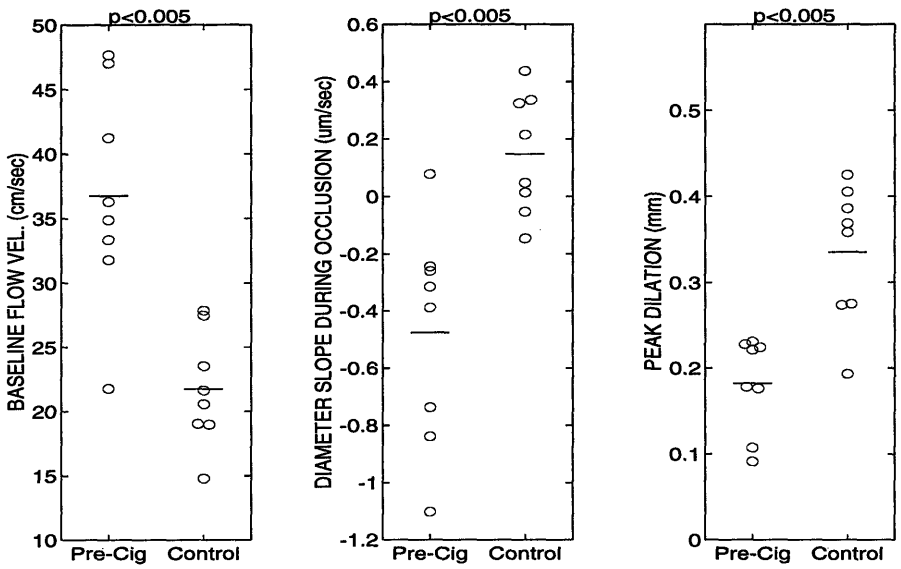

Figure 9-3: The baseline flow velocity (left), slope of diameter during the low-flow state (middle), and the maximum post-release dilation relative to the pre-occlusion diameter (right) in 8 smokers who refrained from cigarettes for at least 2 hours, compared with 8 nonsmoking control subjects. The bars indicate mean values.

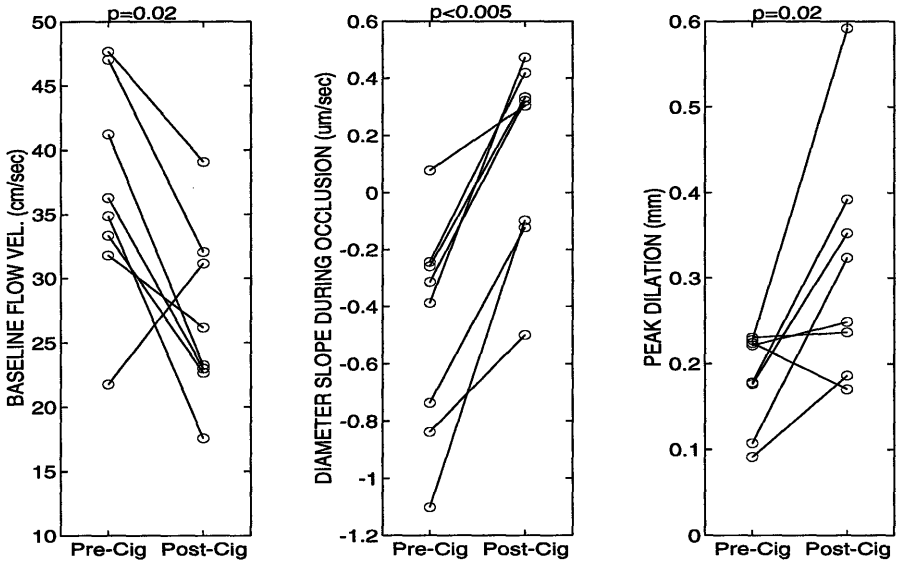

Figure 9-4: The baseline flow velocity (left), slope of diameter during the low-flow state (middle), and the maximum post-release dilation relative to the pre-occlusion diameter (right) in 8 smokers before and after smoking a single cigarette. Acute changes in these parameters after smoking are all in the direction of the results from nonsmoking control subjects, shown above.

upon the arterial dilation 45 to 60 seconds after release of a 5 minute forearm vascular occlusion, relative to the diameter before inflation of the blood pressure cuff. Celermajer reported a mean "flow-mediated dilation" of 10% for the control subjects and 4.0% for smokers with a mean smoking history of 16 pack years [31]. Our results are similar (mean dilation of 9.5% for the control subjects and 4.7% for the pre-cigarette smokers, who had an average smoking history of 18.8 pack years).[1] As demonstrated by the present work (Figure 9-2), the arterial dilation relative to the pre-occlusion diameter depends upon the time since the last cigarette. The smokers in Celermajer et al. [31] were characterized only as having at least one cigarette in the 12 hours before being studied.

Results such as those in Figure 9-2 cast doubt on the proper use of the term "flow-mediated dilation" when describing the change in diameter after release of the cuff. Dilation of the brachial or radial artery in response to increased shear stress has been demonstrated conclusively to result, at least in part, from endothelium-derived nitric oxide [92, 110], a process often called "flow-mediated dilation". However, these studies were conducted on healthy, nonsmoking subjects, whose arteries presumably did not constrict during the low-flow state. In arteries that constrict during the low-flow state (e.g., Figure 7-3, Figure 9-2, and Filitti et al. [60]), the dilation after release of the cuff may be due to a combination of true flow-mediated dilation and simple return of the artery to its basal diameter. We therefore cannot conclude that the significant increase in post-cuff-release dilation after smoking (c.f. Figures 9-2 and 9-4) represents a significant increase in endothelium-dependent or flow-mediated dilation. As we concluded in Chapter 7, the use of nitric-oxide inhibitors with our vasoreactivity measurement technique would be necessary to clarify the role of the endothelium in the observed vasoreactivity.

[1] We prefer to report the absolute dilation, rather than the percent dilation, because smaller arteries are known to produce larger percent dilations than larger arteries [5, 29], and smokers are known to have larger baseline brachial diameters than nonsmokers e.g., Table 9-1 and [31, 33]. Therefore, smokers are inherently biased to have smaller percent dilations.

Vasoreactivity measurements that are based upon diameter measurements at only two time points: before and after temporary forearm vascular occlusion, e.g. [5, 8, 29, 109, 170], overlook the important vasoreactivity that occurs during the low-flow state. We believe that arterial constriction during the low-flow state and reduced dilation in response to a high-flow stimulus are equally important signs of abnormal vasoreactivity. It is interesting to note the similarity between the vasoreactivity of smokers who refrain from smoking (Figure 9-2) and hypercholesterolemic subjects (Figure 7-3 and [60, 150]). In the future, vasoreactivity measurements should include at least three diameter measurements: before cuff inflation, before cuff deflation, and about one minute after cuff deflation.

The current study did not address the cause of abnormal vasoreactivity when smokers refrain from smoking. The abnormal vasoreactivity pre-cigarette and the normalization of vasoreactivity post-cigarette are suggestive of "withdrawal" from a vasoactive substance, perhaps nicotine. Subsequent studies with nicotine supplementation can address this hypothesis. This study also did not address the duration of the "post-cigarette normalization" of peripheral vascular vasoreactivity, or the duration of the abnormal vasoreactivity when chronic smokers permanently quit smoking. Other studies have shown that the reduction of "flow-mediated dilation" in smokers and in passive smokers is dose dependent [31, 33] and appears to be reversible with cessation of smoking over a period of several years [31, 81].

9.4 CONCLUSIONS

- Smokers who temporarily abstain from smoking (for at least 2 hours) demonstrate significantly higher baseline flow velocity in the brachial artery, significant arterial constriction in a low-flow state, and significantly reduced dilation after release of a 5-minute forearm vascular occlusion.
- The above are significantly improved (toward normal values) immediately after smoking one cigarette.
- These results suggest that a portion of the abnormal vasoreactivity in chronic smokers is due to withdrawal from a vasoactive substance, perhaps nicotine.

Table 9-1: Mean ± SEM of the measured parameters ($n = 8$ for each group).

Parameter	**Pre-Cig.**	**Post-Cig.**	**Control**
Age (years)	39.5±4.2	—	40.4±4.3
Systolic BP (mmHg)	113.9±4.1	114.6±4.4	108.9±5.3
Diastolic BP (mmHg)	66.4±3.1	69.3±2.2	70.5±3.3
Pulse (BPM)	80.9±4.1	90.0±4.0**	64.4±2.1**
Total-C (mg/dl)	192.3±20.0	—	186.6±11.1
LDL-C (mg/dl)	117.0±16.8	—	105.3±10.0
HDL-C (mg/dl)	57.5±3.9	—	63.4±5.6
Triglycerides (mg/dl)	98.3±12.9	—	90.6±17.3
BL Diameter (mm)	3.9±0.2	3.9±0.3	3.6±0.3
BL Flow Velocity (cm/sec)	36.8±3.0	26.9±2.4*	21.7±1.6**
Peak Flow Velocity (cm/sec)	146±18	143±14	127±13
Slope† (μm/sec)	-0.48±0.14	0.14±0.12**	0.15±0.07**
ΔD_1 (mm)	0.18±0.02	0.31±0.05*	0.34±0.03**
ΔD_2 (mm)	0.30±0.04	0.23±0.04	0.27±0.03

*: $p < 0.025$ relative to Pre-Cig.

**: $p < 0.005$ relative to Pre-Cig.

C: Cholesterol

BL: Baseline

†: The slope of temporal changes in arterial diameter during the occlusion

ΔD_1: Maximum change in post-release diameter relative to pre-occlusion diameter.

ΔD_2: Maximum change in post-release diameter relative to pre-release diameter.

Chapter 10

Summary and Future Directions

Peripheral vascular ultrasound is a powerful noninvasive and inexpensive technique for assessment of vascular health. Traditionally, the technique has been applied to the assessment of late-stage atherosclerosis, i.e., grading peripheral arterial stenosis. Recently, measurements of arterial vasoreactivity, intima-media thickness, and distensibility have been proposed to study early stages of atherosclerosis. These methods offer new insight to the disease, but the simplicity of the measurement methodology to date has constrained their application.

10.1 SUMMARY

The primary goal of this thesis was to improve upon the above methods for ultrasonic assessment of early atherosclerosis, so that more of the potential of these measurements can be realized. We began by exploring the application of high-resolution echo-tracking methods to the measurement of vasoreactivity. These methods offered the highest known resolution for noninvasive measurement of change in arterial diameter. However, we discovered that the tracking was not robust over the long duration of vasoreactivity measurements. Errors were introduced into the tracking algorithm by motion of the tissue in directions other than the direction of insonation. The

tracking was sufficiently robust, however, for short-duration measurements of arterial distensibility. Tracking errors occurred rarely in distensibility measurements, and the presence of errors could be detected by comparing the tracking results to the original radio-frequency data. The detection of tracking errors is a unique feature of our system.

Our second attempt at high resolution measurement of vasoreactivity involved measurement of change in arterial diameter from B-mode ultrasound images. We argued that the standard technique for measuring arterial diameter, ultrasonic calipers, was subjective and did not make full use of the diameter information available in the image. Also, the standard technique for measuring vasoreactivity, calculation of the difference between caliper measurements at two times, did not make full use of the available temporal information. We improved the accuracy of diameter measurements by applying automated edge detection and model-based estimation techniques. The variability of the time series of diameter estimates was additionally reduced by acquiring images in the skew plane (i.e., a plane rotated about 10 degrees off axis of the artery) and by conducting edge-detection in consistent locations over time. Temporal resolution was exploited in estimates of diameter change by smoothing the diameter time-series measurements.

We then applied the high spatial and temporal resolution of our methods to characterize the response of the human brachial artery after release of a 5-minute forearm vascular occlusion. We demonstrated an initial decrease in brachial artery diameter after release of forearm vascular occlusion, and a delay of 15-30 seconds after release of occlusion for onset of flow-mediated dilation of the brachial artery. The vasoreactivity measurements and the characterization of human peripheral vasoreactivity were then extended to include the periods before, during, and after the forearm vascular occlusion. From the extended measurements, 8 parameters of vasoreactivity were proposed and the reproducibility of the parameters was measured.

The same edge detection techniques were then applied to measurement of common

carotid intima-media thickness (IMT) from B-mode ultrasound images. The accuracy of the measurements was comparable to a similar automated system, but significantly better than other systems that are based on subjective, manual techniques.

The second major goal of this thesis was to test the clinical utility of the new measurement methods. Of the three methods, we decided to focus on vasoreactivity measurements, because of their potential for individual specificity and because of the quantity of potentially-diagnostic information available from our technique. We realized that a complete exploration of the clinical significance of our vasoreactivity measurements would be beyond the scope of a thesis and resolved to conduct several pilot studies to demonstrate potential clinical value.

The first study involved subjects with severe familial hypercholesterolemia that were participating in chronic Heparin-induced Extracorporeal LDL Precipitation (HELP) therapy. Although other laboratories had consistently demonstrated profound abnormalities in flow-mediated dilation of hypercholesterolemic subjects, we found no significant difference in flow-mediated dilation or any of our vasoreactivity parameters between the HELP subjects and matched control subjects with no risk factors for atherosclerosis. On average, the vasoreactivity did not change immediately after LDL removal with HELP, perhaps because the subjects had been treated chronically before our study. However, one HELP subject consistently demonstrated a significant change in vasoreactivity after HELP. This probably represents an important genetic difference in this subject, and suggests individual sensitivity of our measurements. Finally, measurement of HELP subject IMT suggested a reduced rate of IMT progression during chronic therapy.

Next, we measured changes in vasoreactivity after acute increase in plasma homocysteine level via ingestion of methionine. We found rapid but temporary attenuation of flow-mediated dilation in one subject with a high fasting homocysteine level. On average, ingestion of methionine resulted in a significant delay in the time to onset of, and time to peak flow-mediated dilation. This study also suggested individual

sensitivity of our methods.

Finally, we studied vasoreactivity in smokers. We found that habitual smokers who refrained from smoking for at least two hours before measurement of vasoreactivity exhibited profound constriction of the brachial artery during distal occlusion, and reduced dilation of the brachial artery after release of occlusion. Smoking a single cigarette acutely returned the vasoreactivity parameters to or towards normal values, which suggested that the abnormal vasoreactivity in smokers who refrain from smoking may be due to withdrawal from a vasoactive substance such as nicotine. The results from this study were highly specific, achieving a high level of significance with a small number of subjects.

These pilot studies suggest that our measurements of vasoreactivity may be sufficiently sensitive to detect abnormalities in individuals, and may provide sufficient information to distinguish different types of abnormalities of vasoreactivity. Conclusive substantiation of these claims, and establishment of the clinical significance of abnormalities in vasoreactivity are topics for future studies.

10.2 FUTURE DIRECTIONS

This thesis has served to advance the measurement methodology in a field which is largely in its infancy. Therefore, a great number of studies can follow from this work. In our opinion, the most important research directions are to determine the clinical relevance of vasoreactivity, IMT, and distensibility measurements, and to determine whether these three measurements can answer specific questions about the presence, causes, and course of atherosclerosis with individual specificity. We present below several conceptual studies to address these issues.

Clinical Relevance of Abnormal Vasoreactivity: Although the connection between abnormal vasoreactivity and clinical events such as myocardial infarction and stroke can be indirectly inferred by the connection between abnormal vasoreactivity

and atherosclerosis or risk factors for the disease, the former connection has not been directly demonstrated. This study will be very large (perhaps as a part of the Framingham study) and will result in the association of odds ratios for myocardial infarction or stroke with measurements of vasoreactivity, carotid IMT normalized by subject age, and arterial distensibility. The study design will be similar to any epidemiological study of risk factors for atherosclerosis. Importantly, this study would determine whether the three noninvasive measurements of arterial health are more or less predictive of events than measurement of risk factors for atherosclerosis.

Prediction of Atherosclerosis Progression from Vasoreactivity: The goal of this study is to determine whether an individual's rate of change of carotid artery IMT can be predicted from noninvasive measurements of peripheral arterial vasoreactivity. Measurements of vasoreactivity and IMT will be collected in a large population of subjects. The annual rate of IMT progression will be estimated by dividing the IMT by the age of the subject. Several studies have supported this assumption of linear progression of IMT with age [89, 112]. Multivariate regression will be used to determine the overall power of the combined set of vasoreactivity parameters for predicting the rate of progression of IMT. The expected outcome of this analysis is the establishment of a parameter or a combination of parameters of peripheral vasoreactivity that are predictive of the activity of carotid atherosclerosis, and by extrapolation, of atherosclerosis in other parts of the circulation, including the coronary arteries. Such an outcome would suggest a study of the application of this simple noninvasive technique as a rapidly-responding predictor of the efficacy of treatment of atherosclerotic disease, as described below.

Changes in Vasoreactivity and IMT with Therapy: This study will be performed in dyslipidemic patients who are about to undergo treatment of their lipid abnormalities. The goal is to determine whether therapeutic improvement of peripheral vasoreactivity, a rapid response, is predictive of long-term reduction of plaque volume, a slow response measurable by assessment of common carotid intima-media

thickness (IMT). If a link can be demonstrated between normalization of vasoreactivity and arrest of atherosclerosis in a broad patient population, the concept of "individually-validated anti-atherosclerotic therapy" may be realized.

Measurements of vasoreactivity and bilateral IMT will be collected from untreated hypercholesterolemic subjects, before initiation of therapy. Vasoreactivity measurements will be repeated periodically and carotid IMT will be measured annually. All patients will be treated with appropriate diet and medication for their dyslipidemia. This treatment model is expected to provide a wide range of lipid and lipoprotein changes, since patient compliance and response are highly variable. Multivariate regression will be used to determine the relative power of lipid and vasoreactivity parameters to predict progression of IMT. This study will determine whether or not vasoreactivity measurements can predict the long-term efficacy of anti-atherosclerotic therapy.

Specific Abnormalities in Vasoreactivity: The goal of this study is to determine whether specific abnormalities of vasoreactivity, as defined by our techniques, are associated with specific risk factors for atherosclerosis. Brachial arterial reactivity will be compared among several groups of subjects, e.g., hypercholesterolemics, smokers, hyperhomocysteinemics, hypoalphalipoproteinemics, hypertensives, subjects with a family history of atherosclerosis but no other risk factors, and normal subjects. Parameters of vasoreactivity can be compared among the groups with multivariate analysis of variance (MANOVA), and discriminant analysis can be applied to determine the optimal combinations of parameters to discriminate between the subject groups.

Locating the Source of Abnormal Vasoreactivity: In subjects with a strong family history of atherosclerosis and abnormal vasoreactivity, but no other known risk factors, the source of abnormal vasoreactivity may be characterized by a series of vasoreactivity measurements, such as that displayed in Figure 10-1. We believe that there are 4 fundamental sources of abnormal vasoreactivity: 1.) arteries that are non-compliant and cannot respond to stimuli due to mechanical stiffness, 2.) arteries

with abnormalities in smooth muscle cells, such that the signals for vasoreactivity are not properly received or processed, 3.) arteries that inherently cannot produce vasoactive signals such as nitric oxide, and 4.) arteries that cannot produce vasoactive signals due to the presence of humoral "poisons" such as high cholesterol or homocysteine. The flow chart in Figure 10-1 will allow characterization of the source of abnormal vasoreactivity in individuals. First, the response of the brachial artery to 0.4 mg sublingual nitroglycerine will be measured. This exogenous source of nitric oxide will assess the ability of the vessel to respond to nitric oxide. If the response to nitroglycerine is normal (> 15% dilation [8, 32]), either humoral factors or intrinsic endothelial dysfunction (e.g., defective NO synthase) has caused an inability to produce endogenous nitric oxide. These two possibilities will be differentiated by measuring vasoreactivity 2 hours after oral loading with L-arginine (100 mg/kg), the metabolic precursor to nitric oxide [122]. If vasoreactivity remains abnormal after L-arginine loading, the subject most likely has an abnormality in endothelial nitric-oxide synthase (e-NOS). If the response to both nitroglycerine and oral arginine are normal, unrecognized humoral factors are likely to be the cause of insufficient NO production by e-NOS [129]. If the artery does not dilate normally to nitroglycerine, either the nitric-oxide signal transduction pathway is abnormal or the arteries are noncompliant and cannot dilate. These two cases will be differentiated by a distensibility measurement of the carotid arteries. To our knowledge, inherited abnormalities in humans in the production or signal transduction of nitric oxide have not been described previously. This study may result in the identification of such abnormalities, and may lead to future studies of the genetic basis of these abnormalities.

Role of Nitric Oxide in the Observed Vasoreactivity: Finally, as mentioned in Chapters 7 and 9, the role of endothelium-derived nitric oxide in the vasoreactivity observed by our methods is uncertain. To establish this role, vasoreactivity will be measured before and after intra-arterial administration of the L-arginine agonists L-NMMA or L-NAME, which block production of nitric oxide by nitric-oxide synthase

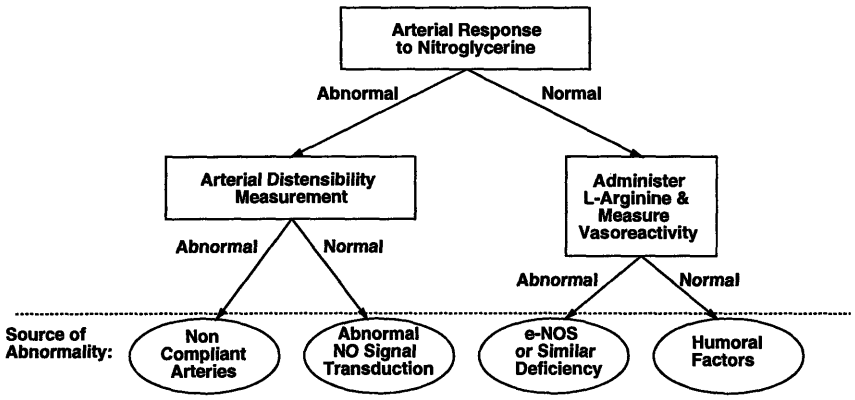

Figure 10-1: Proposed decision tree for localizing the source of abnormal vasoreactivity. Complete characterization of the pathology will provide insight to genetic factors, and may lead to the development of new therapies. NO = nitric oxide, e-NOS = endothelial nitric-oxide synthase

[92, 110]. This experiment will be conducted in subjects with different abnormalities of vasoreactivity, as the contribution of endothelium-derived nitric oxide to vasoreactivity is expected to vary.

If the above studies yield positive results, noninvasive ultrasound techniques such as those described in this thesis may serve as screening tests for early atherosclerosis or risk of atherosclerotic events, and as endpoints for testing and titration of antiatherosclerotic therapies. The end result would be a significant improvement in the prevention of atherosclerosis, and a reduction in health care cost.

Appendix A

Calculation of Vasoreactivity Parameters

The vasoreactivity parameters were automatically calculated from the arterial diameter and flow velocity time series data according to the following algorithm:

The Half Time of Decay of Hyperemia was calculated from the flow velocities between peak flow and 100 seconds after peak flow. The decay rate was determined from a minimum absolute error fit to a single exponential function.

The Diameter Slope During Occlusion was calculated as the slope of a linear regression of the arterial diameter between 20 seconds and 295 seconds after the inflation of the blood pressure cuff.

The diameter and flow velocity time series data was linearly interpolated to achieve a measurement once per second. The pre-occlusion diameter was calculated as the average diameter before cuff inflation and the pre-release diameter was calculated as the average diameter from 40 seconds before to 5 seconds before release of the cuff. The diameter data was then smoothed with a Parks-McClellan lowpass filter [113] of 15 seconds duration.

The Time to Onset of Dilation was calculated as the time after cuff release when the diameter first exceeded the pre-release diameter by 70μm.

The Time to Peak Dilation was selected as the time of maximum diameter after cuff release.

The Peak Diameter Change Relative to Pre-Occlusion Diameter was calculated as the diameter at the time of peak dilation minus the pre-occlusion diameter.

The Peak Diameter Change Relative to Pre-Release Diameter was calculated as the diameter at the time of peak dilation minus the pre-release diameter.

The Mean Diameter Change Relative to Pre-Occlusion or Pre-Release Diameter was calculated as the mean diameter from the time to onset of dilation to 100 seconds after the time to onset of dilation, minus the pre-occlusion or pre-release diameter, respectively. In the event of no dilation, the mean diameter was calculated from 50 seconds before to 50 seconds after the peak post-release diameter (this occurred only in 2 of the post-HELP measurements).

Measurements of percent diameter change were calculated by dividing the maximum or mean diameter by the pre-occlusion or pre-release diameter.

Bibliography

[1] Airaksinen KE, Salmela PI, Linnaluoto MK, Ikaheimo MJ, Ahola K. Diminished arterial elasticity in diabetes: association with fluorescent advanced glycosylation end products in collagen. *Cardiovasc Res.* 1993;27:942-945.

[2] Alva F, Samaniego V, Gonzalez V, Moguel R, Meaney E. Structural and dynamic changes in the elastic arteries due to arterial hypertension and hypercholesterolemia. *Clin Cardiol.* 1993;16:614-618.

[3] Anderson EA, Mark AL. Flow-mediated and reflex changes in large peripheral artery tone in humans. *Circulation.* 1989;79:93-100.

[4] Anderson TJ, Meredith IT, Yeung AC, Frei B, Selwyn AP, Ganz P. The effect of cholesterol-lowering and antioxidant therapy on endothelium-dependent coronary vasomotion. *N Engl J Med.* 1995;332:488-493.

[5] Anderson TJ, Uehata A, Gerhard MD, Meredith IT, Knab S, Delagrange D, Liberman EH, Ganz P, Creager MA, Yeung AC, Selwyn AP. Close relationship of endothelial function in the human coronary and peripheral circulations. *J Am Coll Cardiol.* 1995;26:1235-1241.

[6] Antony I. Lerebours G. Nitenberg A. Loss of flow-dependent coronary artery dilation in patients with hypertension. *Circulation.* 1995;91:1624-1628.

[7] Araki A, Sako Y. Determination of free and total homocysteine in human plasma by high performance liquid chromotography with fluorescence detection. *J Chromatog.* 1987;422:43-52.

[8] Arcaro G, Zenere MB, Travia D, Zenti MG, Covi G, Lechi A, Muggeo M. Non-invasive detection of early endothelial dysfunction in hypercholesterolemic subjects. *Atherosclerosis.* 1995;114:247-254.

[9] Armstrong VW, Windisch M, Wieland H, Fuchs C, Rieger J, Kosterin H, Nebendah K, Scheler F, Seidel D. Selective continuous elimination of low density lipoproteins with heparin at acidic pH. *Trans Am Soc Artif Intern Organs.* 1983;29:323-327.

[10] Arndt JO, Klauske H, Mersch F. The diameter of the intact carotid artery in man and its change with pulse pressure. *Pfluegers Arch.* 1968;301:230-240.

[11] Benetos A, Laurent S, Hoeks APG, Boutouyrie PH, Safar ME. Arterial alterations with aging and high blood pressure. *Arterioscler Thromb.* 1993;13:90-97.

[12] Berglund GL, Riley WA, Barnes RW, Furberg CD. Quality control in ultrasound studies on atherosclerosis. *J Intern Med.* 1994;236;581-586.

[13] Berne RM, Levy MN. *Cardiovascular Physiology.* C. V. Mosby Company, St. Louis, 1986.

[14] Bierenbaum ML, Fleischman AI, Stier A, Somol H, Watson PB. Effect of cigarette smoking upon in vivo platelet function in man. *Thromb Res.* 1978;12:1051-1057.

[15] Blankenhorn DH, Selzer RH, Crawford DW, Barth JD, Liu C-r, Liu C-h, Mack WJ, Alaupovic P. Beneficial effects of cholestipol/niacin therapy on the common carotid artery. *Circulation.* 1993;88:20-28.

[16] Blann AD, McCollum CN. Adverse influence of cigarette smoking on the endothelium. *Thrombosis and Haemostasis.* 1993;70:707-711.

[17] Bonithon-Kopp C, Touboul PJ, Berr C, Leroux C, Mainard F, Courbon D, Ducimetiere P. Relation of intima-media thickness to atherosclerotic plaques in carotid arteries. The vascular aging (EVA) study. *Arterioscler Thromb Vasc Biol.* 1996;16:310-316.

[18] Bonnefous O, Pesque P. Time domain formulation of pulse-Doppler ultrasound and blood velocity estimation by cross correlation. *Ultrason Imaging* 1986;8:73-85.

[19] Bookstein FL. Fitting conic sections to scattered data. *Computer Graphics and Image Processing.* 1979;9:56-71.

[20] Bostom AG, Jacques PF, Nadeau MR, Williams RR, Ellison RC, Selhub J. Post-methionine load hyperhomocysteinemia in persons with normal fasting total plasma homocysteine: initial results from the NHLBI family heart study. *Atherosclerosis.* 1995;116:147-151.

[21] Boutouyrie P, Laurent S, Benetos A, Girerd XJ, Hoeks APG. Opposing effects of aging on distal and proximal large arteries in hypertensives. *J Hypertens Suppl.* 1992;10:S87-S91.

[22] Box GEP, Tiao GC. Intervention analysis with application to economic and environmental problems. *J Am Stat Assoc.* 1975;70:70-79.

[23] Brands PJ, Hoeks APG, Hofstra L, Reneman RS. A noninvasive method to estimate wall shear rate using ultrasound. *Ultrasound Med Biol.* 1995;21:171-185.

[24] Brattstrom L, Israelsson B, Lindgarde F, Hultberg B. Higher total plasma homocysteine in vitamin B12 deficiency than in heterozygosity for homocystinuria due to cystathionine beta-synthase deficiency. *Metabolism.* 1988;37:175-178.

[25] Bratzler RL, Chisolm GM, Colton CK, Smith KA, Lees RS. The distribution of labeled low density lipoproteins across the rabbit aorta in vivo. *Atherosclerosis.* 1977;28:289-307.

[26] Burrus CS, Parks TW. *DFT/FFT and convolution algorithms theory and implementation.* John Wiley and Sons, New York, 1985.

[27] Candipan RC, Wang B, Buitrago R, Tsao PS, Cooke JP. Regression or progression. Dependency on vascular nitric oxide. *Arterioscler Thromb Vasc Biol.* 1996;16:44-50.

[28] Cayatte AJ, Palacino JJ, Horten K, Cohen RA. Chronic inhibition of nitric oxide production accelerates neointima formation and impairs endothelial function in hypercholesterolemic rabbits. *Arterioscler Thromb.* 1994;14:753-759.

[29] Celermajer DS, Sorensen KE, Gooch VM, Spiegelhalter DJ, Miller OI. Noninvasive detection of endothelial dysfunction in children and adults at risk of atherosclerosis. *Lancet.* 1992;340:1111-1115.

[30] Celermajer DS, Sorensen K, Ryalls M, Robinson J, Thomas O, Leonard JV, Deanfield JE. Impaired endothelial function occurs in the systemic arteries of children with homozygous homocystinuria but not in their heterozygous parents. *J Am Coll Cardiol.* 1993;22:854-858.

[31] Celermajer DS, Sorensen KE, Georgakopoulos D, Bull C, Thomas O. Cigarette smoking is associated with dose-related and potentially reversible impairment of endothelium-dependent dilation in healthy young adults. *Circulation.* 1993;88: 2149-2155.

[32] Celermajer DS, Sorensen KE, Bull C, Robinson J, Deanfield JE. Endothelium-dependent dilation in the systemic arteries of asymptomatic subjects relates to coronary risk factors and their interaction. *J Am Coll Cardiol.* 1994;24:1468-1474.

[33] Celermajer DS, Adams MR, Clarkson P, Robinson J, McCredie R, Donald A, Deanfield JE. Passive smoking and impaired endothelium-dependent arterial dilation in healthy young adults. *N Engl J Med.* 1996; 334:150-154.

[34] Chang MY, Lees AM, Lees RS. Time course of ^{125}I-labeled LDL accumulation in the healing, balloon-deendothelialized rabbit aorta. *Arterioscler Thromb.* 1992;12:1088-1098.

[35] Clarke R, Daly L, Robinson K, Naughten E, Cahalane S, Fowler B, Grahan I. Hyperhomocysteinemia: an independent risk factor for vascular disease. *N Engl J Med.* 1991;324:1149-1155.

[36] Cocks TM, Angus JA. Endothelium-dependent relaxation of coronary arteries by noradrenaline and serotonin. *Nature (Lond.)* 1983;305:627-630.

[37] Colton T. *Statistics in medicine* Little, Brown and Company, Inc., 1974.

[38] Cooke JP, Singer AH, Tsao P, Zera P, Rowan RA, Billingham ME. Antiatherogenic effects of L-arginine in the hypercholesterolemic rabbit. *J Clin Invest.* 1992;90:1168-1172.

[39] Cotran RS, Kumar V, Robbins SL. *Robbins Pathologic Basis of Disease 4th Ed.* W.B. Saunders Co., Philadelphia, 1989.

[40] Coulthard J. Ultrasonic cross-correlation flowmeters. *Ultrason.* 1973;11:83-88.

[41] Cox DA, Vita JA, Treasure CB, Fish RD, Alexander RW, Ganz P, Selwyn AP. Atherosclerosis impairs flow-mediated dilation of coronary arteries in humans. *Circulation* 1989;80:458-465.

[42] Craig WY, Palomaki GE, Haddow JE. Cigarette smoking and serum lipid and lipoprotein concentrations: an analysis of published data. *Br Med J.* 1989;298:784-488.

[43] Creager MA, Cooke JP, Mendelsohn ME, Gallagher SJ, Coleman SM, Loscalzo J, Dzau VJ. Impaired Vasodilation of the forearm resistance vessels in hypercholesterolemic humans. *J Clin Invest.* 1990;86:228-234.

[44] Crouse JR, Byington RP, Bond MG, Espeland MA, Craven TE, Sprinkle JW, McGovern ME, Furberg CD. Pravastatin, lipids, and atherosclerosis in the carotid arteries (PLAC-II). *Am J Cardiol.* 1995;75:455-559.

[45] Crouse JR, Craven TE, Hagaman AP, Bond MG. Association of coronary disease with segment-specific intimal-medial thickening of the extracranial carotid artery. *Circulation.* 1995;92:1141-1147.

[46] Deanfield JE, Kensett M, Wilson RA, Shea M, Horlock P, deLandsheere CM, Selwyn AP. Silent myocardial ischemia due to mental stress. *Lancet.* 1984;2:1001-1005.

[47] de Jong PGM, Hoeks APG, Reneman RS. Determination of tissue motion velocity by correlation interpolation of pulsed ultrasonic echo signals. *Ultrason Imaging.* 1990;12:84-98.

[48] de Jong PGM, Arts T, Hoeks APG, Reneman RS. Experimental evaluation of the correlation interpolation technique to measure regional tissue velocity. *Ultrason Imaging.* 1991;13:145-161.

[49] Dovgan PS, Edwards JD, Zhan X, Wilde M, Agrawal DK. Cigarette smoking increases monocyte adherence to cultured endothelial cell monolayer. *Biochem Biophys Res Comm.* 1994;203:929-934.

[50] Drexler H, Zeiher AM. Endothelial function in human coronary arteries in vivo. Focus on hypercholesterolemia. *Hypertension.* 1991;18 (4 Suppl);II90-II99.

[51] Drexler H, Hayoz D, Munzel T, Hornig B, Just H. Endothelial function in chronic congestive heart failure. *Am J Cardiol.* 1992;69:1596-1601.

[52] Duncan GW, Lees RS, Ojemann RG, David SS. Concomitants of atherosclerotic carotid artery stenosis. *Stroke.* 1977;8:665-669.

[53] Egashira K, Inou T, Hirooka Y, Yamada A, Urabe Y, Takeshita A. Evidence of impaired endothelium-dependent coronary vasodilation in patients with angina pectoris and normal coronary angiograms. *N Engl J Med.* 1993;328:1659-1664.

[54] Egashira K, Hirooka Y, Kai H, Sugimachi M, Suzuki S, Inou T, Takeshita A. Reduction in serum cholesterol with pravastatin improves endothelium-dependent coronary vasomotion in patients with hypercholesterolemia. *Circulation.* 1994;89: 2519-2524.

[55] Eisenhauer T, Armstrong VW, Wieland H, Fuchs C, Scheler F, Seidel D. Selective removal of low density lipoproteins (LDL) by precipitation at low pH: first clinical application of the HELP system. *Klin Wochenschr.* 1987;65:161-168.

[56] Embree PM, O'Brien WD. Volumetric blood flow via time-domain correlation: experimental verification. *IEEE Trans Ultrason Ferroelectr Freq Contr.* 1990;37: 176-189.

[57] Ferrara KW, Algazi VR. A new wideband spread target maximum likelihood estimator for blood velocity estimation – Part I: Theory. *IEEE Trans Ultrason Ferroelectr Freq Contr.* 1991;38:1-16.

[58] Ferrara KW, Algazi VR. A new wideband spread target maximum likelihood estimator for blood velocity estimation – Part II: Evaluation of estimators with experimental data. *IEEE Trans Ultrason Ferroelectr Freq Contr.* 1991;38:17-26.

[59] Fielding JE. Smoking: Health effects and control. *N Eng J Med.* 1985;313:491-498.

[60] Filitti V, Giral P, Simon A, Merli I, Del Pino M, Levenson J. Enhanced constriction of the peripheral large artery in response to acute induction of a low flow state in human hypercholesterolemia. *Arterioscler Thromb.* 1991;11:161-166.

[61] Foster SG, Embree PM, O'Brien WD. Flow velocity profile via time-domain correlation: error analysis and computer simulation. *IEEE Trans Ultrason Ferroelectr Freq Contr.* 1990;37:164-175.

[62] Friedewald WT, Levy RI, Friedrickson DS. Estimation of the concentration of low-density lipoprotein cholesterol in plasma, without use of the preparation ultracentrifuge. *Clin Chem.* 1972;18:499-502.

[63] Fujii K, Heistad DD, Faraci FM. Flow-mediated dilation of the basilar artery in vivo. *Circ Res.* 1991;69:697-705.

[64] Furberg CD, Byington RP, Crouse JR, Espeland MA. Pravastatin, lipids, and major coronary events. *Am J Cardiol.* 1994;73:1133-1134.

[65] Furchgott RF, Zawadski JV. The obligatory role of endothelial cells in the relaxation of arterial smooth muscle by acetylcholine. *Nature (London).* 1980;288:373-376.

[66] Fuster V, Stein B, Ambrose JA, Badimon L, Badimon JJ, Chesebro JH. Atherosclerotic plaque rupture and thrombosis: evolving concepts. *Circulation.* 1990;82: II47-II49.

[67] Gage JE, Hess OM, Murakami T, Ritter M, Grimm J, Krayenbuchl HP. Vasoconstriction of stenotic coronary arteries during dynamic exercise in patients with classic angina pectoris: reversibility by nitroglycerine. *Circulation* 1986;73:865-876.

[68] Gardiner HM, Celermajer DS, Sorenson KE, Georgakopoulos D, Robinson J, Thomas O, Deanfield JE. Arterial reactivity is significantly impaired in normotensive young adults after successful repair of aortic coarctation in childhood. *Circulation.* 1994;89:1745-1750.

[69] Gilligan DM, Badar DM, Panza JA, Quyyumi AA, Cannon RO. Effects of estrogen replacement therapy on peripheral vasomotor function in postmenopausal women. *Am J Cardiol.* 1995;75:264-268.

[70] Gillum RF. Trends in acute myocardial infarction and coronary heart disease death in the United States. *J Am Coll Cardiol.* 1993;23:1273-1277.

[71] Glagov S, Weisenberg E, Zarins CK, Stankunavicius R, Kolettis GJ. Compensatory enlargement of human atherosclerotic coronary arteries. *N Engl J Med.* 1987;316: 1371-1375.

[72] Haney MJ, O'Brien WD. Jr. Temperature dependency of ultrasonic propagation properties in biological materials. In: Greenleaf JF. ed. *Tissue characterization with ultrasound.* Boca Raton, Florida: CRC Press; 1986: pp. 15-55.

[73] Hansen F, Mangell P, Sonneson B, Lanne T. Diameter and compliance in the human common carotid artery - variations with age and sex. *Ultrasound Med Biol.* 1995;21:1-9.

[74] Harker LA, Ross R, Slichter SJ, Scott CR. Homocystine-induced arteriosclerosis: the role of endothelial cell injury and platelet response in its genesis. *J Clin Invest.* 1976;58:731-741.

[75] Harrison DG, Armstrong ML, Freiman PC, Heistad DD. Restoration of endothelium-dependent relaxation by dietary treatment of atherosclerosis. *J Clin Invest.* 1987;80:1808-1811.

[76] Hatch FT, Lees RS. Practical methods for plasma lipoprotein analysis *Adv Lipid Res.* 1968;6:1-68.

[77] Hayoz D, Rutschmann B, Perret F, Niederberger M, Tardy T. Conduit artery compliance and distensibility are not necessarily reduced in hypertension. *Hypertension.* 1992;20:1-6.

[78] Hennerici M, Kleophas W, Gries FA. Regression of carotid plaques during low density lipoprotein cholesterol elimination. *Stroke.* 1991;22:989-992.

[79] Herrington DM, Braden GA, Williams JK, Morgan TM. Endothelial-dependent coronary vasomotor responsiveness in postmenopausal women with and without estrogen replacement therapy. *Am J Cardiol.* 1994;73:951-952.

[80] Hickler RB. Aortic and large artery stiffness: current methodology and clinical correlations. *Clin Cardiol.* 1990;13:317-322.

[81] Higman DJ, Strachan AMJ, Powell JT. Reversibility of smoking-induced endothelial dysfunction. *Br J Surg.* 1994;81:977-978.

[82] Hintze TH, Vatner SF. Reactive dilation of large coronary arteries in conscious dogs. *Circ Res.* 1984;54:50-57.

[83] Hoeks APG, Ruissen CJ, Hick P, Reneman RS. Transcutaneous detection of relative changes in artery diameter. *Ultrasound Med Biol.* 1985;11:51-59.

[84] Hoeks APG, Brands PJ, Smeets FAM, Reneman RS. Assessment of the distensibility of superficial arteries. *Ultrasound Med Biol.* 1990;16:121-128.

[85] Hoeks APG, Brands PJ, Reneman RS. Effect of sample window length on the correlation between RF signal and pulsed Doppler signal intensity. *Ultrasound Med Biol.* 1994;20:35-40.

[86] Hoeks APG, Brands PJ, Arts TGJ, Reneman RS. Subsample volume processing of Doppler ultrasound signals. *Ultrasound Med Biol.* 1994;20:953-965.

[87] Hokanson DE, Mozersky DJ, Summer DS, Strandness DE. A phase locked echo-tracking system for recording arterial diameter changes in vivo. *J Appl Physiol.* 1972;32:728-733.

[88] Hopkins PN, Wu LL, Wu J, Hunt SC, James BC, Vincent GM, Williams RR. Higher plasma homocyst(e)ine and increased susceptibility to adverse effects of low folate in early familial coronary artery disease. *Arterioscler Thromb Vasc Biol.* 1995;15:1314-1320.

[89] Howard G, Sharrett AR, Heiss G, Evans GW, Chambless LE, Riley WA, Bruke GL. Carotid artery intimal-medial thickness distribution in general populations as evaluated by B-mode ultrasound. *Stroke.* 1993;24:1297-1304.

[90] Igarashi K, Horimoto M, Takenaka T, Inoue H, Miyata S. Acute cholesterol lowering therapy with LDL-apheresis improves endothelial function of the coronary microcirculation in patients with hypercholesterolemia [abstract] *Circulation* 1995;92 Suppl I:I-452.

[91] Ignarro LJ, Byrns RE, Buga GM, Wood KS. Endothelium-derived relaxing factor from pulmonary artery and vein possesses pharmacologic and chemical properties identical to those of nitric oxide radical. *Circ Res.* 1987;61:866-879.

[92] Joannides R, Haefeli WE, Linder L, Richard V, Bakkali EH. Nitric oxide is responsible for flow-dependent dilation of human peripheral conduit arteries in vivo. *Circulation.* 1995;91:1314-1319.

[93] Johnstone MT, Creager SJ, Scales KM, Cusco JA, Lee BK. Impaired endothelium-dependent vasodilation in patients with insulin-dependent diabetes mellitus. *Circulation.* 1993;88:2510-2516.

[94] Kanai H, Satoh H, Hirose K, Chubachi N. A new method for measuring small local vibrations in the heart using ultrasound. *IEEE Trans Biomed Eng.* 1993;40:1233-1241.

[95] Kasai C, Namekawa K, Koyane A, Omoto R. Real-time two-dimensional blood flow imaging using an autocorrelation technique. *IEEE Trans Sonics Ultrason.* 1985;SU-32:458-463.

[96] Koller A, Kaley G. Endothelium regulates skeletal muscle microcirculation by a blood flow velocity-sensing mechanism. *Am J Physiol.* 1990;258:H916-H920.

[97] Krupski WC. The peripheral vascular consequences of smoking. *Ann Vasc Surg.* 1991;5:291-304.

[98] Kuhn FE, Mohler ER, Satler LF, Reagan K, Lu DY, Rackley CE. Effects of high-density lipoprotein on acetylcholine-induced coronary vasoreactivity. *Am J Cardiol.* 1991;68:1425-1430.

[99] Kou L, Davis MJ, Cannon MS, Chilian WM. Pathophysiological consequences of atherosclerosis extend into the coronary microcirculation. Restoration of endothelium-dependent responses by L-arginine. *Circ Res.* 1992;70:465-476.

[100] Lane DM, Alaupovic P, Knight-Gibson C, Dudley VS, Laughlin LO. Changes in plasma lipid and apolipoprotein levels between heparin-induced extracorporeal low-density lipoprotein (HELP) treatments. *Am J Cardiol.* 1995;75:1124-1129.

[101] Lane DM, McConathy WJ, Laughlin LO, Comp PC, von Albertini B, Bricker LA, Kozlovskis P, Lees RS, Dorrier C. Selective removal of plasma low density lipoprotein with the HELP system: biweekly versus weekly therapy. *Atherosclerosis.* 1995;114:203-211.

[102] Laskey WK, Parker HG, Ferrari VA, Kussmaul WG, Noordergraaf A. Estimation of total systemic arterial compliance in humans. J Appl Physiol. 1990;69:112-119.

[103] Lassila R, Seyberth HW, Haapanen A, Schweer H, Koskenvou M, Laustiola KE. Vasoactive and atherogenic effects of cigarette smoking: a study of monoxygotic twins discordant for smoking. *Br Med J.* 1988;297:955-957.

[104] Laurent S, Lacolley P, Brunel P, Laloux B, Pannier B, Safar M. Flow-dependent vasodilation of brachial artery in essential hypertension. *Am J Physiol.* 1990;258: H1004-H1011.

[105] Laurent S, Mourad J, Lacolley P, Beck L, Boutouyrie P. Elastic modulus of the radial artery wall material is not increased in patients with essential hypertension. *Arterioscler Thromb.* 1994;14:1223-1231.

[106] Leung W, Sanders W, Alderman E. Coronary artery quantitation and data management system for paired cineangiograms. *Cathet Cardiovasc Diagn.* 1991;24:121-134.

[107] Leung W-H, Lau C-P, Wong C-K. Beneficial effect of cholesterol-lowering therapy on coronary endothelium-dependent relaxation in hypercholesterolemic patients. *Lancet.* 1993;341:1496-1500.

[108] Lie M, Sejersted OM, Kiil F. Local regulation of vascular cross section during changes in femoral arterial blood flow in dogs. *Circ Res.* 1970;27:727-737.

[109] Lieberman EH, Gerhard MD, Uehata A, Walsh BW, Selwyn AP, Ganz P, Yeung AC, Creager MA. Estrogen improves endothelium-dependent, flow-mediated vasodilation in postmenopausal women. *Ann Intern Med.* 1994;121:936-941.

[110] Lieberman EH, Knab ST, Creager MA. Nitric oxide mediates the vasodilator response to flow in humans [abstract]. *Circulation.* 1994;90:I-138.

[111] Ludmer PL, Selwyn AP, Shook TL, Wayne RR, Mudge GH, Alexander RW, Ganz P. Paradoxical vasoconstriction induced by acetylcholine in atherosclerotic coronary arteries. *N Engl J Med.* 1986;315:1046-1051.

[112] Mack WJ, Selzer RH, Hodis HN, Erickson JK, Liu C-r, Liu C-h, Crawford DW, Blankenhorn DH. One-year reduction and longitudinal analysis of carotid intima-media thickness associated with colestipol/niacin therapy. *Stroke.* 1993;24:1779-1783.

[113] McClellan JH, Parks TW. A unified approach to the design of optimum FIR linear phase filters. *IEEE Trans Circuit Theory.* 1973;CT-20:697-701.

[114] McLenachan JM, Vita J, Fish RD, Treasure CB, Cox DA, Ganz P, Selwyn AP. Early evidence of endothelial vasodilator dysfunction at coronary branch points. *Circulation.* 1990;82:1169-1173.

[115] Morrison DF. *Multivariate statistical methods* McGraw-Hill, New York, 1990.

[116] Nabel EG, Ganz P, Gordon JB, Alexander RW, Selwyn AP. Dilation of normal and constriction of atherosclerotic coronary arteries caused by cold pressor test. *Circulation.* 1988;53:557-573.

[117] Nabel EG, Selwyn AP, Ganz P. Large coronary arteries in humans are responsive to changing blood flow: an endothelium-dependent mechanism that fails in patients with atherosclerosis. *J Am Coll Cardiol.* 1990;16:349-356.

[118] Nadler JL, Velasco JS, Horton R. Cigarette smoking inhibits prostacyclin formation. *Lancet.* 1983; 1:1248-1250.

[119] Naruse K, Shimizu K, Muramatsu M, Toki Y, Miyazaki Y, Okumura K, Hashimoto H, Ito T. Long-term inhibition of NO synthesis promotes atherosclerosis in the hypercholesterolemic rabbit thoracic aorta. *Arterioscler Thromb.* 1994;14:746-752.

[120] Oppenheim AV, Schafer RW. *Discrete-time signal processing.* Prentice Hall, New Jersey, 1989.

[121] Palmer RM, Ferrige AG, Moncada S. Nitric oxide release accounts for the biological activity of endothelium-derived relaxing factor. *Nature (Lond.)* 1987;327:524-526.

[122] Palmer RM, Ashton DS, Moncada S. Vascular endothelial cells synthesize nitric oxide from L-arginine. *Nature (Lond.)* 1988;333:664-666.

[123] Peach MB, Loeb AL, Singer HA Saye J. Endothelium-derived vascular relaxing factor. *Hypertension.* 1985;7(Suppl I):I94-I100.

[124] Perret F, Mooser V, Hayoz D, Tardy Y, Meister JJ. Evaluation of arterial compliance-pressure curves: effect of antihypertensive drugs. *Hypertension.* 1991;18:II-77–II-83.

[125] Pignoli P, Tremoli E, Poli A. Intimal plus medial thickness of the arterial wall: a direct measurement with ultrasound imaging. *Circulation.* 1986;74:1399-1406.

[126] Pitt B, Mancini GBJ, Ellis SG, Rosman HS, Park J, McGovern ME. Pravastatin limitation of atherosclerosis in the coronary arteries (PLAC I): Reduction in atherosclerosis progression and clinical events. *J Am Coll Cardiol.* 1995;26:1133-1139.

[127] Pittilo RM. Cigarette smoking and endothelial injury: a review. *Adv Exp Med Biol.* 1990;273:61-78.

[128] Pohl U, Holtz J, Busse R, Bassenge E. Crucial role of endothelium in the vasodilator response to increased flow in vivo. *Hypertension.* 1986;8:37-44.

[129] Prichard KA, Groszek L, Smalley DM, Sessa WC, Wu M, Villalon P, Solin MS, Stemerman MB. Native low-density lipoprotein increases endothelial cell nitric oxide synthase generation of superoxide anion. *Circ Res.* 1995;77:510-518.

[130] Prinzmetal M, Kennamer R, Merliss R, Wada T, Bor N. Angina pectoris: I., A variant form of angina pectoris. Preliminary report, *Am J Med.* 1959;27:374.

[131] Reiber JHC, Kooijman CJ, Slager CJ, Gerbrands JJ, Schuurbiers JCH. Coronary artery dimensions from cineangiograms – Methodology and validation of a computer-assisted analysis procedure. *IEEE Trans Med Imaging.* 1984;MI-3:131-141.

[132] Riley WA, Barnes RW, Applegate WB, Dempsey R, Hartwell T, Davis VG, Bond MG, Furberg CD. Reproducibility of noninvasive ultrasonic measurement of carotid atherosclerosis. *Stroke.* 1992;23:1062-1068.

[133] Robinson K, Mayer EL, Miller DP, Green R, van Lente F, Gupta A, Kotte-Marchant K, Savon SR, Selhub J, Nissen S, Kutner M, Topol EJ, Jacobsen DW. Hyperhomocysteinemia and low pyridoxal phosphate. Common and independent reversible risk factors for coronary artery disease. *Circulation.* 1995;92:2285-2830.

[134] Rubanyi GM, Romero JC, Vanhoutte PM. Flow-induced release of endothelium-derived relaxing factor. *Am J Physiol.* 1986;250:H1145-H1149.

[135] Safee-Rad R, Smith KC, Benhabib B, Tchoukanov I. Application of moment and Fourier descriptors to the accurate estimation of elliptical-shape parameters. *Pattern Recognition Lett.* 1992;13:497-508.

[136] Salonen JT, Salonen R. Ultrasound B-mode imaging in observational studies of atherosclerotic progression. *Circulation.* 1993;87 (Suppl. II):II-56-II-65.

[137] Salonen R, Nyyssönen K, Porkkala E, Rummukainen J, Belder R, Park JS, Salonen JT. Kuopio atherosclerosis prevention study (KAPS). A population-based primary preventive trial of the effect of LDL lowering on atherosclerotic progression in carotid and femoral arteries. *Circulation.* 1995;92:1758-1764.

[138] Schuff-Werner P, Gohlke H, Bartmann U, Baggio G, Corti MC, Dinsenbacher A, Eisenhauer T, Grutzmacher P, Keller C, Kettner U, Kleophas W, Koster W, Olbricht CJ, Richter WO, Seidel D, and the HELP study group. The HELP–LDL–apheresis multicentre study, an angiographically assessed trial on the role of LDL–apheresis in the secondary prevention of coronary heart disease. *Eur J Clin Invest.* 1994;24:724-732.

[139] Seidel D, Armstrong VW, Schuff-Werner P, Eisenhauer T. Removal of low-density lipoproteins (LDL) and fibrinogen by precipitation with heparin at low pH: Clinical application and experience. *J Clin Apheresis.* 1988;4:78-81.

[140] Seidel D, Armstrong VW, Schuff-Werner P, and the HELP study group. The HELP–LDL–apheresis multicentre study, an angiographically assessed trial on the role of LDL–apheresis in the secondary prevention of heart disease. I. Evaluation of safety and cholesterol-lowering effects during the first 12 months. *Eur J Clin Invest.* 1991;24:375-383.

[141] Selhub J, Jacques PF, Bostom AG, D'Agnostino RB, Wilson PWF, Belanger AJ, O'Leary DH, Wolf PA, Schaefer EJ, Rosenberg IH. Association between plasma homocysteine concentrations and extracranial carotid-artery stenosis. *N Engl J Med.* 1995;332:286-291.

[142] Sellke FW, Armstrong ML, Harrison DG. Endothelium-dependent vascular relaxation is abnormal in the coronary microcirculation of atherosclerotic primates. *Circulation.* 1990; 81: 1586-1593.

[143] Selzer RH, Hodis HN, Kwong-Fu H, Mack WJ, Lee PL, Liu C-r, Liu C-h. Evaluation of computerized edge tracking for quantifying intima-media thickness of the common carotid artery from B-mode ultrasound images. *Atherosclerosis.* 1994;111:1-11.

[144] Shiode N, Morishima N, Nakayama K, Yamagata T, Matsuura H, Kajiyama G. Flow-mediated vasodilation of human epicardial coronary arteries: effect of inhibition of nitric oxide synthesis. *J Am Coll Cardiol.* 1996;27:304-310.

[145] Simon A, Levenson J. Use of arterial compliance for evaluation of hypertension. *Am J Hypertens.* 1991;4:97-105.

[146] Simon A, Levinson J. Could the identification of subclinical atherosclerosis offer an alternative to the mass drug treatment of hypercholesterolemia? *Atherosclerosis.* 1994;105:245-249.

[147] Sinoway LI, Hendrickson C, Davidson WR, Prophet S, Zelis R. Characterization of flow-mediated brachial artery vasodilation in human subjects. *Circ Res.* 1989;64:32-42.

[148] Smiesko V, Kozik J, Dolezel S. Role of the endothelium in the control of arterial diameter by blood flow. *Blood Vessels.* 1985;22:247-251.

[149] Smiesko V, Lang DJ, Johnson PC. Dilator response of rat mesenteric arcading arterioles to increased blood flow velocity. *Am J Physiol.* 1989;257:H1958-H1965.

[150] Sorensen KE, Celermajer DS, Georgakopoulos D, Hatcher G, Betteridge DJ. Impairment of endothelium-dependent dilation is an early event in children with familial hypercholesterolemia and is related to the lipoprotein (a) level. *J Clin Invest.* 1994;93:50-55.

[151] Stadler RW, Karl WC, Lees RS. New methods for arterial diameter measurement from B-mode images. *Ultrasound Med Biol.* 1996;22:25-34.

[152] Stadler RW, Karl WC, Lees RS. The application of echo-tracking methods to endothelium-dependent vasoreactivity and arterial compliance measurements. *Ultrasound Med Biol.* 1996;22:35-42.

[153] Stadler RW, Karl WC, Ibrahim SF, Lees RS. Characterization of brachial artery and forearm microvascular endothelium-dependent vasoreactivity via duplex ultrasound. Submitted for publication.

[154] Stadler RW, Ibrahim SF, Lees RS. Peripheral vasoreactivity and intima-media thickness in familial hypercholesterolemic subjects treated with heparin-induced extracorporeal LDL precipitation (HELP). Submitted for publication.

[155] Stamler JS, Osborne JA, Jaraki O, Rabbani LE, Mullins M, Singel D, Loscalzo J. Adverse vascular effects of homocysteine are modulated by endothelium-derived relaxing factor and related oxides of nitrogen. *J Clin Invest.* 1993;91:308-318.

[156] Strang G. *Linear algebra and its applications.* 3rd ed. San Diego: Harcourt, Brace and Javanovich; 1988.

[157] Stroes ESG, Koomans HA, de Bruin TWA, Rabelink TJ. Vascular function in the forearm of hypercholesterolemic patients on and off lipid-lowering medication. *Lancet.* 1995;346:467-471.

[158] Tagawa T, Imaizumi T, Endo T, Shiramoto M, Harasawa Y, Takashita A. Role of nitric oxide in reactive hyperemia of human forearm vessels. *Circulation.* 1994;90:2285-2290.

[159] Tardy Y, Meister JJ, Perret F, Brunner HR, Arditi M. Non-invasive estimate of the mechanical properties of peripheral arteries from ultrasonic and photoplethysmographic measurements. *Clin Phys Physiol Meas.* 1991;12:39-54.

[160] Thiery J, Walli AK, Janning G, Seidel D. Low-density lipoprotein plasmapheresis with and without lovastatin in the treatment of the homozygous form of familial hypercholesterolemia. *Eur J Pediatr.* 1990;149:716-721.

[161] Tomita T, Ezaki M, Miwa M, Nakamura K, Inoue Y. Rapid and reversible inhibition by low density lipoprotein of the endothelium-dependent relaxation to hemostatic substances in porcine coronary arteries. *Circ Res.* 1990;66:18-27.

[162] Topol EH, Nissen SE. Our preoccupation with coronary luminology. The dissociation between clinical and angiographic findings in ischemic heart disease. *Circulation.* 1995;92:2333-2342.

[163] Treasure CB, Klein JL, Weintraub WS, Talley JD, Stillabower ME, Kosinski AS, Zhang J, Boccuzzi SJ, Cedarholm JC, Alexander RW. Beneficial effects of cholesterol-lowering therapy on the coronary endothelium in patients with coronary artery disease. *N Engl J Med.* 1995;332:481-487.

[164] U.S. Department of Health and Human Services. The health consequences of smoking: cardiovascular disease. A report of the Surgeon General's office on smoking and health. Rockville, MD: DHHS (PHS 84-50204), 1983.

[165] Vane JR, Anggard EE, Botting RM. Regulatory functions of the vascular endothelium. *New Eng J Med.* 1990;323:27-36.

[166] Van Merode T, Hick PJJ, Hoeks APG, Rahn KH, Reneman RS. Carotid artery wall properties in normotensive and borderline hypertensive subjects of various ages. *Ultrasound Med Biol.* 1988;14:563-569.

[167] Van Merode T, Hick PJJ, Hoeks APG, Smeets FAM, Reneman RS. Differences in carotid artery wall properties between presumed-healthy men and women. *Ultrasound Med Biol.* 1988;14:571-574.

[168] Vita JA, Treasure CB, Ganz P, Cox DA, Fish RD, Selwyn AP. Control of shear stress in the epicardial coronary arteries of humans: impairment by atherosclerosis. *J Am Coll Cardiol.* 1989;14:1193-1199.

[169] Vita JA, Treasure CB, Nabel EG, McLenachan JM, Fish RD, Yeung AC, Vekshtein VI, Selwyn AP, Ganz P. Coronary vasomotor response to acetylcholine relates to risk factors for coronary artery disease. *Circulation.* 1990;81:491-497.

[170] Vogel RA, Corretti MC, Plotnick GD. Changes in flow-mediated brachial arterial vasoactivity with lowering of desirable cholesterol levels in healthy middle-aged men. *Am J Cardiol.* 1996;77:37-40.

[171] Wall RT, Harlan JM, Harker LA, Striker GE. Homocysteine-induced endothelial cell injury in vitro: a model for the study of vascular injury. *Thromb Res.* 1980;18:113-121.

[172] Ward ME, Madger SA, Hussain SN. Role of endothelium-derived 1 relaxing factor in reactive hyperemia in canine diaphragm. *J Appl Physiol.* 1993;74:1606-1612.

[173] Wendelhag I, Gustavvson T, Suurkula M, Berglund G, Wikstrand J. Ultrasound measurement of wall thickness in the carotid artery: fundamental principles and description of a computerized analyzing system. *Clin Physiol.* 1991;11:565-577.

[174] Wendelhag I, Wiklund O, Wikstrand J. Arterial wall thickness in familial hypercholesterolemia. Ultrasound measurement of intima-media thickness in the common carotid artery. *Atheroscler Thromb.* 1992;12:70-77.

[175] Wendelhag I, Wiklund O, Wikstrand J. Atherosclerotic changes in the femoral and carotid arteries in familial hypercholesterolemia. *Arterioscler Thromb.* 1993;13:1404-1411.

[176] Wesseling KH. Finapres, continuous noninvasive finger arterial pressure based on the method of Penaz. in: Meyer-Sabellek W, Anlauf M, Gozen R, Steinfeld L. (eds), *Blood Pressure Measurements: New Techniques in Automatic and 24-hour Indirect Monitoring.* New York, Springer-Verlag, 1990;161-172.

[177] Wikstrand J, Wendelhag L. Methodological considerations of ultrasound investigation of intima-media thickness and lumen diameter. *J Int Med.* 1994;236:555-559.

[178] Wong M, Edelstein J, Wollman J, Bond, MG. Ultrasonic-pathological comparison of the human arterial wall. Verification of intima-media thickness. *Arterioscler Thromb.* 1993;13:482-486.

[179] Yamamoto H, Tomoike H, Hisano K, Inoue T, Mohri M, Nakamura M. Reactive dilation and late-hyperemic constriction of epicardial coronary artery after short coronary occlusion. *Am J Physiol.* 1986;251:H554-H561.

[180] Yamamoto H, Bossaller C, Cartwright J, Henry PD. Videomicroscopic demonstration of defective cholinergic arteriolar vasodilation in atherosclerotic rabbit. *J Clin Invest.* 1988;81:1752-1758.

[181] Yamamoto H. Preserved endothelial function in the spastic segment of the human epicardial coronary artery in patients with variant angina – role of substance P in evaluating endothelial function. *Eur Heart J.* 1993;14 (Suppl 1.):118-122.

[182] Yamane K. Endothelin and collagen vascular disease: a review with special reference to Raynaud's phenomenon and systemic sclerosis. *Internal Med.* 1994;33:579-582.

[183] Zeiher AM, Drexler H, Wollschlager H, Just H. Modulation of coronary vasomotor tone in humans. Progressive endothelial dysfunction with different early stages of coronary atherosclerosis. *Circulation.* 1991;83:391-401.

[184] Zeiher AM, Drexler H, Wollschlager H, Just, H. Endothelial dysfunction of the coronary microvasculature is associated with impaired coronary blood flow regulation in patients with atherosclerosis. *Circulation.* 1991;84:1984-1992.

[185] Zeiher AM, Schachinger V, Minners J. Long-term cigarette smoking impairs endothelium-dependent coronary arterial vasodilator function. *Circulation.* 1995;92:1094-1100.

[186] Zwiener RJ, Uauy R, Petruska ML, Huet BA. Low-density lipoprotein apheresis as long-term treatment for children with homozygous familial hypercholesterolemia. *J Pediatr.* 1995;126:728-735.